Micromorphic approach to crystal plasticity and phase transformation

Samuel Forest [*†], Kais Ammar [*], Benoît Appolaire [**], Nicolas Cordero [*], and Anaïs Gaubert [***],

[*] MINES ParisTech, Centre des matériaux, CNRS UMR 7633, Evry, France
[**] Laboratoire d'étude des microstructures, CNRS/ONERA, Châtillon, France
[***] Dept. of Metallic Materials and Structures, ONERA, Châtillon, France
[†] Corresponding author: samuel.forest@mines-paristech.fr

Abstract Continuum crystal plasticity models are extended to incorporate the effect of the dislocation density tensor on material hardening. The approach is based on generalized continuum mechanics including strain gradient plasticity, Cosserat and micromorphic media. The applications deal with the effect of precipitate size in two–phase single crystals and to the Hall-Petch grain size effect in polycrystals. Some links between the micromorphic approach and phase field models are established. A coupling between phase field approach and elastoviscoplasticity constitutive equations is then presented and applied to the prediction of the influence of viscoplasticity on the kinetics of diffusive precipitate growth and morphology changes.

1 Introduction

Continuum crystal plasticity is a special class of anisotropic elastoviscoplastic behaviour of materials. It relies on the precise knowledge of the kinematics of plastic slip according to crystallographic slip systems and of the driving force for activation of plastic slip, namely the corresponding resolved shear stress. When the number of dislocations inside the material volume element is high enough, a continuum description of plastic deformation and hardening can be formulated as settled in (Mandel, 1965, 1971, 1973) and (Teodosiu and Sidoroff, 1976).

The objectives of this contribution is first to establish the continuum mechanical framework for the formulation of constitutive equations for single crystals including the effect of the dislocation density tensor. We show then than this model class can be used to predict size effects in the response of polycrystals. The considered plastic deformation mechanism is

J. Schröder, K. Hackl (Eds.), *Plasticity and Beyond*, CISM International Centre for Mechanical Sciences, DOI 10.1007/978-3-7091-1625-8_3, © CISM, Udine 2014

crystallographic slip but the formulation can serve as a basis for extensions to climb or twinning since thermomechanical balances and most kinematic considerations are still valid.

There exists an extreme variety of possible constitutive equations for single crystals derived in the last 40 years but the thermomechanical foundation is quite unique and now clearly settled Estrin (1996). We will consider this variety of constitutive laws by introducing generic internal variables without making specific choices. Only generic examples of evolution laws for such internal variables are provided and the reader is referred to (Fivel and Forest, 2004a), and references quoted therein, for a detailed discussion of best–suited constitutive laws for metal single crystals. Also the transition from single to polycrystal behaviour is shortly addressed here but fundamentals for modelling polycrystals can be found in (Fivel and Forest, 2004b; Besson et al., 2009).

The most relevant internal variables for describing the work–hardening of single crystals are undoubtedly dislocation densities, ρ^s, defined as the total length of dislocations belonging to a slip system s divided by the volume of the material volume element. Evolution equations for dislocations densities can be found in (Fivel and Forest, 2004a). In the present contribution, we introduce general isotropic and kinematic hardening variables accounting for monotonic and cyclic responses of crystals. Dislocation densities are generally related to isotropic hardening through forest hardening but recent contributions also aim at establishing dislocation based kinematic hardening dislocation rules.

Another characterisation of the dislocation distribution is the dislocation density tensor introduced by (Nye, 1953). It is defined in section 2.3 and contributes to many size effects observed in crystalline solids: grain size or Hall–Petch effect, precipitate size effect, etc. The dislocation density tensor cannot be handled as a usual internal variable because it is related to the gradient of the plastic deformation field. As a result, higher order partial differential equations arise when hardening laws involve the dislocation density tensor. The development of constitutive models involving the dislocation density tensor is the realm of strain gradient plasticity. Even for the much too simple constitutive equations presented in this work, the model shows that the dislocation density tensor is responsible for a size–dependent kinematic hardening component in the material behaviour.

The final part of this chapter draws a parallel between the micromorphic approach which consists in introducing additional degrees of freedom in the mechanical framework, and the phase field approach dedicated to the simulation of evolution of microstructures. The comparison enables us to combine the elastoviscoplastic behaviour of constitutents and the phase field

model in order to address the question of the influence of nonlinear deformation on the kinetics and morphology evolution during phase transformation (Ammar et al., 2011).

Notations Vectors, second, third and fourth rank tensors are denoted by $\underline{\boldsymbol{a}}, \underline{\underline{\boldsymbol{a}}}, \underline{\underline{\underline{\boldsymbol{a}}}}, \underline{\underline{\underline{\underline{\boldsymbol{a}}}}}$, respectively. The initial and current positions of the material point are denoted by $\underline{\boldsymbol{X}}$ and $\underline{\boldsymbol{x}}$, respectively. Throughout this work, the initial configuration of the body is V_0 whereas V denotes the current one. The associated smooth boundaries are ∂V_0 and ∂V with normal vector $\underline{\boldsymbol{N}}$ and $\underline{\boldsymbol{n}}$. The gradient operators with respect to initial and current coordinates are called $\boldsymbol{\nabla}_X$ and $\boldsymbol{\nabla}_x$ respectively. Similarily, the divergence and curl operators are Div, div and Curl, curl whether they are computed with respect to initial or current positions, respectively. Intrinsic notation is used in general but it is sometimes complemented or replaced by the index notation for clarity. A Cartesian coordinate system is used throughout with respect to the orthonormal basis $(\underline{\boldsymbol{e}}_1, \underline{\boldsymbol{e}}_2, \underline{\boldsymbol{e}}_3)$. The notations for double contraction and gradient operations are:

$$\underline{\underline{\boldsymbol{A}}} : \underline{\underline{\boldsymbol{B}}} = A_{ij}B_{ij}, \quad \underline{\boldsymbol{u}} \otimes \boldsymbol{\nabla}_X = \frac{\partial u_i}{\partial X_j}\, \underline{\boldsymbol{e}}_i \otimes \underline{\boldsymbol{e}}_j \tag{1}$$

2 Crystal plasticity and the dislocation density tensor

2.1 Thermomechanics of single crystal behaviour

Balance equations. Mechanical equilibrium can be expressed in the form of the principle of virtual power

$$-\int_{\mathcal{D}} \underline{\underline{\boldsymbol{\sigma}}} : \underline{\underline{\boldsymbol{D}}}^*\, dv + \int_{\mathcal{D}} \rho(\underline{\boldsymbol{f}} - \underline{\boldsymbol{a}}) \cdot \underline{\boldsymbol{v}}^*\, dv + \int_{\partial\mathcal{D}} \underline{\boldsymbol{t}} \cdot \underline{\boldsymbol{v}}^*\, ds = 0 \tag{2}$$

for all virtual velocity fields and all subdomains, $\mathcal{D}$, of the current configuration Ω of the body. The Cauchy stress tensor is $\underline{\underline{\boldsymbol{\sigma}}}$ and $\underline{\underline{\boldsymbol{D}}}$ is the strain rate tensor. Volume and acceleration forces are denoted by $\underline{\boldsymbol{f}}$ and $\underline{\boldsymbol{a}}$, respectively, whereas $\underline{\boldsymbol{t}}$ is the traction vector. The principle of virtual power implies the following balance of momentum equation

$$\operatorname{div} \underline{\underline{\boldsymbol{\sigma}}} + \rho \underline{\boldsymbol{f}} = \rho \underline{\boldsymbol{a}} \tag{3}$$

The energy balance is the purpose of the first principle of thermodynamics

$$\int_{\mathcal{D}} \rho \dot{e}\, dv - \int_{\mathcal{D}} \rho(\underline{\boldsymbol{a}} - \underline{\boldsymbol{f}}) \cdot \underline{\boldsymbol{v}}\, dv = \int_{\partial\mathcal{D}} \underline{\boldsymbol{t}} \cdot \underline{\boldsymbol{v}}\, ds + \mathcal{Q} \tag{4}$$

or equivalently, after implementing the balance of momentum principle,

$$\int_{\mathcal{D}} \rho \dot{e}\, dv = \int_{\mathcal{D}} \underset{\sim}{\boldsymbol{\sigma}} : \underset{\sim}{\boldsymbol{D}}\, dv + \mathcal{Q} \tag{5}$$

where ρe is the volume density of internal energy. The heat production rate is assumed to take the form

$$\mathcal{Q} = -\int_{\partial\mathcal{D}} \underline{\boldsymbol{q}} \cdot \underline{\boldsymbol{n}}\, ds \tag{6}$$

The local form of the energy principle is then

$$\rho \dot{e} = \underset{\sim}{\boldsymbol{\sigma}} : \underset{\sim}{\boldsymbol{D}} - \operatorname{div} \underline{\boldsymbol{q}} \tag{7}$$

The second principle of thermodynamics stipulates that

$$\int_{\mathcal{D}} \rho \dot{\eta}\, dv + \int_{\partial\mathcal{D}} \frac{\underline{\boldsymbol{q}}}{T} \cdot \underline{\boldsymbol{n}}\, ds \geq 0 \tag{8}$$

where η is the mass density of entropy and T the temperature field. The validity of this principle with respect to all subdomain $\mathcal{D}$ leads to the local form of the entropy principle

$$\rho \dot{\eta} + \operatorname{div} \frac{\underline{\boldsymbol{q}}}{T} \geq 0 \tag{9}$$

Introducing the free energy density $\Psi := e - T\eta$ and taking the balance of energy into account, we are lead to the Clausius inequality

$$\underset{\sim}{\boldsymbol{\sigma}} : \underset{\sim}{\boldsymbol{D}} - \rho \dot{\Psi} - \rho \eta \dot{T} - \underline{\boldsymbol{q}} \cdot \frac{\boldsymbol{\nabla} T}{T} \geq 0 \tag{10}$$

Kinematics of single crystals. It is based on the multiplicative decomposition of the deformation gradient, $\underset{\sim}{\boldsymbol{F}}$, into an elastic part, $\underset{\sim}{\boldsymbol{E}}$, and a plastic part, $\underset{\sim}{\boldsymbol{P}}$:

$$\underset{\sim}{\boldsymbol{F}}(\underline{\boldsymbol{X}}) = \underset{\sim}{\mathbf{1}} + \frac{\partial \underline{\boldsymbol{u}}}{\partial \underline{\boldsymbol{X}}} = \underset{\sim}{\mathbf{1}} + \underline{\boldsymbol{u}} \otimes \boldsymbol{\nabla}_X, \quad \underset{\sim}{\boldsymbol{F}}(\underline{\boldsymbol{X}}) = \underset{\sim}{\boldsymbol{E}}(\underline{\boldsymbol{X}}).\underset{\sim}{\boldsymbol{P}}(\underline{\boldsymbol{X}}) \tag{11}$$

The initial coordinates of the material point in the reference configuration are denoted by $\underline{\boldsymbol{X}}$ and $\boldsymbol{\nabla}_X$ denotes the gradient operator with respect to initial coordinates. The current position of the material point in the current configuration is $\underline{\boldsymbol{x}}$. The displacement vector is $\underline{\boldsymbol{u}} = \underline{\boldsymbol{x}} - \underline{\boldsymbol{X}}$. The multiplicative decomposition (11) is associated with the definition of an intermediate

configuration for which elastic strain is unloaded, see figure 1. The intermediate released configuration is uniquely determined up to a rigid body rotation which is chosen such that the lattice orientation in the intermediate configuration is the same as the initial one. Mandel called it the *isoclinic* intermediate configuration. As a result, lattice rotation and distortion during elastoplastic deformation are contained in the elastic deformation part $\underset{\sim}{\boldsymbol{E}}$, as examined at the end of this section.

The multiplicative decomposition leads to the following partition of the velocity gradient

$$\underline{\boldsymbol{v}} \otimes \boldsymbol{\nabla} = \dot{\underset{\sim}{\boldsymbol{F}}} \cdot \underset{\sim}{\boldsymbol{F}}^{-1} = \dot{\underset{\sim}{\boldsymbol{E}}} \cdot \underset{\sim}{\boldsymbol{E}}^{-1} + \underset{\sim}{\boldsymbol{E}} \cdot \dot{\underset{\sim}{\boldsymbol{P}}} \cdot \underset{\sim}{\boldsymbol{P}}^{-1} \cdot \underset{\sim}{\boldsymbol{E}}^{-1} \tag{12}$$

We introduce the Cauchy–Green and Green–Lagrange elastic strain measures

$$\underset{\sim}{\boldsymbol{C}}^e := \underset{\sim}{\boldsymbol{E}}^T \cdot \underset{\sim}{\boldsymbol{E}}, \quad \underset{\sim}{\boldsymbol{E}}^e = \frac{1}{2}(\underset{\sim}{\boldsymbol{C}}^e - \underset{\sim}{\mathbf{1}}) \tag{13}$$

and note that

$$\begin{aligned} \dot{\underset{\sim}{\boldsymbol{E}}}^e &= \frac{1}{2}(\dot{\underset{\sim}{\boldsymbol{E}}}^T \cdot \underset{\sim}{\boldsymbol{E}} + \underset{\sim}{\boldsymbol{E}}^T \cdot \dot{\underset{\sim}{\boldsymbol{E}}}) = \frac{1}{2}\dot{\underset{\sim}{\boldsymbol{C}}}^e \\ &= \frac{1}{2}\underset{\sim}{\boldsymbol{E}}^T \cdot (\underset{\sim}{\boldsymbol{E}}^{-T} \cdot \dot{\underset{\sim}{\boldsymbol{E}}}^T + \dot{\underset{\sim}{\boldsymbol{E}}} \cdot \underset{\sim}{\boldsymbol{E}}^{-1}) \cdot \underset{\sim}{\boldsymbol{E}} = \underset{\sim}{\boldsymbol{E}}^T \cdot \left(\dot{\underset{\sim}{\boldsymbol{E}}}^e \cdot \underset{\sim}{\boldsymbol{E}}^{-1}\right)^{sym} \cdot \underset{\sim}{\boldsymbol{E}} \end{aligned}$$

where *sym* operator takes the symmetric part of the quantity in brackets. The mass density of the material point with respect to the current (resp. intermediate) configuration is denoted by ρ (resp. ρ_e). The volume density of internal forces with respect to the intermediate configuration is

$$\begin{aligned} J_e \underset{\sim}{\boldsymbol{\sigma}} : \underset{\sim}{\boldsymbol{D}} &= J_e \underset{\sim}{\boldsymbol{\sigma}} : (\dot{\underset{\sim}{\boldsymbol{F}}} \cdot \underset{\sim}{\boldsymbol{F}}^{-1}) = J_e \underset{\sim}{\boldsymbol{\sigma}} : (\dot{\underset{\sim}{\boldsymbol{E}}} \cdot \underset{\sim}{\boldsymbol{E}}^{-1}) + J_e \underset{\sim}{\boldsymbol{\sigma}} : (\underset{\sim}{\boldsymbol{E}} \cdot \dot{\underset{\sim}{\boldsymbol{P}}} \cdot \underset{\sim}{\boldsymbol{P}}^{-1} \cdot \underset{\sim}{\boldsymbol{E}}^{-1}) \\ &= J_e \underset{\sim}{\boldsymbol{\sigma}} : (\dot{\underset{\sim}{\boldsymbol{E}}} \cdot \underset{\sim}{\boldsymbol{E}}^{-1})^{sym} + J_e \underset{\sim}{\boldsymbol{\sigma}} : (\underset{\sim}{\boldsymbol{E}} \cdot \dot{\underset{\sim}{\boldsymbol{P}}} \cdot \underset{\sim}{\boldsymbol{P}}^{-1} \cdot \underset{\sim}{\boldsymbol{E}}^{-1}) \\ &= \underset{\sim}{\boldsymbol{\Pi}}^e : \dot{\underset{\sim}{\boldsymbol{E}}}^e + \underset{\sim}{\boldsymbol{M}} : \dot{\underset{\sim}{\boldsymbol{P}}}.\underset{\sim}{\boldsymbol{P}}^{-1} \end{aligned} \tag{14}$$

where $J_e = \det \underset{\sim}{\boldsymbol{E}}$ is the volume change from the intermediate to the current configuration, $\underset{\sim}{\boldsymbol{\Pi}}^e$ is the second Piola–Kirchhoff stress tensor with respect to the isoclinic intermediate configuration, and $\underset{\sim}{\boldsymbol{M}}$ is the Mandel stress tensor defined as :

$$\underset{\sim}{\boldsymbol{\Pi}}^e = J_e \underset{\sim}{\boldsymbol{E}}^{-1}.\underset{\sim}{\boldsymbol{\sigma}}.\underset{\sim}{\boldsymbol{E}}^{-T}, \quad \underset{\sim}{\boldsymbol{M}} = J_e \underset{\sim}{\boldsymbol{E}}^T.\underset{\sim}{\boldsymbol{\sigma}}.\underset{\sim}{\boldsymbol{E}}^{-T} = \underset{\sim}{\boldsymbol{C}}^e \cdot \underset{\sim}{\boldsymbol{\Pi}}^e \tag{15}$$

Plastic deformation is the result of slip processes according to N slip systems characterised by the slip direction, $\underline{\boldsymbol{m}}^s$, and the normal to the slip plane, $\underline{\boldsymbol{n}}^s$, in the intermediate configuration :

$$\dot{\underset{\sim}{\boldsymbol{P}}}.\underset{\sim}{\boldsymbol{P}}^{-1} = \sum_{s=1}^{N} \dot{\gamma}^s \underline{\boldsymbol{m}}^s \otimes \underline{\boldsymbol{n}}^s \tag{16}$$

Note that plastic deformation induced by dislocation glide is isochoric so that

$$J_p = \det \underset{\sim}{\boldsymbol{P}} = 1, \quad J_e = J = \det \underset{\sim}{\boldsymbol{F}} \tag{17}$$

Constitutive equations Constitutive equations for elastoviscoplastic materials are based on the definition of two potential functions, namely the free energy density function and the dissipation potential. The specific energy density, $\Psi(\underset{\sim}{\boldsymbol{E}}^e, T, \alpha)$, is a function of elastic strain, temperature and internal variables accounting for hardening properties. Writing the Clausius–Duhem inequality (10) with respect to the intermediate isoclinic configuration amounts to multiplying (10) by $\rho_e/\rho = J_e$

$$J_e \underset{\sim}{\boldsymbol{\sigma}} : \underset{\sim}{\boldsymbol{D}} - \rho_e \dot{\Psi} - \rho_e \eta \dot{T} - \underline{\boldsymbol{Q}} \cdot \frac{\boldsymbol{\nabla}_X T}{T} \geq 0 \tag{18}$$

where $\underline{\boldsymbol{Q}} = J_e \underset{\sim}{\boldsymbol{F}}^{-T} \cdot \underline{\boldsymbol{q}}$. Expanding the time derivative of the free energy density, we obtain

$$\left(\underset{\sim}{\boldsymbol{\Pi}}^e - \rho_e \frac{\partial \Psi}{\partial \underset{\sim}{\boldsymbol{E}}^e} \right) : \dot{\underset{\sim}{\boldsymbol{E}}}^e - \rho_e (\eta + \frac{\partial \Psi}{\partial T}) \dot{T} + \underset{\sim}{\boldsymbol{M}} : \dot{\underset{\sim}{\boldsymbol{P}}} \cdot \underset{\sim}{\boldsymbol{P}}^{-1} - \rho_e \frac{\partial \Psi}{\partial \alpha} \dot{\alpha} - \underline{\boldsymbol{Q}} \cdot \frac{\boldsymbol{\nabla}_X}{\partial T} \geq 0 \tag{19}$$

The following state laws provide the hyperelasticity relation and the entropy density :

$$\underset{\sim}{\boldsymbol{\Pi}}^e = \rho_e \frac{\partial \Psi}{\partial \underset{\sim}{\boldsymbol{E}}^e} = \underset{\approx}{\boldsymbol{C}} : \underset{\sim}{\boldsymbol{E}}^e, \quad \eta = -\frac{\partial \Psi}{\partial T}, \quad X = \rho_e \frac{\partial \Psi}{\partial \alpha} \tag{20}$$

where a quadratic potential for elasticity has been proposed, thus introducing the fourth rank tensor of elasticity moduli, $\underset{\approx}{\boldsymbol{C}}$. Such an assumption is realistic for metals since elastic strain usually remains small, as discussed in the next subsection. The thermodynamic forces associated with the internal variables α are called X. The residual dissipation rate is

$$\underset{\sim}{\boldsymbol{M}} : \dot{\underset{\sim}{\boldsymbol{P}}} \cdot \underset{\sim}{\boldsymbol{P}}^{-1} - X \dot{\alpha} - \underline{\boldsymbol{Q}} \cdot \frac{\boldsymbol{\nabla}_X T}{T} \geq 0 \tag{21}$$

The first term is the plastic power. Part of it is stored due to the second contribution whereas the third one denotes thermal dissipation.

At this stage, a dissipation potential $\Omega(\underset{\sim}{\boldsymbol{M}}, X)$ is introduced from which the flow rule and the evolution equation for internal variables are derived

$$\dot{\underset{\sim}{\boldsymbol{P}}} . \underset{\sim}{\boldsymbol{P}}^{-1} = \frac{\partial \Omega}{\partial \underset{\sim}{\boldsymbol{M}}}, \quad \dot{\alpha} = -\frac{\partial \Omega}{\partial X} \tag{22}$$

Positivity of dissipation rate is ensured if the dissipation potential $\Omega(\underset{\sim}{\boldsymbol{M}}, X)$ exhibits specific convexity properties with respect to its arguments (convex with respect to $\underset{\sim}{\boldsymbol{M}}$ and concave with respect to X) and if a Fourier type of heat conduction is chosen

$$\underline{\boldsymbol{Q}} = -\underset{\sim}{\boldsymbol{K}} \cdot \boldsymbol{\nabla}_X(\log T) \tag{23}$$

The dissipation potential is assumed to depend on $\underset{\sim}{\boldsymbol{M}}$ and X via the Schmid yield function

$$f^s(\underset{\sim}{\boldsymbol{M}}, X) = |\tau^s - x^s| - \tau_c^s, \quad \text{with} \quad \tau^s = \underset{\sim}{\boldsymbol{M}} : \underline{\boldsymbol{m}}^s \otimes \underline{\boldsymbol{n}}^s \tag{24}$$

where τ_c^s is the critical resolved shear stress for slip system s, which may evolve due to isotropic hardening. Kinematic hardening is accounted for by means of back-stress components x^s attached to each slip system. The resolved shear stress $\tau^s = \underline{\boldsymbol{m}}^s.\underset{\sim}{\boldsymbol{M}}.\underline{\boldsymbol{n}}^s$ on slip system s is the driving force for activation of slip. This corresponds to the specific choice of hardening variables: $X = (\tau_c^s, x^s)$. So we consider a function

$$\Omega(\underset{\sim}{\boldsymbol{M}}, X) = \sum_{s=1}^{N} \Omega^s(f^s(\underset{\sim}{\boldsymbol{M}}, X)) \tag{25}$$

It follows that

$$\dot{\underset{\sim}{\boldsymbol{P}}}.\underset{\sim}{\boldsymbol{P}}^{-1} = \frac{\partial \Omega}{\partial \underset{\sim}{\boldsymbol{M}}} = \sum_{s=1}^{N} \frac{\partial \Omega^s}{\partial f^s} \frac{\partial f^s}{\partial \underset{\sim}{\boldsymbol{M}}} = \sum_{s=1}^{N} \dot{\gamma}^s \underline{\boldsymbol{m}}^s \otimes \underline{\boldsymbol{n}}^s \tag{26}$$

where the slip rate is computed as

$$\dot{\gamma}^s = \frac{\partial \Omega^s}{\partial f^s} \ \text{sign}\,(\tau^s - x^s) \tag{27}$$

Accordingly, the kinematics (16) is retrieved from the normality rule, showing that the crystal slip kinematics is associated with the Schmid law. Let us call (ρ^s, α^s) internal variables associated with the isotropic and kinematic hardening variables (τ_c^s, x^s). The hardening rules in (22) become

$$\dot{\rho}^s = -\frac{\partial \Omega}{\partial \tau_c^s} = \frac{\partial \Omega^s}{\partial f^s} = |\dot{\gamma}^s|, \quad \dot{\alpha}^s = -\frac{\partial \Omega}{\partial x^s} = \frac{\partial \Omega^s}{\partial f^s} \ \text{sign}\,(\tau^s - x^s) = \dot{\gamma}^s \tag{28}$$

It is worth computing the plastic power after taking the previous relations into account

$$\underset{\sim}{\boldsymbol{M}} : \dot{\underset{\sim}{\boldsymbol{P}}}.\underset{\sim}{\boldsymbol{P}}^{-1} = \sum_{s=1}^{N} \tau^s \dot{\gamma}^s \tag{29}$$

Specific hardening laws including evolution equations for dislocation densities can be found for example in Fivel and Forest (2004a). As an example, we consider here a power law potential

$$\dot{\gamma}^s = \frac{\partial \Omega}{\partial \tau^s} = \left\langle \frac{|\tau^s - x^s| - \tau_c}{K} \right\rangle^n \text{sign}(\tau^s) \tag{30}$$

$$\Omega(\tau^s) = \sum_{s=1}^{N} \frac{K}{n+1} \left\langle \frac{|\tau^s - x^s| - \tau_c}{K} \right\rangle^{n+1} \tag{31}$$

The brackets $\langle x \rangle$ denote the positive part of x. Viscosity parameters are K and n in (31). They can be chosen such that plastic processes are almost rate–independent in a given range of applied strain rates. As an example, we give here simple nonlinear evolution rules for the isotropic and kinematic variables that are used for practical computations

$$\tau_c^s = \tau_c + q \sum_{r=1}^{N} h^{sr}(1 - \exp(-bv^r)), \quad \dot{\alpha}^s = \dot{\gamma}^s - d\dot{v}^s \alpha^s \tag{32}$$

where q, b, d are material parameters. An interaction matrix h^{rs} is necessary to account for interaction between dislocations and is responsible for latent hardening Fivel and Forest (2004a).

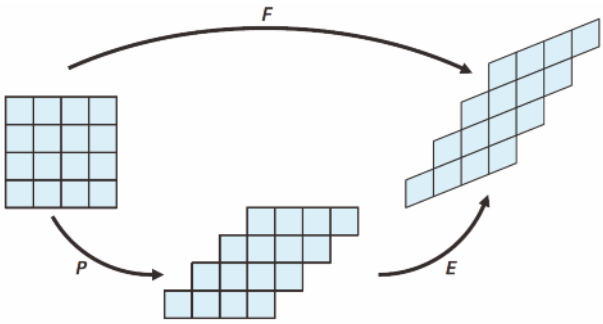

Figure 1. Multiplicative decomposition of the deformation gradient into elastic and plastic parts.

Lattice rotation. The previous continuum mechanical approach makes it possible to distinguish between the transformation of material and lattice

directions. Material lines are made of material points that are subjected to the motion $\underline{\boldsymbol{u}}(\underline{\boldsymbol{X}})$. The tangent to a material line at $\underline{\boldsymbol{X}}$ is a material direction $\underline{\boldsymbol{d}}$ in the reference configuration that transforms into the material direction $\underline{\boldsymbol{d}}'$ in the current configuration by means of the deformation gradient:

$$\underline{\boldsymbol{d}}'(\underline{\boldsymbol{X}}) = \underset{\sim}{\boldsymbol{F}}(\underline{\boldsymbol{X}}) \cdot \underline{\boldsymbol{d}}(\underline{\boldsymbol{X}}) \tag{33}$$

In contrast, lattice directions are not material insofar as they are not necessarily made of the same material points (atoms) in the initial and current configurations due to the passing of dislocations, but keep the same crystallographic meaning. According to the concept of isoclinic configuration, lattice directions are unchanged from the initial to the intermediate configuration of figure 1. Glide of dislocations through, and thus leaving, the material volume element do not distort nor rotate the lattice, although material lines are sheared. According to the continuum theory of dislocations, statistically stored dislocations accumulating in the material volume element affect material hardening but do not change the element shape. Accordingly, an initial lattice direction $\underline{\boldsymbol{d}}^\sharp$ is transformed into $\underline{\boldsymbol{d}}^{\sharp\prime}$ by means of the elastic deformation:

$$\underline{\boldsymbol{d}}^{\sharp\prime}(\underline{\boldsymbol{X}}) = \underset{\sim}{\boldsymbol{E}}(\underline{\boldsymbol{X}}).\underline{\boldsymbol{d}}^\sharp(\underline{\boldsymbol{X}}) \tag{34}$$

The kinematics of elastoplastic deformation recalled in section 2.1 can be expanded in the case of small strains and small rotations, based on the polar decompositions of total, elastic and plastic deformations:

$$\underset{\sim}{\boldsymbol{E}} = \underset{\sim}{\boldsymbol{R}}^e.\underset{\sim}{\boldsymbol{U}}^e \simeq (\underset{\sim}{\mathbf{1}} + \underset{\sim}{\boldsymbol{\omega}}^e).(\underset{\sim}{\mathbf{1}} + \underset{\sim}{\boldsymbol{\varepsilon}}^e) \simeq \underset{\sim}{\mathbf{1}} + \underset{\sim}{\boldsymbol{\varepsilon}}^e + \underset{\sim}{\boldsymbol{\omega}}^e \tag{35}$$

$$\underset{\sim}{\boldsymbol{P}} = \underset{\sim}{\boldsymbol{R}}^p.\underset{\sim}{\boldsymbol{U}}^p \simeq (\underset{\sim}{\mathbf{1}} + \underset{\sim}{\boldsymbol{\omega}}^p).(\underset{\sim}{\mathbf{1}} + \underset{\sim}{\boldsymbol{\varepsilon}}^p) \simeq \underset{\sim}{\mathbf{1}} + \underset{\sim}{\boldsymbol{\varepsilon}}^p + \underset{\sim}{\boldsymbol{\omega}}^p \tag{36}$$

where $\underset{\sim}{\boldsymbol{R}}^e, \underset{\sim}{\boldsymbol{R}}^p$ and $\underset{\sim}{\boldsymbol{U}}^e, \underset{\sim}{\boldsymbol{U}}^p$ are rotations and symmetric stretch tensors, respectively. Accordingly, $\underset{\sim}{\boldsymbol{\varepsilon}}^e, \underset{\sim}{\boldsymbol{\omega}}^e$ (resp. $\underset{\sim}{\boldsymbol{\varepsilon}}^p, \underset{\sim}{\boldsymbol{\omega}}^p$) represent small elastic (resp. plastic) strain and rotation. The elastic rotation accounts for lattice rotation, as follows from the proposed kinematics of plastic slip. Similarly, the following holds for the total deformation:

$$\underset{\sim}{\boldsymbol{F}} = \underset{\sim}{\boldsymbol{R}}.\underset{\sim}{\boldsymbol{U}} = (\underset{\sim}{\mathbf{1}} + \underset{\sim}{\boldsymbol{\omega}}).(\underset{\sim}{\mathbf{1}} + \underset{\sim}{\boldsymbol{\varepsilon}}) \simeq \underset{\sim}{\mathbf{1}} + \underset{\sim}{\boldsymbol{\varepsilon}} + \underset{\sim}{\boldsymbol{\omega}} \tag{37}$$

so that

$$\underset{\sim}{\boldsymbol{\varepsilon}} = \underset{\sim}{\boldsymbol{\varepsilon}}^e + \underset{\sim}{\boldsymbol{\varepsilon}}^p, \quad \underset{\sim}{\boldsymbol{\omega}} = \underset{\sim}{\boldsymbol{\omega}}^e + \underset{\sim}{\boldsymbol{\omega}}^p \tag{38}$$

where all strain tensors are symmetric whereas all ω tensors are skew–symmetric.

In metals, elastic strain remains small whereas lattice rotations can become very large. That is why the kinematics of crystallographic slip is very often approximated as

$$\underset{\sim}{\boldsymbol{F}} \simeq \underset{\sim}{\boldsymbol{R}}^e \cdot \underset{\sim}{\boldsymbol{P}} \tag{39}$$

especially for the simulation of metal forming processes. Lattice rotation is then directly given by $\underset{\sim}{\boldsymbol{R}}^e$.

Let us consider also rotation rates by introducing the material spin tensor $\underset{\sim}{\boldsymbol{W}}$ which is the skew–symmetric part of the velocity gradient

$$\dot{\underset{\sim}{\boldsymbol{F}}} \cdot \underset{\sim}{\boldsymbol{F}}^{-1} = \underset{\sim}{\boldsymbol{D}} + \underset{\sim}{\boldsymbol{W}} = \dot{\underset{\sim}{\boldsymbol{E}}} \cdot \underset{\sim}{\boldsymbol{E}}^{-1} + \underset{\sim}{\boldsymbol{E}} \cdot \dot{\underset{\sim}{\boldsymbol{P}}} \cdot \underset{\sim}{\boldsymbol{P}}^{-1} \cdot \underset{\sim}{\boldsymbol{E}}^{-1} = \underset{\sim}{\boldsymbol{D}}^e + \underset{\sim}{\boldsymbol{W}}^e + \underset{\sim}{\boldsymbol{D}}^p + \underset{\sim}{\boldsymbol{W}}^p \tag{40}$$

where the elastic and plastic contributions have been split into their symmetric and skew–symmetric parts. The elastic spin tensor is therefore defined as

$$\underset{\sim}{\boldsymbol{W}}^e = \left(\dot{\underset{\sim}{\boldsymbol{E}}} \cdot \underset{\sim}{\boldsymbol{E}}^{-1} \right)^{skew} = \left(\dot{\underset{\sim}{\boldsymbol{R}}}^e \cdot \underset{\sim}{\boldsymbol{R}}^{e-1} + \underset{\sim}{\boldsymbol{R}}^e \cdot \dot{\underset{\sim}{\boldsymbol{U}}}^e \cdot \underset{\sim}{\boldsymbol{U}}^e \cdot \underset{\sim}{\boldsymbol{R}}^{e-1} \right)^{skew} \tag{41}$$

$$\simeq \dot{\underset{\sim}{\boldsymbol{R}}}^e \cdot \underset{\sim}{\boldsymbol{R}}^{e-1} = \dot{\underset{\sim}{\boldsymbol{R}}}^e \cdot \underset{\sim}{\boldsymbol{R}}^{eT} \tag{42}$$

where the exponent *skew* denotes the skew–symmetric part of the tensor in brackets. The latter approximation is valid when elastic strain rates can be neglected compared to rotation rates, which is generally the case for metals at sufficiently high total strains. Note that for any rotation $\underset{\sim}{\boldsymbol{Q}}$, the rotation rate $\dot{\underset{\sim}{\boldsymbol{Q}}} \cdot \underset{\sim}{\boldsymbol{Q}}^{-1} = \dot{\underset{\sim}{\boldsymbol{Q}}} \cdot \underset{\sim}{\boldsymbol{Q}}^{T}$ is a skew–symmetric tensor due to the fact that a rotation is an orthogonal tensor[1]. The plastic spin rate is

$$\begin{aligned}
\underset{\sim}{\boldsymbol{W}}^p &= \left(\underset{\sim}{\boldsymbol{E}} \cdot \left(\sum_{s=1}^{N} \dot{\gamma}^s \underline{\boldsymbol{m}}^s \otimes \underline{\boldsymbol{n}}^s \right) \cdot \underset{\sim}{\boldsymbol{E}}^{-1} \right)^{skew} \\
&\simeq \left(\underset{\sim}{\boldsymbol{R}}^e \cdot \left(\sum_{s=1}^{N} \dot{\gamma}^s \underline{\boldsymbol{m}}^s \otimes \underline{\boldsymbol{n}}^s \right) \cdot \underset{\sim}{\boldsymbol{R}}^{eT} \right)^{skew} \\
&\simeq \underset{\sim}{\boldsymbol{R}}^e \cdot \left(\sum_{s=1}^{N} \dot{\gamma}^s \left(\underline{\boldsymbol{m}}^s \otimes \underline{\boldsymbol{n}}^s \right)^{skew} \right) \cdot \underset{\sim}{\boldsymbol{R}}^{eT}
\end{aligned}$$

In the case of small elastic strain and rotations, the expressions simplify

[1] meaning that $\underset{\sim}{\boldsymbol{Q}} \cdot \underset{\sim}{\boldsymbol{Q}}^T = \underset{\sim}{\boldsymbol{Q}}^T \cdot \underset{\sim}{\boldsymbol{Q}} = \underset{\sim}{\boldsymbol{1}}$

and we obtain

$$\underset{\sim}{\boldsymbol{D}}^p \simeq \underset{\sim}{\dot{\boldsymbol{\varepsilon}}}^p = \sum_{s=1}^{N} \dot{\gamma}^s \left(\underline{\boldsymbol{m}}^s \otimes \underline{\boldsymbol{n}}^s\right)^{sym} \tag{43}$$

$$\underset{\sim}{\boldsymbol{W}}^p \simeq \underset{\sim}{\dot{\boldsymbol{\omega}}}^p = \sum_{s=1}^{N} \dot{\gamma}^s \left(\underline{\boldsymbol{m}}^s \otimes \underline{\boldsymbol{n}}^s\right)^{skew} \tag{44}$$

$$\underset{\sim}{\boldsymbol{D}}^e \simeq \underset{\sim}{\dot{\boldsymbol{\varepsilon}}}^e = \underset{\sim}{\dot{\boldsymbol{\varepsilon}}} - \underset{\sim}{\dot{\boldsymbol{\varepsilon}}}^p, \quad \underset{\sim}{\dot{\boldsymbol{W}}}^e \simeq \underset{\sim}{\dot{\boldsymbol{\omega}}}^e = \underset{\sim}{\dot{\boldsymbol{\omega}}} - \underset{\sim}{\dot{\boldsymbol{\omega}}}^p \tag{45}$$

2.2 Elements of tensor analysis

The Euclidean space is endowed with an arbitrary coordinate system characterizing the points $M(q^i)$. The basis vectors are defined as

$$\underline{\boldsymbol{e}}_i = \frac{\partial M}{\partial q^i} \tag{46}$$

The reciprocal basis $(\underline{\boldsymbol{e}}^i)_{i=1,3}$ of $(\underline{\boldsymbol{e}}_i)_{i=1,3}$ is the unique triad of vectors such that

$$\underline{\boldsymbol{e}}^i \cdot \underline{\boldsymbol{e}}_j = \delta^i_j \tag{47}$$

If a Cartesian orthonormal coordinate system is chosen, then both bases coincide.

The gradient operator for a tensor field $T(\underline{\boldsymbol{X}})$ of arbitrary rank is then defined as

$$\operatorname{grad} T = T \otimes \boldsymbol{\nabla} := \frac{\partial T}{\partial q^i} \otimes \underline{\boldsymbol{e}}^i \tag{48}$$

The gradient operation therefore increases the tensor rank by one.

The divergence operator for a tensor field $T(\underline{\boldsymbol{X}})$ of arbitrary rank is then defined as

$$\operatorname{div} T = T \cdot \boldsymbol{\nabla} := \frac{\partial T}{\partial q^i} \cdot \underline{\boldsymbol{e}}^i \tag{49}$$

The divergence operation therefore decreases the tensor rank by one.

The curl operator[2] for a tensor field $T(\underline{\boldsymbol{X}})$ of arbitrary rank is then defined as

$$\operatorname{curl} T = T \wedge \boldsymbol{\nabla} := \frac{\partial T}{\partial q^i} \wedge \underline{\boldsymbol{e}}^i \tag{50}$$

where the vector product is $\wedge$. The curl operation therefore leaves the tensor rank unchanged. The vector product on an oriented Euclidean space is

$$\underline{\boldsymbol{a}} \wedge \underline{\boldsymbol{b}} = \epsilon_{ijk} a_j b_k \, \underline{\boldsymbol{e}}_i = \underset{\sim}{\boldsymbol{\epsilon}} : (\underline{\boldsymbol{a}} \otimes \underline{\boldsymbol{b}}) \tag{51}$$

[2] or rotational operator.

The component ϵ_{ijk} of the third rank permutation tensor is the signature of the permutation of $(1,2,3)$.

With respect to a Cartesian orthonormal basis, the previous formula simplify. We give the expressions for a second rank tensor $\underset{\sim}{\boldsymbol{T}}$

$$\begin{aligned} \operatorname{grad} \underset{\sim}{\boldsymbol{T}} &= T_{ij,k}\, \underline{\boldsymbol{e}}_i \otimes \underline{\boldsymbol{e}}_j \otimes \underline{\boldsymbol{e}}_k \quad (52) \\ \operatorname{div} \underset{\sim}{\boldsymbol{T}} &= T_{ij,j}\, \underline{\boldsymbol{e}}_i \quad (53) \end{aligned}$$

We consider then successively the curl of a vector field and of a second rank vector field, in a Cartesian orthonormal coordinate frame

$$\operatorname{curl} \underline{\boldsymbol{u}} = \frac{\partial \underline{\boldsymbol{u}}}{\partial X_j} \wedge \underline{\boldsymbol{e}}_j = u_{i,j}\, \underline{\boldsymbol{e}}_i \wedge \underline{\boldsymbol{e}}_j = \epsilon_{kij} u_{i,j}\, \underline{\boldsymbol{e}}_k \quad (54)$$

$$\operatorname{curl} \underset{\sim}{\boldsymbol{A}} = \frac{\partial \underset{\sim}{\boldsymbol{A}}}{\partial x_k} \wedge \underline{\boldsymbol{e}}_k = A_{ij,k} \underline{\boldsymbol{e}}_i \otimes \underline{\boldsymbol{e}}_j \wedge \underline{\boldsymbol{e}}_k = \epsilon_{mjk} A_{ij,k}\, \underline{\boldsymbol{e}}_i \otimes \underline{\boldsymbol{e}}_m \quad (55)$$

We also recall the Stokes formula for a vector field for a surface $\mathcal{S}$ with unit normal vector $\underline{\boldsymbol{n}}$ and oriented closed border line $\mathcal{L}$:

$$\oint_{\mathcal{L}} \underline{\boldsymbol{u}} \cdot \underline{\boldsymbol{dl}} = -\int_{\mathcal{S}} (\operatorname{curl} \underline{\boldsymbol{u}}) \cdot \underline{\boldsymbol{n}}\, ds, \quad \oint_{\mathcal{L}} u_i dl_i = -\epsilon_{kij} \int_{\mathcal{S}} u_{i,j} n_k\, ds \quad (56)$$

Applying the previous formula to $u_j = A_{ij}$ at fixed i leads to the Stokes formula for a tensor field of rank 2:

$$\oint_{\mathcal{L}} \underset{\sim}{\boldsymbol{T}} \cdot \underline{\boldsymbol{dl}} = -\int_{\mathcal{S}} (\operatorname{curl} \underset{\sim}{\boldsymbol{T}}) \cdot \underline{\boldsymbol{n}}\, ds, \quad \oint_{\mathcal{L}} A_{ij} dl_i = -\epsilon_{kij} \int_{\mathcal{S}} A_{ij,k} n_m\, ds \quad (57)$$

2.3 Dislocation density tensor

In continuum mechanics, the previous differential operators are used with respect to the initial coordinates $\underline{\boldsymbol{X}}$ or with respect to the current coordinates $\underline{\boldsymbol{x}}$ of the material points. In the latter case, the notation $\boldsymbol{\nabla}, \operatorname{grad}, \operatorname{div}$ and curl are used but in the former case we adopt $\boldsymbol{\nabla}_X, \operatorname{Grad}, Div$ and Curl. For instance,

$$\underset{\sim}{\boldsymbol{F}} = \underset{\sim}{\mathbf{1}} + \operatorname{Grad} \underline{\boldsymbol{u}} \quad \Longrightarrow \quad \operatorname{Curl} \underset{\sim}{\boldsymbol{F}} = 0 \quad (58)$$

This result expresses the fact that the deformation gradient is a compatible field which derives from the displacement vector field. This is generally not the case for elastic and plastic deformation:

$$\operatorname{Curl} \underset{\sim}{\boldsymbol{E}} \neq 0, \quad \operatorname{Curl} \underset{\sim}{\boldsymbol{P}} \neq 0 \quad (59)$$

Elastic and plastic deformations are generally incompatible tensor fields, even though the product $\underset{\sim}{\boldsymbol{F}} = \underset{\sim}{\boldsymbol{E}} \cdot \underset{\sim}{\boldsymbol{P}}$ is compatible. It may happen incidentally that elastic deformation be compatible for instance when plastic or elastic deformation is homogeneous.

A consequence of the incompatibility of the elastic deformation is that, for an oriented surface $\mathcal{S} \subset \Omega$ of the body, with border $\mathcal{L}$, the vector $\underline{\boldsymbol{B}}$ belonging to the intermediate isoclinic configuration

$$\underline{\boldsymbol{B}} = \oint_{\mathcal{L}} \underset{\sim}{\boldsymbol{E}}^{-1} \cdot \underline{\boldsymbol{dl}} = -\int_{\mathcal{S}} (\operatorname{curl} \underset{\sim}{\boldsymbol{E}}^{-1}) \cdot \underline{\boldsymbol{n}}\, ds \tag{60}$$

does not vanish in general. It can be interpreted as the continuum Burgers vector for the circuit $\mathcal{L}$. It represents a generalization of the concept of Burgers vector for dislocations. This geometric definition was introduced by Bilby et al. (1957); Teodosiu (1970); Kröner and Teodosiu (1972) within the context of the continuum theory of dislocations. The previous calculation leads to the definition of the dislocation density tensor

$$\underset{\sim}{\boldsymbol{\alpha}} := -\operatorname{curl} \underset{\sim}{\boldsymbol{E}}^{-1} = -\epsilon_{jkl} E^{-1}_{ik,l}\, \underline{\boldsymbol{e}}_i \otimes \underline{\boldsymbol{e}}_j \tag{61}$$

which is used to compute the resulting Burgers vector for dislocations crossing the surface $\mathcal{S}$:

$$\underline{\boldsymbol{B}} = \int_{\mathcal{S}} \underset{\sim}{\boldsymbol{\alpha}} \cdot \underline{\boldsymbol{n}}\, ds \tag{62}$$

The Burgers vector can also be computed by means of a closed circuit $\mathcal{L}_0 \subset \Omega_0$ convected from $\mathcal{L} \subset \Omega$:

$$\underline{\boldsymbol{B}} = \oint_{\mathcal{L}} \underset{\sim}{\boldsymbol{E}}^{-1} \cdot \underline{\boldsymbol{dx}} = \oint_{\mathcal{L}_0} \underset{\sim}{\boldsymbol{E}}^{-1} \cdot \underset{\sim}{\boldsymbol{F}} \cdot \underline{\boldsymbol{dX}} = \oint_{\mathcal{L}_0} \underset{\sim}{\boldsymbol{P}} \cdot \underline{\boldsymbol{dX}} \tag{63}$$

$$= \int_{\mathcal{S}_0} (\operatorname{Curl} \underset{\sim}{\boldsymbol{P}}) \cdot \underline{\boldsymbol{dS}} = \int_{\mathcal{S}} (\operatorname{Curl} \underset{\sim}{\boldsymbol{P}}) \cdot \underset{\sim}{\boldsymbol{F}}^T \cdot \frac{\underline{\boldsymbol{dS}}}{J} \tag{64}$$

Nanson's formula[3] has been used. We obtain the alternative definition of the dislocation density tensor

$$\underset{\sim}{\boldsymbol{\alpha}} = \operatorname{curl} \underset{\sim}{\boldsymbol{E}}^{-1} = \frac{1}{J} (\operatorname{Curl} \underset{\sim}{\boldsymbol{P}}) \cdot \underset{\sim}{\boldsymbol{F}}^T \tag{65}$$

The present modern treatment of the dislocation density tensor was settled by Cermelli and Gurtin (2001); Svendsen (2002). A statistical mechanics perspective of the dislocation density tensor can be found in Kröner (1969).

It can be noticed that the relation (65) implies

$$J(\operatorname{curl} \underset{\sim}{\boldsymbol{E}}^{-1}) \cdot \underset{\sim}{\boldsymbol{E}}^{-T} = (\operatorname{Curl} \underset{\sim}{\boldsymbol{P}}) \cdot \underset{\sim}{\boldsymbol{P}}^T \tag{66}$$

which is a consequence of (58), $\operatorname{curl} \underset{\sim}{\boldsymbol{F}} = \operatorname{curl}(\underset{\sim}{\boldsymbol{E}} \cdot \underset{\sim}{\boldsymbol{P}}) = 0$.

[3] $\underline{\boldsymbol{ds}} = J \underset{\sim}{\boldsymbol{F}}^{-T} \cdot \underline{\boldsymbol{dS}}$

Within the small perturbation framework, we introduce the notations

$$\underset{\sim}{\boldsymbol{H}} = \operatorname{Grad} \underline{\boldsymbol{u}} = \underset{\sim}{\boldsymbol{H}}^e + \underset{\sim}{\boldsymbol{H}}^p, \quad \text{with} \quad \underset{\sim}{\boldsymbol{H}}^e = \underset{\sim}{\boldsymbol{\varepsilon}}^e + \underset{\sim}{\boldsymbol{\omega}}^e, \quad \underset{\sim}{\boldsymbol{H}}^p = \underset{\sim}{\boldsymbol{\varepsilon}}^p + \underset{\sim}{\boldsymbol{\omega}}^p \tag{67}$$

We have

$$\underset{\sim}{\boldsymbol{E}}^{-1} \simeq \underset{\sim}{\mathbf{1}} - \underset{\sim}{\boldsymbol{H}}^e \tag{68}$$

so that the dislocation density tensor can be computed as

$$\underset{\sim}{\boldsymbol{\alpha}} \simeq \operatorname{Curl} \underset{\sim}{\boldsymbol{H}}^e = -\operatorname{Curl} \underset{\sim}{\boldsymbol{H}}^p \tag{69}$$

since $\operatorname{Curl} \underset{\sim}{\boldsymbol{H}} = 0$ due to the compatibility of the deformation gradient.

2.4 Lattice curvature

Experimental techniques like EBSD provide the field of lattice orientation and, consequently, of lattice rotation $\underset{\sim}{\boldsymbol{R}}^e$ during deformation. Since

$$\underset{\sim}{\boldsymbol{\alpha}} = -\operatorname{curl} \underset{\sim}{\boldsymbol{E}}^{-1} = -\operatorname{curl}(\underset{\sim}{\boldsymbol{U}}^{e-1} \cdot \underset{\sim}{\boldsymbol{R}}^{eT}) \tag{70}$$

the hypothesis of small elastic strain implies

$$\underset{\sim}{\boldsymbol{\alpha}} \simeq -\operatorname{curl} \underset{\sim}{\boldsymbol{R}}^{eT} \tag{71}$$

If, in addition, elastic rotations are small, we have

$$\underset{\sim}{\boldsymbol{\alpha}} \simeq -\operatorname{curl}(\underset{\sim}{\mathbf{1}} - \underset{\sim}{\boldsymbol{\omega}}^e) = \operatorname{curl} \underset{\sim}{\boldsymbol{\omega}}^e \tag{72}$$

The small rotation axial vector is defined as

$$\overset{\times}{\underline{\boldsymbol{\omega}}}{}^e = -\frac{1}{2} \underset{\approx}{\boldsymbol{\epsilon}} : \underset{\sim}{\boldsymbol{\omega}}^e, \quad \underset{\sim}{\boldsymbol{\omega}}^e = -\underset{\approx}{\boldsymbol{\epsilon}} \cdot \overset{\times}{\underline{\boldsymbol{\omega}}}{}^e \tag{73}$$

or, in matrix notations,

$$[\underset{\sim}{\boldsymbol{\omega}}^e] = \begin{bmatrix} 0 & \omega_{12}^e & -\omega_{31}^e \\ -\omega_{12}^e & 0 & \omega_{23}^e \\ \omega_{31}^e & -\omega_{23}^e & 0 \end{bmatrix} = \begin{bmatrix} 0 & -\overset{\times}{\omega}{}_3^e & \overset{\times}{\omega}{}_2^e \\ \overset{\times}{\omega}{}_3^e & 0 & -\overset{\times}{\omega}{}_1^e \\ -\overset{\times}{\omega}{}_2^e & \overset{\times}{\omega}{}_1^e & 0 \end{bmatrix} \tag{74}$$

The gradient of the lattice rotation field delivers the lattice curvature tensor. In the small deformation context, the gradient of the rotation tensor is represented by the gradient of the axial vector:

$$\underset{\sim}{\boldsymbol{\kappa}} := \overset{\times}{\underline{\boldsymbol{\omega}}}{}^e \tag{75}$$

One can establish a direct link between $\operatorname{curl}\underset{\sim}{\boldsymbol{\omega}}^e$ and the gradient of the axial vector associated with $\underset{\sim}{\boldsymbol{\omega}}$. For that purpose, the matrix form of $\operatorname{curl}\underset{\sim}{\boldsymbol{\omega}}^e$ is derived according to (55):

$$[\operatorname{curl}\underset{\sim}{\boldsymbol{\omega}}^e] = \begin{bmatrix} \omega^e_{12,3} + \omega^e_{31,2} & -\omega^e_{31,1} & -\omega^e_{12,1} \\ -\omega^e_{23,2} & \omega^e_{12,3} + \omega^e_{23,1} & -\omega^e_{12,2} \\ -\omega^e_{23,3} & -\omega^e_{31,3} & \omega^e_{23,1} + \omega^e_{31,2} \end{bmatrix} \tag{76}$$

or equivalently

$$[\operatorname{curl}\underset{\sim}{\boldsymbol{\omega}}^e] = \begin{bmatrix} -\overset{\times}{\omega}{}^e_{3,3} - \overset{\times}{\omega}{}^e_{2,2} & \overset{\times}{\omega}{}^e_{2,1} & \overset{\times}{\omega}{}^e_{3,1} \\ \overset{\times}{\omega}{}^e_{1,2} & -\overset{\times}{\omega}{}^e_{3,3} - \overset{\times}{\omega}{}^e_{1,1} & \overset{\times}{\omega}{}^e_{3,2} \\ \overset{\times}{\omega}{}^e_{1,3} & \overset{\times}{\omega}{}^e_{2,3} & -\overset{\times}{\omega}{}^e_{1,1} - \overset{\times}{\omega}{}^e_{2,2} \end{bmatrix} \tag{77}$$

from which it becomes apparent that

$$\underset{\sim}{\boldsymbol{\alpha}} = \underset{\sim}{\boldsymbol{\kappa}}^T - (\operatorname{trace}\underset{\sim}{\boldsymbol{\kappa}})\underset{\sim}{\mathbf{1}}, \quad \underset{\sim}{\boldsymbol{\kappa}} = \underset{\sim}{\boldsymbol{\alpha}}^T - \frac{1}{2}(\operatorname{trace}\underset{\sim}{\boldsymbol{\alpha}})\underset{\sim}{\mathbf{1}} \tag{78}$$

This is a remarkable relation linking, with the context of small elastic strains[4] and rotations, the dislocation density tensor to lattice curvature. It is known as Nye's formula Nye (1953).

3 Micromorphic crystal plasticity

The links between the micromorphic continuum and the plasticity of crystalline materials has been recognized very early by Eringen himself (Claus and Eringen, 1969; Eringen and Claus, 1970). Lattice directions in a single crystal can be regarded as directors that rotate and deform as they do in a micromorphic continuum. The fact that lattice directions can be rotated and stretched in a different way than material lines connecting individual atoms, especially in the presence of static or moving dislocations, illustrates the independence between directors and material lines in a micromorphic continuum, even though their deformations can be related at the constitutive level.

The identification of a micromorphic continuum from the discrete atomic single crystal model is possible based on proper averaging relations proposed in (Chen and Lee, 2003a,b). These works contain virial formula for

[4] and in fact of small gradient of elastic strain.

the higher order stress tensors arising in the micromorphic theory. This atomistic–based approach can be used to predict phonon dispersion relations (Chen and Lee, 2003c). Claus and Eringen (1971) also studied the dispersion of waves in a dislocated crystal.

Analytical solutions have been provided that give the generalized stress fields around individual screw or edge dislocations embedded in an elastic generalized continuum medium, like the micromorphic medium. The physical meaning of such a calculation is the account of non–local elasticity at the core of dislocations that may suppress or limit the singularity of the stress fields. For instance, non singular force and couple stress were determined by (Lazar and Maugin, 2004) for a screw dislocation embedded in a gradient micropolar medium that combines the first strain gradient with independent rotational degrees of freedom. The unphysical singularities at the core of straight screw and edge dislocations are also removed when the second gradient of strain is introduced in the theory, while the first strain gradient is not sufficient, see (Lazar et al., 2006). Other crystal defects in a large range of microcontinua were analysed by Lazar and Maugin (2007).

The next step is to consider the collective behaviour of dislocations in a single crystal by means of the continuum theory of dislocations. The material volume element is now assumed to contain a large enough number of dislocations for the continuum theory of dislocation to be applicable. Non–homogeneous plastic deformations induce material and lattice incompatibilities that are resolved by a suitable distribution of the dislocation density tensor field which is a second rank statistical mean for a population of arbitrary dislocations inside a material volume element (Kröner, 1969; Cermelli and Gurtin, 2001). Nye's fundamental relation linearly connects the dislocation density tensor to the lattice curvature field of the crystal. This fact has prompted many authors to treat a continuously dislocated crystal as a Cosserat continuum (Günther, 1958; Kröner, 1963; Schäfer,H., 1969; Forest et al., 2000). The Cosserat approach records only the lattice curvature of the crystal but neglects the effect of the rotational part of the elastic strain tensor, which is a part of the total dislocation density tensor (Cordero et al., 2010). Full account of plastic incompatibilities is taken in strain gradient plasticity theories, starting from the original work by Aifantis (1984) up to recent progress by Gurtin (2002). Formulation of crystal plasticity within the micromorphic framework is more recent and was suggested by Clayton et al. (2005) for a large spectrum of crystal defects, including point defects and disclinations. Limiting the discussion to dislocation density tensor effects, also called geometrically necessary dislocation (GND) effects, Cordero et al. (2010) showed, within a small deformation setting, how the micromorphic model can be used to predict grain and precipitate

size effects in laminate crystalline materials. In particular, the micromorphic model is shown to deliver more general scaling laws than conventional strain gradient plasticity. These models represent extensions of the conventional crystal plasticity theory, see for instance (Teodosiu and Sidoroff, 1976), that accounts for single crystal hardening and lattice rotation but does not incorporate the effect of the dislocation density tensor.

The objective of the present work is, first, to formulate a finite deformation micromorphic extension of conventional crystal plasticity to account for GND effects in single crystals, and, second, to show that the micromorphic approach can also be used to introduce cleavage induced damage in a single crystal model. The first part, see Section 3, represents an extension to finite deformation of the model proposed by Aslan et al. (2011). It also provides new analytical predictions of size effects on the yield stength and kinematic hardening of laminate microstructures made of an elastic layer and an elastic–plastic single crystal layer undergoing single slip. The theory is called the *microcurl* model because the evaluation of the curl of the microdeformation, instead of its full gradient, is sufficient to account for the effect of the dislocation density tensor.

The models proposed in this work for single crystals fall in the class of anisotropic elastoviscoplastic micromorphic media for which constitutive frameworks at finite deformations have been proposed in (Forest and Sievert, 2003; Lee and Chen, 2003; Grammenoudis and Tsakmakis, 2009; Sansour et al., 2010; Regueiro, 2010). The introduction of damage variables was performed in (Grammenoudis et al., 2009). In fact, the micromorphic approach can be applied not only to the total deformation by introducing the micro–deformation field, but can also be restricted to plastic deformation, for specific application to size effects in plasticity, or to damage variables for application to regularized simulation of crack propagation, as proposed in (Forest, 2009; Hirschberger and Steinmann, 2009).

3.1 Model formulation

Balance equations. The degrees of freedom of the proposed theory are the displacement vector $\underline{\boldsymbol{u}}$ and the microdeformation variable $\underset{\sim}{\hat{\boldsymbol{\chi}}}^p$, a generally non–symmetric second rank tensor. The field $\underset{\sim}{\hat{\boldsymbol{\chi}}}^p(\underline{\boldsymbol{X}})$ is generally not compatible, meaning that it does not derive from a vector field. The exponent ^{p} indicates, in advance, that this variable will eventually be constitutively related to plastic deformation occurring at the material point. In particular, the microdeformation $\underset{\sim}{\hat{\boldsymbol{\chi}}}^p$ is treated as an invariant quantity with respect to rigid body motion. The constitutive model will eventually ensure this invariance property. This is in contrast to the general microdeforma-

tion degrees of freedom of the original micromorphic theory. A first gradient theory is considered with respect to the degrees of freedom. However, the influence of the microdeformation gradient is limited to its curl part because of the aimed relation to the dislocation density tensor associated with the curl of plastic distortion. The following sets of degrees of freedom and of their gradients are therefore defined:

$$DOF = \{\underline{\boldsymbol{u}}, \quad \underset{\sim}{\hat{\boldsymbol{\chi}}}^p\}, \quad GRAD = \{\underset{\sim}{\boldsymbol{F}} := \underset{\sim}{\mathbf{1}} + \underline{\boldsymbol{u}} \otimes \boldsymbol{\nabla}_X, \quad \underset{\sim}{\boldsymbol{K}} := \mathrm{Curl}\, \underset{\sim}{\hat{\boldsymbol{\chi}}}^p\} \tag{79}$$

The following definition of the Curl operator is adopted:

$$\mathrm{Curl}\, \underset{\sim}{\hat{\boldsymbol{\chi}}}^p := \frac{\partial \underset{\sim}{\hat{\boldsymbol{\chi}}}^p}{\partial X_k} \times \underline{\boldsymbol{e}}_k, \quad K_{ij} := \epsilon_{jkl} \frac{\partial \hat{\chi}^p_{ik}}{\partial X_l} \tag{80}$$

where ϵ_{ijk} is the permutation tensor.
The method of virtual power is used to derive the balance and boundary conditions, following (Germain, 1973b). For that purpose, we define the power density of internal forces as a linear form with respect to the velocity fields and their Eulerian gradients:

$$p^{(i)} = \underset{\sim}{\boldsymbol{\sigma}} : (\dot{\underline{\boldsymbol{u}}} \otimes \boldsymbol{\nabla}_x) + \underset{\sim}{\boldsymbol{s}} : \dot{\underset{\sim}{\hat{\boldsymbol{\chi}}}}^p + \underset{\sim}{\boldsymbol{M}} : \mathrm{curl}\, \dot{\underset{\sim}{\hat{\boldsymbol{\chi}}}}^p, \quad \forall \underline{\boldsymbol{x}} \in V \tag{81}$$

where the conjugate quantities are the Cauchy stress tensor $\underset{\sim}{\boldsymbol{\sigma}}$, which is symmetric for objectivity reasons, the microstress tensor, $\underset{\sim}{\boldsymbol{s}}$, and the generalized couple stress tensor $\underset{\sim}{\boldsymbol{M}}$. The curl of the microdeformation rate is defined as

$$\mathrm{curl}\, \dot{\underset{\sim}{\hat{\boldsymbol{\chi}}}}^p := \epsilon_{jkl} \frac{\partial \dot{\hat{\chi}}^p_{ik}}{\partial x_l} \underline{\boldsymbol{e}}_i \otimes \underline{\boldsymbol{e}}_j = \dot{\underset{\sim}{\boldsymbol{K}}} \cdot \underset{\sim}{\boldsymbol{F}}^{-1} \tag{82}$$

The form of the power density of internal forces dictates the form of the power density of contact forces:

$$p^{(c)} = \underline{\boldsymbol{t}} \cdot \dot{\underline{\boldsymbol{u}}} + \underset{\sim}{\boldsymbol{m}} : \dot{\underset{\sim}{\hat{\boldsymbol{\chi}}}}^p, \quad \forall \underline{\boldsymbol{x}} \in \partial V \tag{83}$$

where $\underline{\boldsymbol{t}}$ is the usual simple traction vector and $\underset{\sim}{\boldsymbol{m}}$ the double traction tensor. The principle of virtual power is stated in the static case and in the absence of volume forces for the sake of brevity:

$$-\int_D p^{(i)}\, dV + \int_{\partial D} p^{(c)}\, dS = 0 \tag{84}$$

for all virtual fields $\dot{\underline{\boldsymbol{u}}}, \dot{\underset{\sim}{\hat{\boldsymbol{\chi}}}}^p$, and any subdomain $D \subset V$. By application of Gauss divergence theorem, assuming sufficient regularity of the fields, this

statement expands into:

$$\int_V \frac{\partial \sigma_{ij}}{\partial x_j}\dot{u}_i\, dV + \int_V \left(\epsilon_{kjl}\frac{\partial M_{ik}}{\partial x_l} - s_{ij}\right)\dot{\chi}^p_{ij}\, dV$$
$$+ \int_{\partial V} (t_i - \sigma_{ij}n_j)\,\dot{u}_i\, dS + \int_{\partial V} (m_{ik} - \epsilon_{jkl}M_{ij}n_l)\,\dot{\chi}^p_{ik}\, dS = 0, \quad \forall \dot{u}_i, \forall \dot{\chi}^p_{ij}$$

which leads to the two field equations of balance of momentum and generalized balance of moment of momentum:

$$\operatorname{div} \underset{\sim}{\boldsymbol{\sigma}} = 0, \quad \operatorname{curl} \underset{\sim}{\boldsymbol{M}} + \underset{\sim}{\boldsymbol{s}} = 0, \quad \forall \underline{\boldsymbol{x}} \in V \tag{85}$$

and two boundary conditions

$$\underline{\boldsymbol{t}} = \underset{\sim}{\boldsymbol{\sigma}} \cdot \underline{\boldsymbol{n}}, \quad \underset{\sim}{\boldsymbol{m}} = \underset{\sim}{\boldsymbol{M}} \cdot \underset{\approx}{\boldsymbol{\epsilon}} \cdot \underline{\boldsymbol{n}}, \quad \forall \underline{\boldsymbol{x}} \in \partial V \tag{86}$$

the index notation of the latter relation being $m_{ij} = M_{ik}\epsilon_{kjl}n_l$.

Constitutive equations. The deformation gradient is decomposed into elastic and plastic parts in the form

$$\underset{\sim}{\boldsymbol{F}} = \underset{\sim}{\boldsymbol{F}}^e \cdot \underset{\sim}{\boldsymbol{F}}^p \tag{87}$$

The isoclinic intermediate configuration is defined in a unique way by keeping the crystal orientation unchanged from the initial to the intermediate configuration following (Mandel, 1973). The plastic distortion $\underset{\sim}{\boldsymbol{F}}^p$ is invariant with respect to rigid body motions that are carried by $\underset{\sim}{\boldsymbol{F}}^e$. The current mass density is ρ whereas the mass density of the material element in the intermediate configuration is ρ_i, such that $\rho_i/\rho = J_e := \det \underset{\sim}{\boldsymbol{F}}^e$. The elastic strain is defined as

$$\underset{\sim}{\boldsymbol{E}}^e := \frac{1}{2}(\underset{\sim}{\boldsymbol{F}}^{eT} \cdot \underset{\sim}{\boldsymbol{F}}^e - \underset{\sim}{\mathbf{1}}) \tag{88}$$

The microdeformation is linked to the plastic deformation via the introduction of a relative deformation measure defined as

$$\underset{\sim}{\boldsymbol{e}}^p := \underset{\sim}{\boldsymbol{F}}^{p-1} \cdot \underset{\sim}{\hat{\boldsymbol{\chi}}}^p - \underset{\sim}{\mathbf{1}} \tag{89}$$

It measures the departure of the microdeformation from the plastic deformation, which will be associated with a cost in the free energy potential. When $\underset{\sim}{\boldsymbol{e}}^p \equiv 0$, the microdeformation coincides with the plastic deformation. The state variables are assumed to be the elastic strain, the relative deformation, the curl of microdeformation and some internal variables, α:

$$STATE := \{\underset{\sim}{\boldsymbol{E}}^e, \quad \underset{\sim}{\boldsymbol{e}}^p, \quad \underset{\sim}{\boldsymbol{K}}, \quad \alpha\} \tag{90}$$

The specific Helmholtz free energy density, ψ, is assumed to be a function of this set of state variables. In particular, in this simple version of the model, the curl of microdeformation is assumed to contribute entirely to the stored energy. In more sophisticated models, as proposed in (Forest and Sievert, 2003, 2006; Forest, 2009; Gurtin and Anand, 2009), the relative deformation, the microdeformation and its gradient can be split into elastic plastic parts. This is not necessary for the size effects to be described in the present work.

When the internal constraint $\underset{\sim}{\boldsymbol{e}}^p \equiv 0$ is enforced, the plastic microdeformation coincides with the plastic deformation so that the curl of the plastic microdformation is directly related to the dislocation density tensor:

$$\underset{\sim}{\boldsymbol{K}} := \mathrm{Curl}\,\underset{\sim}{\hat{\boldsymbol{\chi}}}^p \equiv \mathrm{Curl}\,P = J\underset{\sim}{\boldsymbol{\alpha}} \cdot \underset{\sim}{\boldsymbol{F}}^{-T} \tag{91}$$

The micromorphic model then reduces to strain gradient plasticity according to Gurtin (2002).

The dissipation rate density is the difference:

$$D := p^{(i)} - \rho\dot{\psi} \geq 0 \tag{92}$$

which must be positive according to the second principle of thermodynamics. When the previous strain measures are introduced, the power density of internal forces takes the following form:

$$\begin{aligned} p^{(i)} &= \underset{\sim}{\boldsymbol{\sigma}} : \dot{\underset{\sim}{\boldsymbol{F}}}^e \cdot \underset{\sim}{\boldsymbol{F}}^{e-1} + \underset{\sim}{\boldsymbol{\sigma}} : \underset{\sim}{\boldsymbol{F}}^e \cdot \dot{\underset{\sim}{\boldsymbol{F}}}^p \cdot \underset{\sim}{\boldsymbol{F}}^{p-1} \cdot \underset{\sim}{\boldsymbol{F}}^{e-1} \\ &+ \underset{\sim}{\boldsymbol{s}} : (\underset{\sim}{\boldsymbol{F}}^p \cdot \dot{\underset{\sim}{\boldsymbol{e}}}^p + \dot{\underset{\sim}{\boldsymbol{F}}}^p \cdot \underset{\sim}{\boldsymbol{e}}^p) + \underset{\sim}{\boldsymbol{M}} : \dot{\underset{\sim}{\boldsymbol{K}}} \cdot \underset{\sim}{\boldsymbol{F}}^{-1} \\ &= \frac{\rho}{\rho_i}\underset{\sim}{\boldsymbol{\Pi}}^e : \dot{\underset{\sim}{\boldsymbol{E}}}^e + \frac{\rho}{\rho_i}\underset{\sim}{\boldsymbol{\Pi}}^M : \dot{\underset{\sim}{\boldsymbol{F}}}^p \cdot \underset{\sim}{\boldsymbol{F}}^{p-1} \\ &+ \underset{\sim}{\boldsymbol{s}} : (\underset{\sim}{\boldsymbol{F}}^p \cdot \dot{\underset{\sim}{\boldsymbol{e}}}^p + \dot{\underset{\sim}{\boldsymbol{F}}}^p \cdot \underset{\sim}{\boldsymbol{e}}^p) + \underset{\sim}{\boldsymbol{M}} : \dot{\underset{\sim}{\boldsymbol{K}}} \cdot \underset{\sim}{\boldsymbol{F}}^{-1} \end{aligned} \tag{93}$$

where $\underset{\sim}{\boldsymbol{\Pi}}^e$ is the second Piola–Kirchhoff stress tensor with respect to the intermediate configuration and $\underset{\sim}{\boldsymbol{\Pi}}^M$ is the Mandel stress tensor:

$$\underset{\sim}{\boldsymbol{\Pi}}^e := J_e\underset{\sim}{\boldsymbol{F}}^{e-1} \cdot \underset{\sim}{\boldsymbol{\sigma}} \cdot \underset{\sim}{\boldsymbol{F}}^{e-T}, \quad \underset{\sim}{\boldsymbol{\Pi}}^M := J_e\underset{\sim}{\boldsymbol{F}}^{eT} \cdot \underset{\sim}{\boldsymbol{\sigma}} \cdot \underset{\sim}{\boldsymbol{F}}^{e-T} = \underset{\sim}{\boldsymbol{F}}^{eT} \cdot \underset{\sim}{\boldsymbol{F}}^e \cdot \underset{\sim}{\boldsymbol{\Pi}}^e \tag{94}$$

On the other hand,

$$\rho\dot{\psi} = \rho\frac{\partial\psi}{\partial\underset{\sim}{\boldsymbol{E}}^e} : \dot{\underset{\sim}{\boldsymbol{E}}}^e + \rho\frac{\partial\psi}{\partial\underset{\sim}{\boldsymbol{e}}^p} : \dot{\underset{\sim}{\boldsymbol{e}}}^p + \rho\frac{\partial\psi}{\partial\underset{\sim}{\boldsymbol{K}}} : \dot{\underset{\sim}{\boldsymbol{K}}} + \rho\frac{\partial\psi}{\partial\alpha}\dot{\alpha} \tag{95}$$

We compute

$$\begin{aligned} J_e D &= (\underset{\sim}{\boldsymbol{\Pi}}^e - \rho_i \frac{\partial \psi}{\partial \underset{\sim}{\boldsymbol{E}}^e}) : \dot{\underset{\sim}{\boldsymbol{E}}}^e + (J_e \underset{\sim}{\boldsymbol{F}}^{pT} \cdot \underset{\sim}{\boldsymbol{s}} - \rho_i \frac{\partial \psi}{\partial \underset{\sim}{\boldsymbol{e}}^p}) : \dot{\underset{\sim}{\boldsymbol{e}}}^p \\ &+ (J_e \underset{\sim}{\boldsymbol{M}} \cdot \underset{\sim}{\boldsymbol{F}}^{-T} - \rho_i \frac{\partial \psi}{\partial \underset{\sim}{\boldsymbol{K}}}) : \dot{\underset{\sim}{\boldsymbol{K}}} \\ &+ (\underset{\sim}{\boldsymbol{\Pi}}^M + J_e \underset{\sim}{\boldsymbol{s}} \cdot \underset{\sim}{\hat{\boldsymbol{\chi}}}^{pT}) : \dot{\underset{\sim}{\boldsymbol{F}}}^p \cdot \underset{\sim}{\boldsymbol{F}}^{p-1} - \rho_i \frac{\partial \psi}{\partial \alpha} \dot{\alpha} \geq 0 \end{aligned} \tag{96}$$

Assuming that the processes associated with $\dot{\underset{\sim}{\boldsymbol{E}}}^e$, $\dot{\underset{\sim}{\boldsymbol{e}}}^p$ and $\dot{\underset{\sim}{\boldsymbol{K}}}$ are non–dissipative, the state laws are obtained:

$$\underset{\sim}{\boldsymbol{\Pi}}^e = \rho_i \frac{\partial \psi}{\partial \underset{\sim}{\boldsymbol{E}}^e}, \quad \underset{\sim}{\boldsymbol{s}} = J_e^{-1} \underset{\sim}{\boldsymbol{F}}^{p-T} \cdot \rho_i \frac{\partial \psi}{\partial \underset{\sim}{\boldsymbol{e}}^p}, \quad \underset{\sim}{\boldsymbol{M}} = J_e^{-1} \rho_i \frac{\partial \psi}{\partial \underset{\sim}{\boldsymbol{K}}} \cdot \underset{\sim}{\boldsymbol{F}}^T \tag{97}$$

The residual dissipation rate is

$$J_e D = (\underset{\sim}{\boldsymbol{\Pi}}^M + J_e \underset{\sim}{\boldsymbol{s}} \cdot \underset{\sim}{\hat{\boldsymbol{\chi}}}^{pT}) : \dot{\underset{\sim}{\boldsymbol{F}}}^p \cdot \underset{\sim}{\boldsymbol{F}}^{p-1} - R\dot{\alpha} \geq 0, \quad \text{with} \quad R := \rho_i \frac{\partial \psi}{\partial \alpha} \tag{98}$$

At this stage, a dissipation potential, function of stress measures, $\Omega(\underset{\sim}{\boldsymbol{\mathcal{S}}}, R)$, is introduced in order to formulate the evolution equations for plastic flow and internal variables:

$$\dot{\underset{\sim}{\boldsymbol{F}}}^p \cdot \underset{\sim}{\boldsymbol{F}}^{p-1} = \frac{\partial \Omega}{\partial \underset{\sim}{\boldsymbol{\mathcal{S}}}}, \quad \text{with} \quad \underset{\sim}{\boldsymbol{\mathcal{S}}} := \underset{\sim}{\boldsymbol{\Pi}}^M + J_e \underset{\sim}{\boldsymbol{s}} \cdot \underset{\sim}{\hat{\boldsymbol{\chi}}}^{pT} \tag{99}$$

$$\dot{\alpha} = -\frac{\partial \Omega}{\partial R} \tag{100}$$

where R is the thermodynamic force associated with the internal variable α, and $\underset{\sim}{\boldsymbol{\mathcal{S}}}$ is the effective stress conjugate to plastic strain rate, the driving force for plastic flow.

In the case of crystal plasticity, a generalized Schmid law is adopted for each slip system s in the form:

$$f^s(\underset{\sim}{\boldsymbol{\mathcal{S}}}, \tau_c^s) = |\underset{\sim}{\boldsymbol{\mathcal{S}}} : \underset{\sim}{\boldsymbol{P}}^s| - \tau_c^s \geq 0, \quad \text{with} \quad \underset{\sim}{\boldsymbol{P}}^s = \underline{\boldsymbol{l}}^s \otimes \underline{\boldsymbol{n}}^s \tag{101}$$

for activation of slip system s with slip direction, $\underline{\boldsymbol{l}}^s$, and normal to the slip plane, $\underline{\boldsymbol{n}}^s$. We call $\underset{\sim}{\boldsymbol{P}}^s$ the orientation tensor. The critical resolved shear stress is τ_c^s which may be a function of R in the presence of isotropic hardening. The kinematics of plastic slip follows from the choice of a dissipation potential, $\Omega(f^s)$, that depends on the stress variables through the yield function itself, f^s:

$$\dot{\underset{\sim}{\boldsymbol{F}}}^p \cdot \underset{\sim}{\boldsymbol{F}}^{p-1} = \sum_{s=1}^{N} \frac{\partial \Omega}{\partial f^s} \frac{\partial f^s}{\partial \underset{\sim}{\boldsymbol{\mathcal{S}}}} = \sum_{s=1}^{N} \dot{\gamma}^s \underset{\sim}{\boldsymbol{P}}^s, \quad \text{with} \quad \dot{\gamma}^s = \frac{\partial \Omega}{\partial f^s} \text{sign}(\underset{\sim}{\boldsymbol{\mathcal{S}}} : \underset{\sim}{\boldsymbol{P}}^s) \tag{102}$$

A possible viscoplastic potential is then:

$$\Omega(f^s) = \frac{K}{n+1} < \frac{f^s}{K} >^{n+1} \tag{103}$$

where K, n are viscosity parameters associated with viscoplastic slip, and the brackets stand for $< \cdot >= Max(0, \cdot)$. The generalized resolved shear stress can be decomposed into two contributions:

$$\underset{\sim}{\boldsymbol{\mathcal{S}}} : \underset{\sim}{\boldsymbol{P}}^s = \tau^s - x^s, \quad \text{with} \quad \tau^s = \underset{\sim}{\boldsymbol{\Pi}}^M : \underset{\sim}{\boldsymbol{P}}^s \quad \text{and} \quad x^s = -\underset{\sim}{\boldsymbol{s}} \cdot \underset{\sim}{\hat{\boldsymbol{\chi}}}^{pT} : \underset{\sim}{\boldsymbol{P}}^s \tag{104}$$

The usual resolved shear stress is τ^s whereas x^s can be interpreted as an internal stress or back–stress leading to kinematic hardening. The fact that the introduction of the effect of the dislocation density tensor or, more generally, of gradient of plastic strain tensor, leads to the existence of internal stresses induced by higher order stresses has already been noticed by (Steinmann, 1996), see also (Forest, 2008). The back–stress component is induced by the microstress $\underset{\sim}{\boldsymbol{s}}$ or, equivalently, by the curl of the generalized couple stress tensor, $\underset{\sim}{\boldsymbol{M}}$, via the balance equation (85).

When deformations and rotations remain sufficiently small, the previous equations can be linearized as follows:

$$\underset{\sim}{\boldsymbol{F}} = \underset{\sim}{\boldsymbol{1}} + \underset{\sim}{\boldsymbol{H}} \simeq \underset{\sim}{\boldsymbol{1}} + \underset{\sim}{\boldsymbol{H}}^e + \underset{\sim}{\boldsymbol{H}}^p, \quad \underset{\sim}{\boldsymbol{H}}^e = \underset{\sim}{\boldsymbol{\varepsilon}}^e + \omega^e, \quad \underset{\sim}{\boldsymbol{H}}^p = \underset{\sim}{\boldsymbol{\varepsilon}}^p + \omega^p \tag{105}$$

where $\underset{\sim}{\boldsymbol{\varepsilon}}^e, \underset{\sim}{\boldsymbol{\omega}}^e$ (resp. $\underset{\sim}{\boldsymbol{\varepsilon}}^p, \underset{\sim}{\boldsymbol{\omega}}^p$) are the symmetric and skew–symmetric parts of $\underset{\sim}{\boldsymbol{F}}^e - \underset{\sim}{\boldsymbol{1}}$ (resp. $\underset{\sim}{\boldsymbol{F}}^p - \underset{\sim}{\boldsymbol{1}}$). When microdeformation is small, the relative deformation is linearized as

$$\underset{\sim}{\boldsymbol{e}}^p = (\underset{\sim}{\boldsymbol{1}} + \underset{\sim}{\boldsymbol{H}}^p)^{-1} \cdot (\underset{\sim}{\boldsymbol{1}} + \underset{\sim}{\boldsymbol{\chi}}^p) - \underset{\sim}{\boldsymbol{1}} \simeq \underset{\sim}{\boldsymbol{\chi}}^p - \underset{\sim}{\boldsymbol{H}}^p, \quad \text{with} \quad \underset{\sim}{\boldsymbol{\chi}}^p = \underset{\sim}{\hat{\boldsymbol{\chi}}}^p - \underset{\sim}{\boldsymbol{1}} \tag{106}$$

When linearized, the state laws (97) become:

$$\underset{\sim}{\boldsymbol{\sigma}} = \rho \frac{\partial \psi}{\partial \underset{\sim}{\boldsymbol{\varepsilon}}^e}, \quad \underset{\sim}{\boldsymbol{s}} = \rho \frac{\partial \psi}{\partial \underset{\sim}{\boldsymbol{e}}^p}, \quad \underset{\sim}{\boldsymbol{M}} = \rho \frac{\partial \psi}{\partial \underset{\sim}{\boldsymbol{K}}} \tag{107}$$

The evolution equations read then:

$$\dot{\underset{\sim}{\boldsymbol{\varepsilon}}}^p = \frac{\partial \Omega}{\partial (\underset{\sim}{\boldsymbol{\sigma}} + \underset{\sim}{\boldsymbol{s}})}, \quad \dot{\alpha} = -\frac{\partial \Omega}{\partial R} \tag{108}$$

We adopt the most simple case of a quadratic free energy potential:

$$\rho\psi(\underset{\sim}{\boldsymbol{\varepsilon}}^e, \underset{\sim}{\boldsymbol{e}}^p, \underset{\sim}{\boldsymbol{K}}) = \frac{1}{2} \underset{\sim}{\boldsymbol{\varepsilon}}^e : \underset{\approx}{\boldsymbol{C}} : \underset{\sim}{\boldsymbol{\varepsilon}}^e + \frac{1}{2} H_\chi \underset{\sim}{\boldsymbol{e}}^p : \underset{\sim}{\boldsymbol{e}}^p + \frac{1}{2} A \underset{\sim}{\boldsymbol{K}} : \underset{\sim}{\boldsymbol{K}} \tag{109}$$

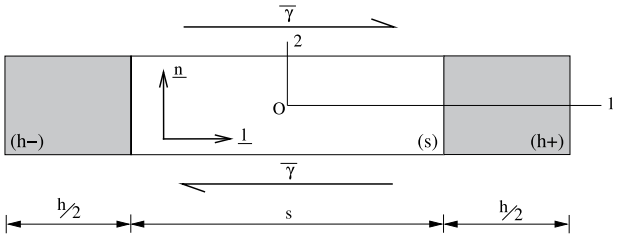

Figure 2. Single slip in a periodic two–phase single crystal laminate under simple shear: the grey phase (h) displays a purely linear elastic behaviour whereas the inelastic deformation of the white elasto–plastic phase (s) is controlled by a single slip system $(\underline{\boldsymbol{n}}, \underline{\boldsymbol{l}})$.

The usual four–rank tensor of elastic moduli is denoted by $\underset{\approx}{\boldsymbol{C}}$. The higher order moduli have been limited to only two additional parameters: H_χ (unit MPa) and A (unit MPa.mm^2). Their essential impact on the prediction of size effect will be analyzed in the next section. It follows that:

$$\underset{\sim}{\boldsymbol{\sigma}} = \underset{\approx}{\boldsymbol{C}} : \underset{\sim}{\boldsymbol{\varepsilon}}^e, \quad \underset{\sim}{\boldsymbol{s}} = H_\chi \underset{\sim}{\boldsymbol{e}}^p, \quad \underset{\sim}{\boldsymbol{M}} = A\underset{\sim}{\boldsymbol{K}} \tag{110}$$

Large values of H_χ ensure that $\underset{\sim}{\boldsymbol{e}}^p$ remains small so that $\hat{\underset{\sim}{\boldsymbol{\chi}}}^p$ remains close to $\underset{\sim}{\boldsymbol{H}}^p$ and $\underset{\sim}{\boldsymbol{K}}$ is close to the dislocation density tensor. The yield condition for each slip system becomes:

$$f^s = |\tau^s - x^s| - \tau_c^s \tag{111}$$

with

$$x^s = -\underline{\boldsymbol{s}} : \underline{\boldsymbol{P}}^s = (\operatorname{curl} \underline{\boldsymbol{M}}) : \underline{\boldsymbol{P}}^s = A(\operatorname{curl}\operatorname{curl} \underline{\boldsymbol{\chi}}^p) : \underline{\boldsymbol{P}}^s \tag{112}$$

3.2 Size effects in a two-phase single crystal laminate

Let us consider a periodic two–phase single crystal laminate under simple shear as in (Forest and Sedláček, 2003), (Forest, 2008) and (Cordero et al., 2010). This microstructure is described in Fig. 2; it is composed of a hard elastic phase (h) and a soft elasto–plastic phase (s) where one slip system with slip direction normal to the interface between (h) and (s) is considered. A mean simple glide $\bar{\gamma}$ is applied in the crystal slip direction of the phase (s). We consider a displacement and microdeformation fields of the form:

$$u_1 = \bar{\gamma} x_2, \quad u_2(x_1), \quad u_3 = 0, \quad \chi^p_{12}(x_1), \quad \chi^p_{21}(x_1) \tag{113}$$

within the context of small deformation theory. It follows that

$$\left[\underset{\sim}{\boldsymbol{H}}\right] = \begin{bmatrix} 0 & \bar{\gamma} & 0 \\ u_{2,1} & 0 & 0 \\ 0 & 0 & 0 \end{bmatrix}$$

$$\left[\underset{\sim}{\boldsymbol{H}}^p\right] = \begin{bmatrix} 0 & \gamma & 0 \\ 0 & 0 & 0 \\ 0 & 0 & 0 \end{bmatrix} \quad \left[\underset{\sim}{\boldsymbol{H}}^e\right] = \begin{bmatrix} 0 & \bar{\gamma}-\gamma & 0 \\ u_{2,1} & 0 & 0 \\ 0 & 0 & 0 \end{bmatrix}$$

$$\left[\underset{\sim}{\boldsymbol{\chi}}^p\right] = \begin{bmatrix} 0 & \chi^p_{12}(x_1) & 0 \\ \chi^p_{21}(x_1) & 0 & 0 \\ 0 & 0 & 0 \end{bmatrix} \quad \left[\operatorname{curl}\underset{\sim}{\boldsymbol{\chi}}^p\right] = \begin{bmatrix} 0 & 0 & -\chi^p_{12,1} \\ 0 & 0 & 0 \\ 0 & 0 & 0 \end{bmatrix}$$

The resulting stress tensors are:

$$\left[\underset{\sim}{\boldsymbol{\sigma}}\right] = \mu \begin{bmatrix} 0 & \bar{\gamma}-\gamma+u_{2,1} & 0 \\ \bar{\gamma}-\gamma+u_{2,1} & 0 & 0 \\ 0 & 0 & 0 \end{bmatrix}$$

$$\left[\underset{\sim}{\boldsymbol{s}}\right] = -H_\chi \begin{bmatrix} 0 & \gamma-\chi^p_{12} & 0 \\ -\chi^p_{21} & 0 & 0 \\ 0 & 0 & 0 \end{bmatrix}$$

$$\left[\underset{\sim}{\boldsymbol{M}}\right] = \begin{bmatrix} 0 & 0 & -A\chi^p_{12,1} \\ 0 & 0 & 0 \\ 0 & 0 & 0 \end{bmatrix} \quad \left[\operatorname{curl}\underset{\sim}{\boldsymbol{M}}\right] = \begin{bmatrix} 0 & -A\chi^p_{12,11} & 0 \\ 0 & 0 & 0 \\ 0 & 0 & 0 \end{bmatrix}$$

These forms of matrices are valid for both phases, except that $\gamma \equiv 0$ in the hard elastic phase. Each phase possesses its own material parameters, H_χ and A, the shear modulus, μ, being assumed for simplicity to be identical in both phases. The balance equation, $\underset{\sim}{\boldsymbol{s}} = -\operatorname{curl}\underset{\sim}{\boldsymbol{M}}$, gives $\chi^p_{21} = 0$ and the plastic slip:

$$\gamma = \chi^p_{12} - \frac{A}{H_\chi}\chi^p_{12,11}. \tag{114}$$

In the soft phase, the plasticity criterion stipulates that

$$\sigma_{12} + s_{12} = \tau_c + H\gamma_{cum}, \tag{115}$$

where H is a linear hardening modulus considered in this phase and γ_{cum} is the accumulated plastic slip as $\dot{\gamma}_{cum} = |\dot{\gamma}|$. The following analytical resolution is done for the first loading branch, under monotonic loading. The slip direction, $\underline{\boldsymbol{l}}$, has been chosen such that $\gamma > 0$ for this first loading branch, so that we have: $\gamma_{cum} = \gamma$. Considering Eqs. (114) and (115),

we obtain the second order differential equation for the microdeformation variable in the soft phase, χ_{12}^{ps},

$$\frac{1}{\omega^{s2}}\,\chi_{12,11}^{ps} - \chi_{12}^{ps} = \frac{\tau_c - \sigma_{12}}{H}, \quad \text{with} \quad \omega^s = \sqrt{\frac{H_\chi^s H}{A^s\left(H_\chi^s + H\right)}}. \tag{116}$$

where $1/\omega^s$ is the characteristic length of the soft phase for this boundary value problem. The force stress balance equation requires σ_{12} to be uniform. It follows that the non–homogeneous part of the differential equation is constant and then the hyperbolic profile of χ_{12}^{ps} takes the form:

$$\chi_{12}^{ps} = C^s \cosh\left(\omega^s x\right) + D, \tag{117}$$

where C^s and D are constants to be determined. Symmetry conditions $(\chi_{12}^{ps}(-s/2) = \chi_{12}^{ps}(s/2))$ have been taken into account.
In the elastic phase, where the plastic slip vanishes, an hyperbolic profile of the microdeformation variable, χ_{12}^{ph}, is also obtained:

$$\chi_{12}^{ph} = C^h \cosh\left(\omega^h\left(x \pm \frac{s+h}{2}\right)\right), \quad \text{with} \quad \omega^h = \sqrt{\frac{H_\chi^h}{A^h}}, \tag{118}$$

where, again, C^h is a constant to be determined and symmetry conditions have been taken into account. It is remarkable that the plastic microvariable, χ_{12}^{ph}, does not vanish in the elastic phase, close to the interfaces, although no plastic deformation takes place. This is due to the transmission of double traction. Such a transmission has been shown in (Cordero et al., 2010) to be essential for size effects to occur. This point will be discussed in section 3.3. The meaning of the linear constitutive equation for the double stress tensor in (110) can be interpreted, for the elastic phase, as non–local elasticity. That is why the corresponding characteristic length, $1/\omega^h$, will be kept of the order of nanometer in the presented simulation.

Note that the same boundary value problem was handled in (Cordero et al., 2010) in the case of a perfectly plastic phase (s), i.e., without linear isotropic hardening. It showed that χ_{12}^{ps} has a parabolic profile over (s), the profile of χ_{12}^{ph} remaining hyperbolic in the hard phase (h). In the following of this section we will show how the additional isotropic hardening affects the local and macroscopic behaviors while the main effects of the *microcurl* model as presented in (Cordero et al., 2010) remain.
The coefficients C^s, D and C^h can be identified using the interface and periodicity conditions:

- Continuity of χ_{12}^p at $x = \pm s/2$:

$$C^s \cosh\left(\omega^s \frac{s}{2}\right) + D = C^h \cosh\left(\omega^h \frac{h}{2}\right). \tag{119}$$

- Continuity of the double traction, as given in Eq. (86), $m_{12} = -M_{13}$ at $x = \pm s/2$:

$$A^s \omega^s C^s \sinh\left(\omega^s \frac{s}{2}\right) = -A^h \omega^h C^h \sinh\left(\omega^h \frac{h}{2}\right). \tag{120}$$

- Periodicity of displacement component u_2. We have the constant stress component

$$\sigma_{12} = \mu(\bar{\gamma} - \gamma + u_{2,1}) \tag{121}$$

whose value is obtained from the plasticity criterion in the soft phase (Eq. 115):

$$\sigma_{12} = \tau_c + H\gamma_{cum} - A^s \chi_{12,11}^{ps}. \tag{122}$$

Still considering the first loading branch for which $\gamma_{cum} = \gamma$, it follows that

$$u_{2,1}^s = \frac{\sigma_{12}}{\mu} - \bar{\gamma} + \gamma = \frac{\tau_c}{\mu} - \bar{\gamma} + \frac{A^s \omega^{s2} C^s}{H} \cosh(\omega^s x) + \frac{H+\mu}{\mu} D \tag{123}$$

in the soft phase and

$$u_{2,1}^h = \frac{\sigma_{12}}{\mu} - \bar{\gamma} = \frac{\tau_c}{\mu} - \bar{\gamma} + \frac{H}{\mu} D \tag{124}$$

in the hard phase. The average on the whole structure,

$$\int_{-(s+h)/2}^{(s+h)/2} u_{2,1}\, dx = 0, \tag{125}$$

must vanish for periodicity reasons and gives

$$\left(\frac{\tau_c}{\mu} - \bar{\gamma}\right)(s+h) + \frac{2A^s \omega^s C^s}{H} \sinh\left(\omega^s \frac{s}{2}\right) + \frac{H(s+h) + \mu s}{\mu} D = 0 \tag{126}$$

The resolution of Eqs. (119), (120) and (126) gives

$$C^s = \left(\frac{\tau_c}{\mu} - \bar{\gamma}\right) \left[\frac{A^s \omega^s \sinh\left(\omega^s \frac{s}{2}\right)}{s+h} \right.$$

$$\left(\frac{H\,(s+h)+\mu s}{\mu} \left(\frac{\coth\left(\omega^s \dfrac{s}{2}\right)}{A^s\omega^s} + \frac{\coth\left(\omega^h \dfrac{h}{2}\right)}{A^h\omega^h} \right) - \frac{2}{H} \right)^{-1} \tag{127}$$

$$D = -A^s\omega^s C^s \sinh\left(\omega^s \frac{s}{2}\right) \left(\frac{\coth\left(\omega^s \dfrac{s}{2}\right)}{A^s\omega^s} + \frac{\coth\left(\omega^h \dfrac{h}{2}\right)}{A^h\omega^h} \right) \tag{128}$$

$$C^h = -C^s \frac{A^s\omega^s \sinh\left(\omega^s \dfrac{s}{2}\right)}{A^h\omega^h \sinh\left(\omega^h \dfrac{h}{2}\right)}. \tag{129}$$

Fig. 3 shows the profiles of plastic microdeformation and double traction in the two–phase laminate for different sets of material parameters and for a fraction of soft phase (s), $f_s = 0.7$. These profiles clearly show the continuity of χ^p_{12} and m_{12} at the interfaces. The different shapes presented are obtained for various values of the modulus A^s, the other material parameters being fixed and given in Table 1. Varying A^s modifies the mismatch with respect to the modulus A^h of the phase (h). Without mismatch the profile of χ^p_{12} is smooth at interfaces while stronger mismatches lead to sharper transitions between the phases. Varying A^s also changes the intrinsic length scale $1/\omega^s$ of the phase (s). When the intrinsic length scale is small compared to the size of the microstructure, the microdeformation gradient can develop inside the phase (s) which leads to a rounded profile of the plastic microdeformation χ^{ps}_{12} and to a double traction m_{12} localized at the interfaces. When the intrinsic length scale increases, the value of the double traction also increases at the interfaces (or equivalently, when decreasing the microstructure length scale, $l = s + h$, for a fixed intrinsic length scale). When the intrinsic length scale becomes of the order of the size of the microstructure or even larger, the model starts to saturate so that χ^{ps}_{12} becomes quasi–homogeneous (flat profile) and the double traction is not localized anymore (linear profile). χ^{ps}_{12} is affected by A^s in the same way as in (Cordero et al., 2010) where the hardening modulus, H, was not considered; in this latter case, the plastic microdeformation profile was parabolic, so that m_{12}, as a linear function of $\chi^{ps}_{12,1}$, always displayed a linear evolution in the phase (s), even for very small intrinsic length scales.

From Eq. (122) we derive the expression of the macroscopic stress tensor component, Σ_{12}, defined as the mean value of the stress component σ_{12} over

Table 1. Set of material parameters used in the simulations. The intrinsic length scales, defined as $1/\omega^{h,s}$, induced by these parameters is of the order of 10 nm for the elastic phase (h) and 500 nm for the plastic phase (s).

	μ [MPa]	τ_c [MPa]	H [MPa]	H_χ [MPa]	A [MPa.mm^2]
Phase (s)	35000	40	5000	500000	1.10^{-3}
Phase (h)	35000	-	-	500000	5.10^{-5}

the microstructure size, $l = (s + h)$:

$$\Sigma_{12} =< \sigma_{12} >= \frac{1}{l}\int_{-\frac{l}{2}}^{\frac{l}{2}} \sigma_{12}\, dx = \tau_c + \frac{H}{f_s}\langle\gamma^{cum}\rangle - \frac{A^s}{f_s}\langle\chi^{ps}_{12,11}\rangle, \tag{130}$$

where brackets <> denote the average values over the microstructure unit cell. We obtain the mean plastic slip for the first loading branch from Eq. (114):

$$\langle\gamma\rangle = \left\langle \chi^{ps}_{12} - \frac{A^s}{H^s_\chi}\chi^{ps}_{12,11}\right\rangle = \frac{2A^s\omega^s C^s \sinh\left(\omega^s\dfrac{f_s l}{2}\right)}{Hl} + f_s D \tag{131}$$

where f_s is the fraction of soft phase. From this we obtain alternative expressions of C^s and D as functions of $\langle\gamma\rangle$,

$$C^s = -\langle\gamma\rangle\left[A^s\omega^s \sinh\left(\omega^s\frac{f_s l}{2}\right)\right.$$
$$\left.\left(f_s\left(\frac{\coth\left(\omega^s\dfrac{f_s l}{2}\right)}{A^s\omega^s} + \frac{\coth\left(\omega^h\dfrac{(1-f_s)\,l}{2}\right)}{A^h\omega^h}\right) - \frac{2}{Hl}\right)\right]^{-1} \tag{132}$$

$$D = \langle\gamma\rangle\left[f_s - \frac{2}{Hl}\left(\frac{\coth\left(\omega^s\dfrac{f_s l}{2}\right)}{A^s\omega^s} + \frac{\coth\left(\omega^h\dfrac{(1-f_s)\,l}{2}\right)}{A^h\omega^h}\right)^{-1}\right]^{-1} \tag{133}$$

which contain contributions from both the back–stress and the isotropic hardening. The macroscopic stress takes the form:

$$\Sigma_{12} = \tau_c + HD. \tag{134}$$

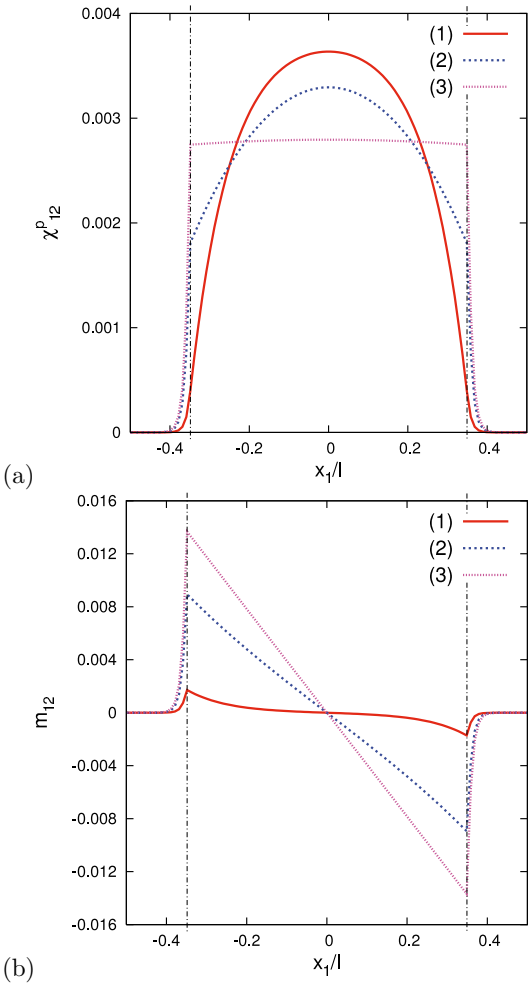

Figure 3. Profiles of (a) plastic microdeformation χ^p_{12} and (b) double traction m_{12} in the two–phase microstructure with the *microcurl* model at 0.2% overall plastic strain obtained with the set of material parameters given in Table 1 and: (1) with no mismatch between the moduli of the two phases, $A^h = A^s = 5.10^{-5}$ MPa.mm^2, (2) with a stronger mismatch, $A^h = 5.10^{-5}$ MPa.mm^2 and $A^s = 1.10^{-3}$ MPa.mm^2 and (3) $A^h = 5.10^{-5}$ MPa.mm^2 and $A^s = 5.10^{-2}$ MPa.mm^2. The associated intrinsic length scales, $1/\omega^s$, are respectively: 100 nm, 449 nm and 3.2 μm. In all three cases, the fraction of soft phase $f_s = 0.7$ and the microstructure size is fixed, $l = 1$ μm. The vertical lines indicate the position of interfaces.

The hardening produced by the model is a combination of the kinematic hardening arising from the higher order back–stress component and the linear isotropic hardening introduced in (115). Its modulus, H^{tot}, is size–dependent and is obtained using Eqs. (133) and (134):

$$H^{tot} = H\left[f_s - \frac{2}{Hl}\left(\frac{\coth\left(\omega^s \frac{f_s l}{2}\right)}{A^s\omega^s} + \frac{\coth\left(\omega^h \frac{(1-f_s)\,l}{2}\right)}{A^h\omega^h}\right)^{-1}\right]^{-1} \tag{135}$$

The macroscopic stress–strain curves shown in Fig. 4 illustrate the additional hardening predicted by the *microcurl* model in comparison to a conventional crystal plasticity theory. One cycle of deformation $\bar{\gamma}$ has been considered to illustrate the kinematic hardening effects. The first loading branch is described by the previous analytical solution, whereas the remaining of the loop has been computed numerically. In the absence of gradient effects (classical case, dashed line), only isotropic hardening is visible. The *microcurl* model leads to an additional kinematic hardening component. When the size of the elasto-plastic phase (s) becomes large compared to the intrinsic length scale $1/\omega_s$, strain gradient effect is small and the kinematic hardening arising from the *microcurl* model tends to vanish. Then the model reduces to conventional crystal plasticity theory and the limit of the 0.2% macroscopic flow stress is:

$$\lim_{l\to\infty} \Sigma_{12|0.2} = \tau_c + \frac{H}{f_s}\langle\gamma^{cum}\rangle. \tag{136}$$

In contrast, the maximum extra–stress, $\Delta\Sigma$, predicted by the model at small microstructure sizes can be computed as:

$$\Delta\Sigma = \lim_{l\to 0} \Sigma_{12}(<\gamma>) - \lim_{l\to\infty} \Sigma_{12|0.2} = \frac{1-f_s}{f_s} H_\chi \langle\gamma\rangle\,. \tag{137}$$

Fig. 5 presents the predicted evolution of the macroscopic flow stress $\Sigma_{12|0.2}$ at 0.2% plastic strain (obtained by setting $\langle\gamma\rangle = 0.002$) as a function of the microstructure length scale l in a log–log diagram. This evolution is plotted using the material parameters given in Table 1 and for various values of the coupling modulus, $H^s_\chi = H^h_\chi = H_\chi$. The four lower curves are obtained for finite values of the modulus H_χ, they exhibit a *tanh*–shape with saturation for large ($l > 10^{-2}$ mm) and small ($l < 10^{-5}$ mm) values of l. These saturations can be characterized by the limit given in Eq. (136) and the maximum extra–stress, $\Delta\Sigma$, given in Eq. (137) respectively. A transition

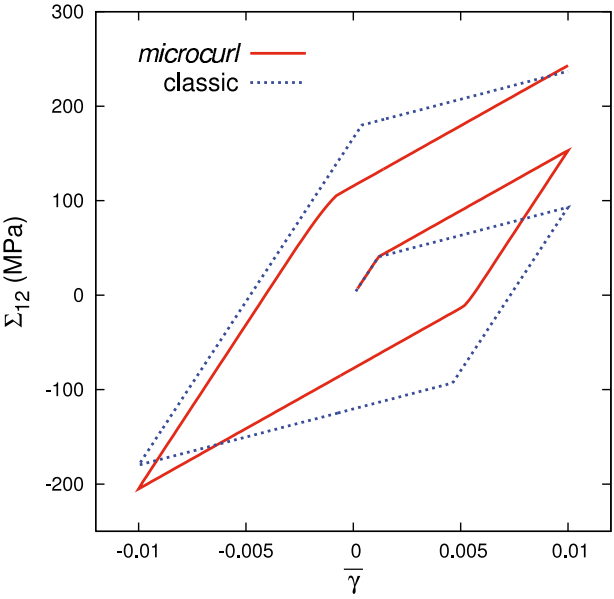

Figure 4. Macroscopic stress–strain response of the two–phase microstructure under cyclic shear loading conditions: comparison between the behaviour from a conventional crystal plasticity theory and the behaviour according to the *microcurl* model in which an additional kinematic hardening is predicted. Results obtained by finite element simulations for: $l = 1\mu$m, $f_s = 0.7$ and the material parameters given in Table 1.

domain with strong size dependence is observed between these two plateaus. The limits and the maximum extra–stress, the position of the transition zone and the scaling law exponent in the size dependent domain (slope in the log–log diagram) are directly related to the material parameters used in the model. In fact, the position of the size dependent domain is controlled by the moduli $A^{h,s}$ (not illustrated here) while the maximum extra–stress and the scaling law exponent are both controlled by the modulus H_χ, both increasing for higher values of H_χ as suggested by Fig. 5.
When H_χ is very small, we can deduce from Eq. (137) that $\Delta\Sigma$ vanishes and consequently the scaling law exponent will tend to 0. The upper curve is obtained for $H_\chi \to \infty$, it no longer exhibits a *tanh*–shape as no saturation occurs for small values of l, the limit $\Delta\Sigma \to \infty$ follows. This limit case will

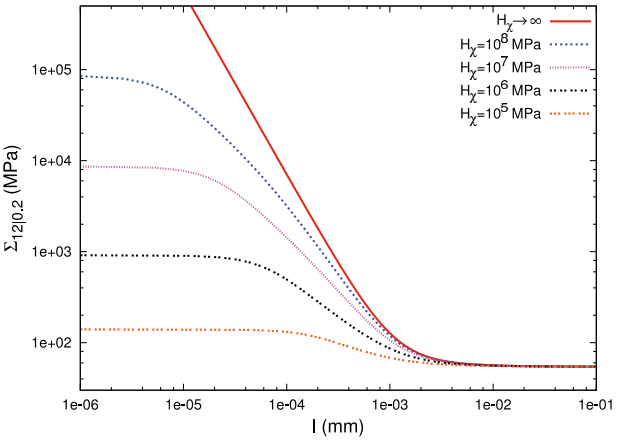

Figure 5. Evolution of the macroscopic flow stress $\Sigma_{12|0.2}$ at 0.2% plastic strain as a function of the microstructure length scale l, plotted for different coupling moduli H_χ ($= H^s_\chi = H^h_\chi$). The other material parameters are given in Table 1 and $f_s = 0.7$.

be described in next subsection, it will be shown that in that case a scaling law exponent of -2 is reached. Finally the *microcurl* model can produce scaling law exponents ranging from 0 to -2.

3.3 Strain gradient plasticity as a limit case

In the proposed *microcurl* model, the modulus H_χ introduces a coupling between micro and macro variables. A high value of H_χ forces the plastic microdeformation $\underset{\sim}{\boldsymbol{\chi}}^p$ to remain as close as possible to the macro plastic deformation $\underset{\sim}{\boldsymbol{H}}^p$. Consequently, it enforces the condition that $\underset{\sim}{\boldsymbol{K}}$ coincides with the dislocation density tensor. In this case, the *microcurl* model degenerates into the strain gradient plasticity model by (Gurtin, 2002). When applied to the laminate microstructure, the strain gradient plasticity model leads to the indeterminacy of the double traction vector at the interfaces, due to the fact that no strain gradient effect occurs in the elastic phase, see (Cordero et al., 2010). The *microcurl* model can then be used to derive the missing interface condition to be applied at the interface, by means of a limit process in the previous solution of the boundary value problem.
The limit $H_\chi \to \infty$ of the *microcurl* model can be used to determine the

value of the double traction to be imposed at the interface.

$$\begin{aligned}\lim_{H_\chi\to\infty} m_{12}(s/2) &= \lim_{H_\chi\to\infty} A^s\chi^{ps}_{12,1}(s/2)\\ &= \lim_{H_\chi\to\infty} A^s\omega^s \sinh\left(\omega^s\frac{f_s l}{2}\right) C^s\end{aligned}$$

$$= \lim_{H_\chi\to\infty}\langle\gamma\rangle\left[\frac{2}{Hl} - f_s\left(\frac{\coth\left(\omega^s\frac{f_s l}{2}\right)}{A^s\omega^s} + \frac{\coth\left(\omega^h\frac{(1-f_s)\,l}{2}\right)}{A^h\omega^h}\right)\right]^{-1}$$

Since $H_\chi \to \infty$, $1/\omega^h \to 0$ and $\coth\left(\omega^h h/2\right) \to 1$. Moreover, $\omega^s_\infty := \omega^s \to \sqrt{H/A^s}$. Consequently,

$$\lim_{H_\chi\to\infty} m_{12}(s/2) = \langle\gamma\rangle\left[\frac{2}{Hl} - f_s\frac{\coth\left(\omega^s_\infty\frac{f_s l}{2}\right)}{A^s\omega^s_\infty}\right]^{-1} \tag{138}$$

Accordingly, the double traction is found to depend on the mean plastic slip. The characteristic length in the soft phase for the strain gradient plasticity model is found to be related to the ratio between the hardening modulus and the higher order modulus, A^s.

The limiting process can also be used to predict the response of the strain gradient plasticity model in the size effect zone. For that purpose, let us consider the limit of $\Sigma_{12|0.2}$, when H_χ goes to infinity. Indeed, when H_χ tends to infinity, the expression of D in Eq. (133) can be simplified. We consider sizes of the microstructures in the size effect zone, i.e. intermediate values of l. Since H_χ is very high, the term $\tanh\left(\omega^h(1-f_s)l/2\right)$ tends to 1. Considering that l is small enough, the term $l\left(\tanh\left(\omega_s f_s l/2\right)\right)$ can be approximated by its Taylor expansion at the order 2, which leads to D of the form:

$$D \approx \frac{al+b}{cl^2+dl+e} \tag{139}$$

where

$$a = \frac{\langle\gamma\rangle f_s}{2\sqrt{H_\chi}}, \quad b = \langle\gamma\rangle f_s A^h\left(1+\frac{H}{H_\chi}\right) \tag{140}$$

$$c = -\frac{f_s^3 H\sqrt{A^h}}{12}, \quad d = \frac{f_s^2 H}{2\sqrt{H_\chi}}, \quad e = -\frac{f_s\sqrt{A^h}H}{H_\chi} \tag{141}$$

The terms a, d and e tend to 0 when $H_\chi \to \infty$, so that

$$D \approx \frac{12 A_s \langle \gamma \rangle}{f_s^3 H l^2} \tag{142}$$

and for the macroscopic stress:

$$\Sigma_{12} \approx \tau_c + \frac{12 A_s \langle \gamma \rangle}{f_s^3 l^2} \tag{143}$$

This expression is the same as that found in the absence of isotropic hardening in (Cordero et al., 2010). It indicates a l^{-2} scaling law for the strain gradient plasticity model. This scaling law differs from Hall–Petch relation, $l^{-1/2}$, typical for grain size effects, and from Orowan's law, l^{-1}, valid for precipitate size effects.

4 Continuum modelling of size effects in polycrystals

The model is now applied to simulate the response of polycrystals and the effects of grain size.

The interface conditions at grain boundaries play a major role in the simulated size effects in the polycrystal behaviour. No special interface law is considered in this work, although such physically motivated interface conditions exist in the literature, see (Gurtin and Anand, 2008). Instead we consider the canonical interface conditions that arise from the formulation of the balance equations of the *microcurl* continuum model. These conditions are the continuity of displacement, $\underline{\boldsymbol{u}}$, and the continuity of plastic micro–deformation, $\underset{\sim}{\boldsymbol{\chi}}^p$. These conditions also include the continuity of the simple and double tractions, $\underline{\boldsymbol{t}}$ and $\underset{\sim}{\boldsymbol{M}}$, described in Eq. (86). Continuity of displacement excludes grain boundary cracking and sliding. Continuity of plastic micro–deformation is reminiscent of the fact that dislocations generally do not cross grain boundaries, especially for such random grain boundaries. Note that in the *microcurl* model, only the kinematic degrees of freedom $\underset{\sim}{\boldsymbol{\chi}}^p$ are continuous. This is not the case of the plastic deformation, $\underset{\sim}{\boldsymbol{H}}^p$, which is treated here as an internal variable. However, due to the internal constraint discussed in section 3.1, $\underset{\sim}{\boldsymbol{H}}^p$ closely follows the plastic micro–deformation, so that it is quasi–continuous at grain boundaries when the penalty coefficient, H_χ, is high enough. Conversely, lower values of H_χ may allow slightly discontinuous plastic deformation, which may be tentatively interpreted as dislocation sinking inside grain boundaries. The continuity of the associated tractions expresses the transmission of classical and generalised internal forces from one grain to another through grain

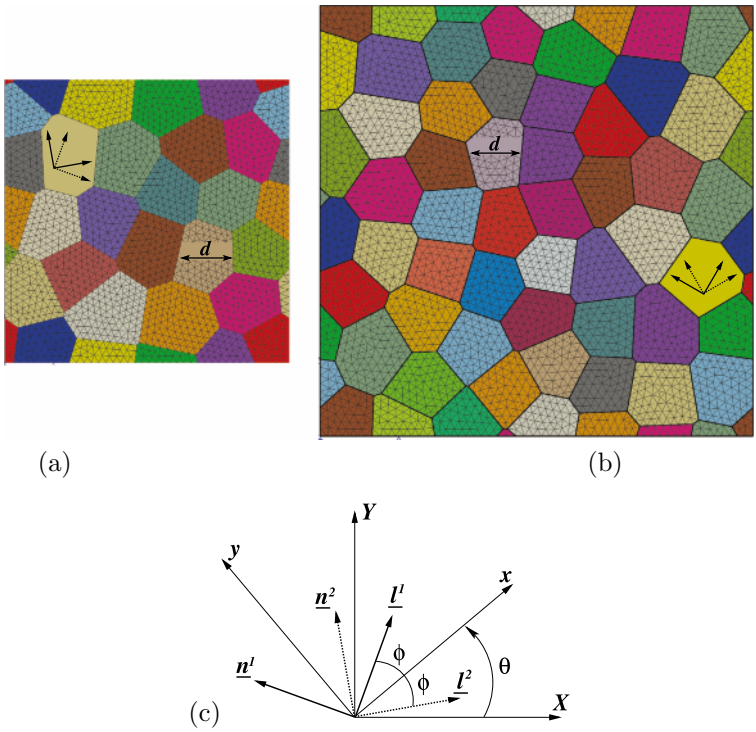

Figure 6. Periodic meshes of the 2D periodic aggregates used in the finite element simulations: (a) 24 grains, (b) 52 gains. Two slip systems are taken into account in each randomly oriented grain. Various mean grain sizes, d, ranging from tens of nanometers to hundreds of microns, are investigated. (c) Description of the two effective slip systems for 2D planar double slip.

boundaries. Such continuum models are then able to mimic in that way the development of dislocation pile–ups at grain boundaries (Forest and Sedláček, 2003).

4.1 Boundary value problem for polycrystals

The size effects exhibited by the solution of the boundary value problem are linked to an intrinsic length scale, l_s, introduced through the generalised

moduli H_χ and A of Eq. (110) and defined as:

$$l_s = \sqrt{\frac{A}{H_\chi}}. \tag{144}$$

This intrinsic length scale has to be consistent with the fact that plasticity effects occur at scales ranging from hundreds of nanometers to a few microns. In addition, as stated in section 3.1, the coupling modulus, H_χ, has to be chosen high enough to ensure that $\underset{\sim}{\boldsymbol{\chi}}^p$ and $\underset{\approx}{\boldsymbol{H}}^p$ are close. H_χ also determines the scaling law exponent. These requirements are guidelines for the choice of relevant generalised moduli H_χ and A. The sets of material parameters used in this paper are chosen in that way.

The finite element simulations have been made on periodic 2D meshes of periodic polycrystalline aggregates generated by a method based on Voronoi tessellations (Fig. 6(a)(b)). The integration order of elements is quadratic. The Voronoi polyhedra represent the grains, the random distribution of their centers has been controlled so that their sizes are sensibly the same, that is why we can reasonably assume that the mean grain size, d, is sufficient to characterise the microstructure of our aggregates. A random orientation is assigned to each grain and two slip systems are taken into account. In 2D, the plastic behaviour of f.c.c. crystals can be simulated with 2D planar double slip by considering two effective slip systems separated by an angle of 2ϕ (Asaro, 1983; Bennett and McDowell, 2003). Figure 6(c) describes the geometry. The slip system pair is oriented by the angle θ which is the grain orientation randomly fixed for each grain. For a f.c.c. crystal $\phi = 35.1°$, it corresponds to the orientation of the close–packed planes in the crystal lattice of the grain.

Periodic homogenization for generalised continua is used to predict the effective response of the polycrystal. The displacement field is assumed to be of the form

$$\underline{\boldsymbol{u}}\,(x) = \underset{\sim}{\boldsymbol{E}}.\underline{\boldsymbol{x}} + \underline{\boldsymbol{v}}\,(x), \tag{145}$$

with the fluctuation $\underline{\boldsymbol{v}}$ periodic, meaning that it takes identical values at homologous points of the unit cell (Forest et al., 2001). The plastic micro–deformation field, $\underset{\sim}{\boldsymbol{\chi}}^p$, is assumed to be periodic, meaning that no rotational macroscopic plastic deformation is imposed to the unit cell. Its components are equal at homologous opposite nodes. According to periodic homogenization, the simple and double tractions $\underline{\boldsymbol{t}}$ and $\underset{\sim}{\boldsymbol{m}}$ are anti–periodic at homologous points of the unit cell.

Polycrystals are random materials so that the periodicity constraint may lead to a bias in the estimation of the effective properties. This boundary

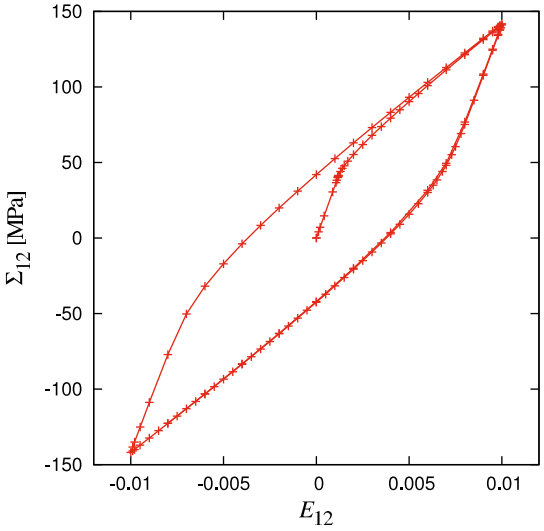

Figure 7. Macroscopic stress–strain response of the 24–grain aggregate under cyclic simple shear loading conditions with a mean gain size $d \approx 0.2\mu$m. The set of material parameters used is labelled (c) in Table 2.

effect can be alleviated by considering several realization of the microstructure and performing ensemble averaging (Zeghadi et al., 2007).

4.2 Overall cyclic response of a polycrystalline aggregate

The finite element simulations of the boundary value problem presented previously have been conducted under generalised plane strain conditions on aggregates with a relatively small number of grains. The aim here is not to obtain a representative response but to catch the grain size effects and to explore qualitatively the impact of different sets of material parameters. In this section, a virtual material is considered with various intrinsic length scales. The macroscopic stress–strain curve shown in Fig. 7 is obtained by applying a cyclic simple shear loading controlled by the average stress component E_{12} on the aggregate of 24 grains with $d = 0.2\mu$m and the set of material parameters labelled (c) in Table 2. The mean stress component Σ_{12} is then computed:

$$\Sigma_{12} = \frac{1}{V}\int_V \sigma_{12}\, dV, \quad E_{12} = \frac{1}{V}\int_V \varepsilon_{12}\, dV, \tag{146}$$

Table 2. Sets of material parameters used in the 24–grain aggregate case (Fig 6(a)). The intrinsic length scale, $l_s = \sqrt{A/H_\chi}$, is given for each set.

Set	μ [MPa]	τ_c [MPa]	H_χ [MPa]	A [MPa mm^2]	l_s [μm]
a	35000	40	$3.0\,10^6$	$1.0\,10^{-2}$	$5.8\,10^{-2}$
b	35000	40	$1.0\,10^6$	$1.0\,10^{-2}$	$1.0\,10^{-1}$
c	35000	40	$3.5\,10^5$	$1.0\,10^{-2}$	$1.7\,10^{-1}$
d	35000	40	$8.8\,10^4$	$1.0\,10^{-3}$	$1.1\,10^{-1}$

where V denotes each polycrystal unit cell. The simulated response illustrates the kinematic hardening produced by the *microcurl* model. The stress–strain curves obtained in the next case (see Fig. 9) show that this kinematic hardening is size dependent: it increases for smaller grains. Note that the observed overall kinematic hardening has two distinct sources: the intragranular back–stress induced by plastic strain gradients, and the intergranular internal stress that originate from the grain to grain plastic strain incompatibilities. The latter contribution is also predicted by classical crystal plasticity models.

Figure 8 presents the effect of the mean grain size, d, on the macroscopic flow stress at 1% plastic strain in the 24–grain aggregate in a log–log diagram for different intrinsic length scales, l_s, introduced through the sets of material parameters (labelled a, b, c and d) given in Table 2. The curves exhibit two plateaus for large ($d > 20\mu$m) and small ($d < 0.1\mu$m) mean grain sizes with a transition domain in between. This *tanh*–shape indicates that when d is large compared to the intrinsic length scale, l_s, strain gradient effects are small and the kinematic hardening arising from the *microcurl* model vanishes. The model saturates when d is of the order of l_s or smaller. The transition domain exhibits a strong size dependence, the polycrystalline aggregate becoming harder for decreasing grain sizes. The position of the transition zone, the maximum extra–stress (the distance between the two plateaus) and the scaling law exponent, m, in the size dependent domain are controlled by the material parameters used in the model. The two latter effects are controlled by the coupling modulus, H_χ, they both increase for higher values of H_χ as shown in Fig. 8. The scaling exponent is defined as the slope in the log–log diagram in the inflection domain, reflecting the scaling law:

$$\Sigma_{12} \propto d^m. \tag{147}$$

It is obtained with the sets of material parameters given in Table 2. The found values range from -0.26 to -0.64 including the well–known Hall–

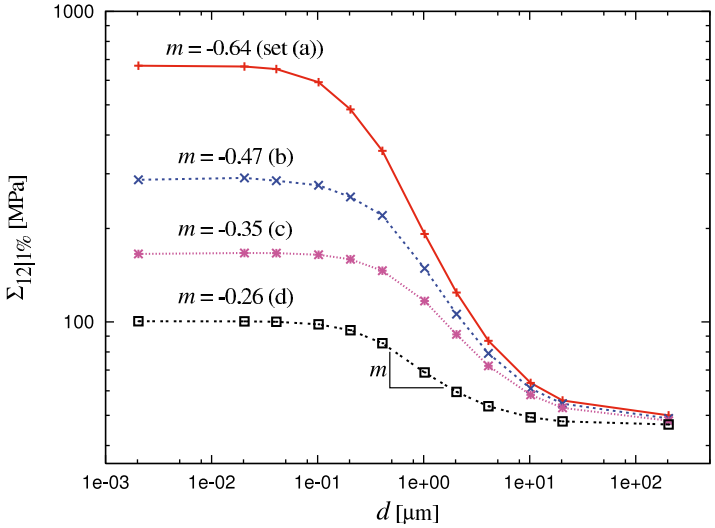

Figure 8. Effect of the mean grain size, d, on the macroscopic flow stress, $\Sigma_{12|1\%}$, at 1% plastic strain. The results are obtained for the 24–grain aggregate using the different sets of material parameters given in Table 2. The scaling law exponent, m, is identified in each case.

Petch exponent $m = -0.5$. In fact it was shown in (Cordero et al., 2010) that values of m ranging from 0 to -2 can be simulated with the *microcurl* model in the case of two–phase microstructures. In each case, these values are obtained without classical isotropic hardening, meaning that the linear kinematic hardening produced by the model is able to reproduce a wide range of scaling laws. Note that conventional strain gradient plasticity models do not lead to *tanh*–shape curves but rather to unbounded stress increase for vanishingly small microstructures (Cordero et al., 2010).

4.3 Grain size effects in idealised aluminium polycrystals

Similar finite element simulations have been performed on idealised aluminium aggregates of 52 grains shown in Fig. 6(b). An additional isotropic hardening component is added as in (Méric et al., 1991) to obtain a more realistic response of large aluminium grains. The size–independent hardening

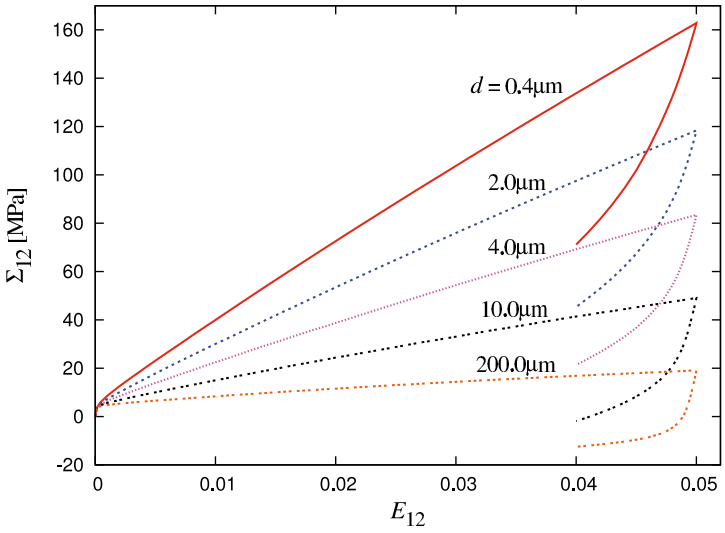

Figure 9. Macroscopic stress–strain response of the 52–grain aggregate under simple shear for various mean grain sizes, d. The set of material parameters used is labelled (g) in Table 3.

law reads:

$$R^\alpha = \tau_c + Q \sum_\beta^n h^{\alpha\beta} \left(1 - \exp\left(-b\,\gamma^\beta_{\rm cum}\right)\right), \tag{148}$$

where n is the number of slip systems (here $n = 2$), Q and b are material coefficients defining non–linear isotropic hardening, $h^{\alpha\beta}$ is the interaction matrix and $\gamma^\beta_{\rm cum}$ is the accumulated micro–plastic slip on the slip system β. Cumulative plastic slip results from the integration of the differential equation $\dot\gamma^\beta_{\rm cum} = |\dot\gamma^\beta|$. The material parameters used in these simulations are given in Table 3. The macroscopic stress–strain curves presented in Fig. 9 are obtained by applying a simple shear loading controlled by the average strain component E_{12} on the 52–grain aggregate with various mean grain sizes, d, taken in the size dependent domain. The chosen set of material parameters has the label (g) in Table 3. These parameters are such that an acceptable description of aluminium polycrystals is obtained for large grains and that a Hall–Petch–like behaviour is found in a plausible range of grain sizes. However we did not attempt to calibrate the amplitude of the extra–hardening so that simulation predictions remain qualitative. The

Table 3. Sets of material parameters used in the 52–grain aggregate case (Fig 6(b)).

Set	μ [MPa]	τ_c [MPa]	Q [MPa]	b	$h^{\alpha\alpha}$	$h^{\alpha\beta,\,\alpha\neq\beta}$
e	27000	0.75	7.9	10.2	1	4.4
f	27000	0.75	7.9	10.2	1	4.4
g	27000	0.75	7.9	10.2	1	4.4

Set	H_χ [MPa]	A [MPa mm^2]	l_s [μm]
e	$1.0\,10^6$	$1.0\,10^{-2}$	$1.0\,10^{-1}$
f	$3.5\,10^5$	$1.0\,10^{-2}$	$1.7\,10^{-1}$
g	$5.0\,10^4$	$1.0\,10^{-2}$	$4.5\,10^{-1}$

curves of Fig. 9 show again that the kinematic hardening produced by the model is strongly size dependent. The evolution of the macroscopic flow stress at 1% plastic strain in the 52–grain aggregate is shown in Fig. 10 in the same way as it was done in Fig. 8. The set of material parameters (g) of Table 3 gives the ideal Hall–Petch scaling law exponent $m = -0.5$.

An important output of the simulations is the dependence of the stress and strain fields in the grains of the polycrystal on grain size. Figures 11 and 12 show the contour plots of the field of accumulated plastic slip, computed as

$$\dot{p} = \sqrt{\frac{2}{3}\underset{\sim}{\dot{\varepsilon}}^p : \underset{\sim}{\dot{\varepsilon}}^p}, \tag{149}$$

where $\underset{\sim}{\varepsilon}^p$ is the symmetric part of the plastic deformation, $\underset{\sim}{\boldsymbol{H}}^p$, and the contour plots of the norm Γ of the dislocation density tensor,

$$\Gamma = \sqrt{\underset{\sim}{\boldsymbol{\Gamma}} : \underset{\sim}{\boldsymbol{\Gamma}}}, \tag{150}$$

respectively. The considered grain sizes are taken in the size dependent domain where the evolution of the fields is assumed to be physically relevant. The chosen set of material parameters has the label (g) in Table 3, it corresponds to an intrinsic length scale $l_s = 0.45\mu$m and gives a scaling law exponent $m = -0.5$. The mean value of the accumulated plastic slip is the same in every case, only its distribution varies with the size of the microstructure as shown in Fig. 11.

The first contour plot of each figure is obtained for $d = 200\mu\text{m} \gg l_s = 0.45\mu$m, at the very beginning of the size–dependent behaviour domain according to Fig. 10. At this size, the simulated fields show that p is quite inhomogeneous and that some deformation bands appear; Γ is localised at

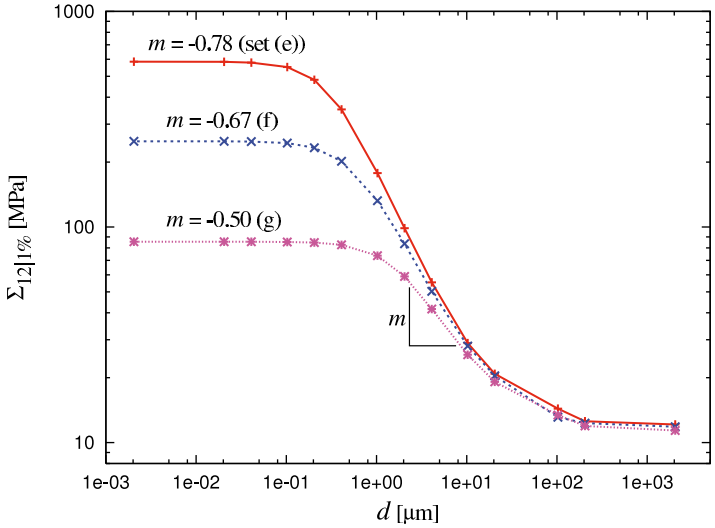

Figure 10. Effect of the mean grain size, d, on the macroscopic flow stress, $\Sigma_{12|1\%}$, at 1% plastic strain. The results are obtained for the 52–grain aggregate using the different sets of material parameters given in Table 3. The scaling law exponent, m, is identified in each case.

the grain boundaries and almost vanishes in the grain cores. The contour plots obtained for $2\mu\text{m} < d < 20\mu\text{m}$ show a significant evolution of both fields. One observes the progressive building of a network of strain localization bands. These bands are slip bands as they are parallel to the slip plane directions represented on the 1μm contour plot of Fig. 11. They compensate the larger blue zones where plastic strain cannot develop due to the higher energy cost associated with its gradient. Plastic strain becomes stronger inside the localization bands. This is due to the fact that the contour plots are given for fixed mean value of p, which implies that the applied total strain is higher for small grain sizes as suggested by Fig. 9. The field of the norm of the dislocation density tensor is still high close to grain boundaries and spreads over the grain cores. The last contour plot of each figure is obtained for $d = 1\mu$m, a size close to l_s. Here the model starts to saturate, which can be seen from the simulated fields. The field of p does not evolve anymore and Γ decreases. In fact, as l_s controls the strain gradient effects, strong strain gradients cannot develop because they become energetically too expensive when the microstructure size is too small.

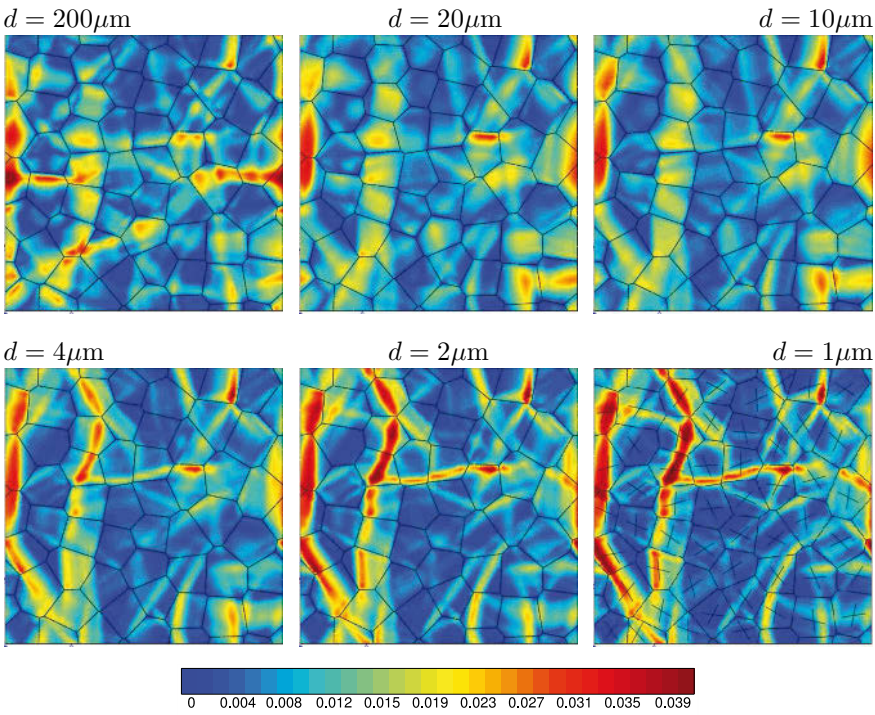

Figure 11. Grain size effect on the accumulated plastic slip. These contour plots are obtained with the 52–grain aggregate for the same mean value of $p = 0.01$. The set of material parameters (g) of Table 3 is used. The pairs of slip plane directions are represented for each grain on the 1μm contour plot.

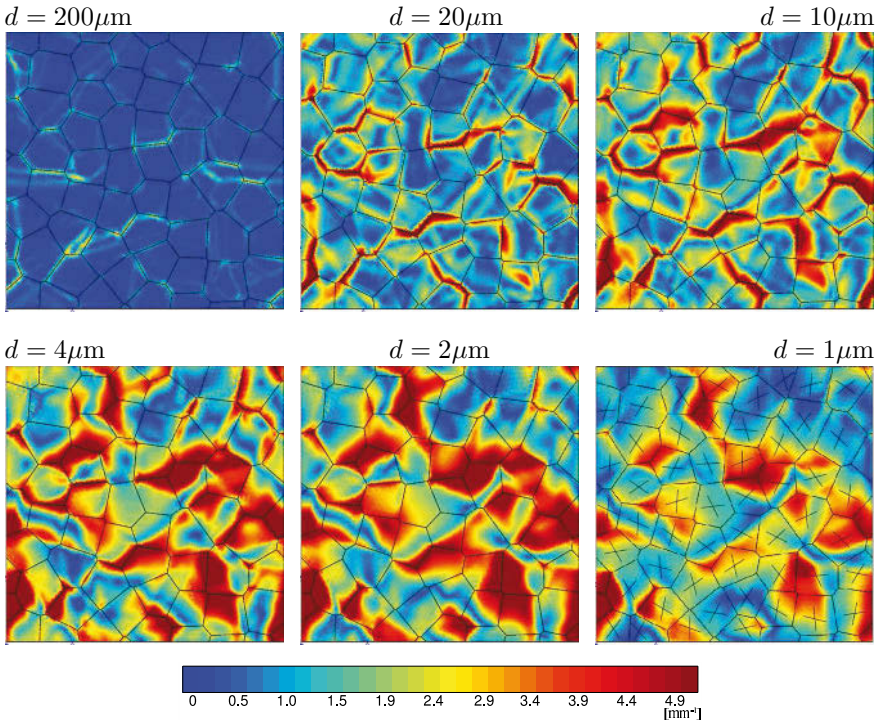

Figure 12. Grain size effect on the norm of the dislocation density tensor. These contour plots are obtained with the 52–grain aggregate for the same mean value of $p = 0.01$. The set of material parameters (g) of Table 3 is used. The pairs of slip plane directions are represented for each grain on the 1μm contour plot.

5 Micromorphic approach vs. phase field models

There are strong links between generalized continuum mechanics and phase field models which are striving in modern field theories of materials. Mindlin's and Casal's second gradient model of mechanics and the Cahn–Hilliard diffusion theory were developed almost simultaneously. More generally, the necessity of introducing additional degrees of freedom in continuum models arose in the 1960s in order to account for microstructure effects on the overall material's response. However, generalized continuum mechanics, with paradigms like Eringen's micromorphic model and Aifantis strain gradient plasticity, developed along an independent track from phase field approach embodied by Khachaturyan's views, for instance.

The links have been seen recently within the context of plasticity and damage mechanics. The computational mechanics community aimed at introducing the evolution of microstructures into their simulations (Ubachs et al., 2004; Ammar et al., 2009a) whereas physicists started introducing plasticity into the thermodynamical setting (Gaubert et al., 2008). Cooperation between these communities becomes necessary when tackling damage mechanics and crack propagation simulation (Aslan and Forest, 2009; Miehe et al., 2010a). First attempts to present a general constitutive framework encompassing classical enhanced mechanical and thermodynamical models have been proposed recently (Forest, 2009; Aslan and Forest, 2011; Miehe, 2011). Such an approach is presented in this chapter and extended to sophisticated descriptions of interactions between viscoplasticity and phase transformations.

The micromorphic model originates from Eringen's introduction of microdeformation tensor at each material point that accounts for the changes of a triad of microstructure vectors. In the present chapter, the micromorphic approach denotes an extension of this theory to other variables than total deformation, namely plastic strain, hardening variables, and even temperature and concentration. The gist of the micromorphic model is to associate a microstructure quantity (e.g. microdeformation) to an overall quantity (e.g. macroscopic deformation). The deviation of the microvariable from the macrovariable and the gradient of the microvariable are sources of stored energy and dissipation. They are controlled by generalized stresses which contribute to the power of internal forces.

On the other hand, the phase field approach has proved to be an efficient method to model the motion of interfaces and growth of precipitates based on a sound thermodynamical formulation including non convex free energy potentials (Finel et al., 2010). The effect of microelasticity on the morphological aspects and kinetics of phase transformation is classically studied but

the occurrence of plasticity is recent (Ubachs et al., 2004; Gaubert et al., 2008, 2010). Beyond plasticity, damage and crack propagation are the subject of both generalized continuum and phase field approaches (Frémond and Nedjar, 1996; Ubachs et al., 2007; Aslan and Forest, 2009; Miehe et al., 2010a,b). Phase field simulations usually rely on finite differences or fast Fourier methods. More recently, the finite element method was also used in order to tackle more general boundary conditions (Ammar et al., 2009a; Miehe et al., 2010a; Rajagopal et al., 2010).

The objective of the present chapter is to formulate a thermomechanical theory of continua with additional degrees of freedom. It is shown in a first part that the theory encompasses available generalized continuum theories and phase field models provided that well–suited free energy and dissipation potentials are selected. The current strain gradient plasticity models are then extended to account simultaneously for plastic strain gradient and plastic strain rate gradient in order to address viscoplastic instabilities occurring in metal plasticity like dynamic strain ageing. The second part of the work exposes how the well–known elastoviscoplastic constitutive framework can be incorporated into the available phase field approach in order to investigate the coupling between viscoplasticity and phase transformation. An original approach is proposed that resorts to standard homogenization techniques used in the mechanics of heterogeneous materials.

5.1 Thermomechanics with additional degrees of freedom

General setting. The displacement variables of mechanics can be complemented by additional degrees of freedom (dof), ϕ, that can be scalars as well as tensor variables of given rank:

$$DOF = \{\underline{\boldsymbol{u}}\,, \quad \phi\}, \tag{151}$$

A first gradient theory is built on the basis of this set of degrees of freedom :

$$STRAIN = \{\underline{\underline{\boldsymbol{\varepsilon}}}, \quad \phi, \quad \boldsymbol{\nabla}\phi\} \tag{152}$$

The strain tensor, $\underline{\underline{\boldsymbol{\varepsilon}}}$, is the symmetric part of the gradient of the displacement field. The main assumption of the proposed theory is that the gradient of the additional degrees of freedom contribute to the work of internal forces in the energy equation, in contrast to internal variables and concentration in diffusion theory. Depending on the invariance properties of the variable ϕ, it can itself contribute to the work of internal forces together with its gradient. It is not the case for the displacement itself which is not an objective vector. The virtual power of internal forces is then extended to the

virtual power done by the additional variable and its first gradient:

$$\mathcal{P}^{(i)}(\underline{\dot{\boldsymbol{u}}}^{\star},\dot{\phi}^{\star}) = -\int_{\mathcal{D}} p^{(i)}(\underline{\dot{\boldsymbol{u}}}^{\star},\dot{\phi}^{\star})\,dV$$

$$p^{(i)}(\underline{\dot{\boldsymbol{u}}}^{\star},\dot{\phi}^{\star}) = \underset{\sim}{\boldsymbol{\sigma}} : \boldsymbol{\nabla}\underline{\dot{\boldsymbol{u}}}^{\star} + a\dot{\phi}^{\star} + \underline{\boldsymbol{b}}.\boldsymbol{\nabla}\dot{\phi}^{\star} \tag{153}$$

where $\mathcal{D}$ is a subdomain of the current configuration Ω of the body. Stars denote virtual fields. The Cauchy stress tensor is $\underset{\sim}{\boldsymbol{\sigma}}$ and a and $\underline{\boldsymbol{b}}$ are generalized stresses associated with the additional dof and its first gradient, respectively. Similarly, the power of contact forces must be extended as follows:

$$\mathcal{P}^{(c)}(\underline{\dot{\boldsymbol{u}}}^{\star},\dot{\phi}^{\star}) = \int_{\mathcal{D}} p^{(c)}(\underline{\dot{\boldsymbol{u}}}^{\star},\dot{\phi}^{\star})\,dV, \quad p^{(c)}(\underline{\dot{\boldsymbol{u}}}^{\star},\dot{\phi}^{\star}) = \underline{\boldsymbol{t}}.\underline{\dot{\boldsymbol{u}}}^{\star} + a^{c}\ \dot{\phi}^{\star} \tag{154}$$

where $\underline{\boldsymbol{t}}$ is the traction vector and a^c a generalized traction. In general, the power of forces acting at a distance must also be extended in the form:

$$\mathcal{P}^{(e)}(\underline{\dot{\boldsymbol{u}}}^{\star},\dot{\phi}^{\star}) = \int_{\mathcal{D}} p^{(e)}(\underline{\dot{\boldsymbol{u}}}^{\star},\dot{\phi}^{\star})\,dV, \quad p^{(e)}(\underline{\dot{\boldsymbol{u}}}^{\star},\dot{\phi}^{\star}) = \rho\underline{\boldsymbol{f}}.\underline{\dot{\boldsymbol{u}}}^{\star} + a^{e}\dot{\phi}^{\star} + \underline{\boldsymbol{b}}^{e}.\boldsymbol{\nabla}\dot{\phi}^{\star} \tag{155}$$

where $\rho\underline{\boldsymbol{f}}$ accounts for given simple body forces and a^e for generalized volume forces. The power of inertial forces also requires, for the sake of generality, the introduction of an inertia I associated with the acceleration of the additional degrees of freedom :

$$\mathcal{P}^{(a)}(\underline{\dot{\boldsymbol{u}}}^{\star},\dot{\phi}^{\star}) = \int_{\mathcal{D}} p^{(a)}(\underline{\dot{\boldsymbol{u}}}^{\star},\dot{\phi}^{\star})\,dV, \quad p^{(a)}(\underline{\dot{\boldsymbol{u}}}^{\star},\dot{\phi}^{\star}) = -\rho\underline{\ddot{\boldsymbol{u}}}.\underline{\dot{\boldsymbol{u}}}^{\star} - I\ddot{\phi}\,\dot{\phi}^{\star} \tag{156}$$

Following (Germain, 1973a), given body couples and double forces working with the gradient of the velocity field, could also be introduced in the theory. The generalized principle of virtual power with respect to the velocity and additional dof, is formulated as

$$\mathcal{P}^{(i)}(\underline{\dot{\boldsymbol{u}}}^{\star},\dot{\phi}^{\star}) + \mathcal{P}^{(e)}(\underline{\dot{\boldsymbol{u}}}^{\star},\dot{\phi}^{\star}) + \mathcal{P}^{(c)}(\underline{\dot{\boldsymbol{u}}}^{\star},\dot{\phi}^{\star}) + \mathcal{P}^{(a)}(\underline{\dot{\boldsymbol{u}}}^{\star},\dot{\phi}^{\star}) = 0,\ \forall\mathcal{D}\subset\Omega, \forall\underline{\dot{\boldsymbol{u}}}^{\star},\dot{\phi} \tag{157}$$

The method of virtual power according to (Maugin, 1980) is used then to derive the standard local balance of momentum equation:

$$\operatorname{div}\underset{\sim}{\boldsymbol{\sigma}} + \rho\underline{\boldsymbol{f}} = \rho\underline{\ddot{\boldsymbol{u}}}, \quad \forall\underline{\boldsymbol{x}}\in\Omega \tag{158}$$

and the generalized balance of micromorphic momentum equation:

$$\operatorname{div}(\underline{\boldsymbol{b}} - \underline{\boldsymbol{b}}^{e}) - a + a^{e} = I\ddot{\phi}, \quad \forall\underline{\boldsymbol{x}}\in\Omega \tag{159}$$

The method also delivers the associated boundary conditions for the simple and generalized tractions:

$$\underline{\boldsymbol{t}} = \underset{\sim}{\boldsymbol{\sigma}}.\underline{\boldsymbol{n}}, \quad a^c = (\underline{\boldsymbol{b}} - \underline{\boldsymbol{b}}^e).\underline{\boldsymbol{n}}, \quad \forall \underline{\boldsymbol{x}} \in \partial\mathcal{D} \tag{160}$$

The local balance of energy is also enhanced by the generalized power already included in the power of internal forces (153):

$$\rho\dot{\epsilon} = p^{(i)} - \operatorname{div} \underline{\boldsymbol{q}} + \rho r \tag{161}$$

where ϵ is the specific internal energy, $\underline{\boldsymbol{q}}$ the heat flux vector and r denotes external heat sources. The entropy principle takes the usual local form:

$$-\rho(\dot{\psi} + \eta\dot{T}) + p^{(i)} - \frac{\underline{\boldsymbol{q}}}{T}.\boldsymbol{\nabla} T \geq 0 \tag{162}$$

where it is assumed that the entropy production vector is still equal to the heat vector divided by temperature, as in classical thermomechanics. Again, the enhancement of the theory goes through the enriched power density of internal forces (153). The entropy principle is exploited according to classical continuum thermodynamics to derive the state laws. At this stage it is necessary to be more specific on the dependence of the state functions $\psi, \eta, \underset{\sim}{\boldsymbol{\sigma}}, a, \underline{\boldsymbol{b}}$ on state variables and to distinguish between dissipative and non–dissipative mechanisms. The introduction of dissipative mechanisms may require an increase in the number of state variables. These different situations are considered in the following subsections.

Micromorphic model as a special case. The micromorphic model as initially proposed by Eringen (Eringen and Suhubi, 1964) and Mindlin (Mindlin, 1964) amounts to introducing a generally non compatible microdeformation field:

$$\phi \equiv \underset{\sim}{\boldsymbol{\chi}}$$

where $\underset{\sim}{\boldsymbol{\chi}}$ is a generally non–symmetric second order tensor defined at each material point. When the microdeformation reduces to its skew symmetric part, the Cosserat model is retrieved (Ehlers and Volk, 1998; Forest and Sievert, 2006). The microdeformation is to be compared to the deformation gradient:

$$\underset{\sim}{\boldsymbol{e}} = \underline{\boldsymbol{u}} \otimes \boldsymbol{\nabla} - \underset{\sim}{\boldsymbol{\chi}} \tag{163}$$

If the internal constraint $\underset{\sim}{\boldsymbol{e}} \equiv 0$ is enforced, the microdeformation coincides with the deformation and the micromorphic model reduces to Mindlin's second gradient theory. The free energy density depends of the following state variables:

$$STATE = \{\underset{\sim}{\boldsymbol{\varepsilon}}, \quad \underset{\sim}{\boldsymbol{e}}, \quad \underset{\approx}{\boldsymbol{K}} := \underset{\sim}{\boldsymbol{\chi}} \otimes \boldsymbol{\nabla}, \quad T, \quad \alpha\}$$

where α denotes the set of internal variables required to represent dissipative mechanical phenomena. The Clausius–Duhem inequality (162) becomes, in the isothermal case,

$$(\underset{\sim}{\boldsymbol{\sigma}} - \rho\frac{\partial\psi}{\partial\underset{\sim}{\boldsymbol{\varepsilon}}}) : \dot{\underset{\sim}{\boldsymbol{\varepsilon}}} + (\underset{\sim}{\boldsymbol{a}} - \rho\frac{\partial\psi}{\partial\underset{\sim}{\boldsymbol{e}}}) : \dot{\underset{\sim}{\boldsymbol{e}}} + (\underline{\underline{\boldsymbol{b}}} - \rho\frac{\partial\psi}{\partial\underline{\underline{\boldsymbol{K}}}}) \dot{:} \dot{\underline{\underline{\boldsymbol{K}}}} - (\rho\eta + \rho\frac{\partial\psi}{\partial T})\dot{T} - \rho\frac{\partial\psi}{\partial T}\dot{\alpha} \geq 0 \tag{164}$$

where $\underset{\sim}{\boldsymbol{a}}$ was taken as the stress conjugate to the relative deformation rate $\dot{\underset{\sim}{\boldsymbol{e}}}$ in the power of internal forces, which corresponds to an alternative form for (153). The state laws for micromorphic media are obtained by assuming that the first four contribution are non–dissipative:

$$\underset{\sim}{\boldsymbol{\sigma}} = \rho\frac{\partial\psi}{\partial\underset{\sim}{\boldsymbol{\varepsilon}}}, \quad \underset{\sim}{\boldsymbol{a}} = \rho\frac{\partial\psi}{\partial\underset{\sim}{\boldsymbol{e}}}, \quad \underline{\underline{\boldsymbol{b}}} = \rho\frac{\partial\psi}{\partial\underline{\underline{\boldsymbol{K}}}}, \quad \eta = -\frac{\partial\psi}{\partial T} \tag{165}$$

Elastoviscoplastic micromorphic media are then obtained by a specific choice of the internal variables α and their evolution rules (Forest and Sievert, 2006).

Phase field model as a special case. Enhancing the mechanical power in the energy balance is plausible in the presence of microstructure induced mechanical phenomena, as proposed by Eringen. However, this is also possible in other contexts, namely when the dof ϕ has a more general meaning of an order parameter. Fried and Gurtin (Fried and Gurtin, 1993; Gurtin, 1996) suggested to consider the following reduced state space:

$$STATE = \{\underset{\sim}{\boldsymbol{\varepsilon}}, \quad \phi, \quad \boldsymbol{\nabla}\phi, \quad T, \quad \alpha\} \tag{166}$$

and the following state laws

$$\underset{\sim}{\boldsymbol{\sigma}} = \rho\frac{\partial\psi}{\partial\underset{\sim}{\boldsymbol{\varepsilon}}}, \quad \underline{\boldsymbol{b}} = \rho\frac{\partial\psi}{\partial\boldsymbol{\nabla}\phi}, \quad \eta = -\frac{\partial\psi}{\partial T} \tag{167}$$

so that, in the isothermal case, the dissipation rate reduces to

$$a^v\dot{\phi} + X\dot{\alpha} \geq 0, \quad \text{with} \quad a^v = a - \rho\frac{\partial\psi}{\partial\phi}, \quad X = -\rho\frac{\partial\psi}{\partial\alpha} \tag{168}$$

The choice of a convex potential $\Omega(a^v, X)$ providing the evolution laws:

$$\dot{\phi} = \frac{\partial\Omega}{\partial a^v}, \quad \dot{\alpha} = \frac{\partial\Omega}{\partial X} \tag{169}$$

ensures the positivity of the dissipation rate.
As an illustration, let us consider a quadratic contribution of a^v to the

dissipation potential. We are lead to the following relationships

$$\dot{\phi} = \frac{1}{\beta} a^v = \frac{1}{\beta}(a - \rho \frac{\partial \psi}{\partial \phi}) \tag{170}$$

where β is a material parameter. The latter equation can be combined with the balance law (159), in the absence of volume or inertial forces, and the state law (167) to derive

$$\beta \dot{\phi} = \mathrm{div}\left(\rho \frac{\partial \psi}{\partial \boldsymbol{\nabla} \phi}\right) - \rho \frac{\partial \psi}{\partial \phi} \tag{171}$$

which corresponds to a general Ginzburg-Landau equation.
The authors in (Ubachs et al., 2004) have combined the micromorphic approach and the Cahn–Hilliard approach to diffusion in order to derive an alternative equation to Cahn–Hilliard.

5.2 Constitutive framework for gradient and micromorphic viscoplasticity

We now exploit the established general structure to propose a constitutive framework for elastoviscoplastic materials exhibiting plastic strain gradient. The attention is focused on an isotropic elastoviscoplastic medium characterized by the cumulated plastic strain, p. The proposed formulation encompasses Aifantis–like strain gradient plasticity models and introduces additional strain rate gradient effects. The total strain is split into its elastic and plastic parts: $\underset{\sim}{\boldsymbol{\varepsilon}} = \underset{\sim}{\boldsymbol{\varepsilon}}^e + \underset{\sim}{\boldsymbol{\varepsilon}}^p$. In this context, the additional dof ϕ has the meaning of a microplastic strain (Forest and Aifantis, 2010) to be compared with p itself.

Two variants of the constitutive framework are considered which handle in a slightly different way the dissipative contribution due to the generalized stresses.

Introduction of viscous generalized stresses The free energy density is assumed to depend on the following state variables:

$$STATE = \{\underset{\sim}{\boldsymbol{\varepsilon}}^e, \quad e := \phi - p, \quad p, \quad \underline{\boldsymbol{K}} := \boldsymbol{\nabla}\phi\} \tag{172}$$

The isothermal Clausius–Duhem inequality take the form:

$$(\underset{\sim}{\boldsymbol{\sigma}} - \rho \frac{\partial \psi}{\partial \underset{\sim}{\boldsymbol{\varepsilon}}^e}) : \dot{\underset{\sim}{\boldsymbol{\varepsilon}}}^e + (a - \rho \frac{\partial \psi}{\partial e}) : \dot{e} + (\underline{\boldsymbol{b}} - \rho \frac{\partial \psi}{\partial \underline{\boldsymbol{K}}}) \cdot \dot{\underline{\boldsymbol{K}}} + \underset{\sim}{\boldsymbol{\sigma}} : \dot{\underset{\sim}{\boldsymbol{\varepsilon}}}^p + a\dot{p} - \rho \frac{\partial \psi}{\partial T} \dot{\alpha} \geq 0 \tag{173}$$

The following state laws are adopted

$$\underset{\sim}{\boldsymbol{\sigma}} = \rho \frac{\partial \psi}{\partial \underset{\sim}{\boldsymbol{\varepsilon}}^e}, \quad R = \rho \frac{\partial \psi}{\partial p} \tag{174}$$

To ensure the positivity of the dissipation rate associated with the generalized stress a and $\underline{\boldsymbol{b}}$, we adopt the viscoelastic constitutive equations

$$a = \rho \frac{\partial \psi}{\partial e} + \beta \dot{e}, \quad \underline{\boldsymbol{b}} = \rho \frac{\partial \psi}{\partial \underline{\boldsymbol{K}}} + \kappa \dot{\underline{\boldsymbol{K}}} \tag{175}$$

where β and κ are generalized viscosity coefficients. This viscoelastic formulation amounts to splitting the generalized stresses a and $\underline{\boldsymbol{b}}$ into elastic (reversible) and viscous parts. Regarding viscoplastic deformation, a viscoplastic potential $\Omega(\underset{\sim}{\boldsymbol{\sigma}}, a - R)$ is chosen such that:

$$\dot{\underset{\sim}{\boldsymbol{\varepsilon}}}^p = \frac{\partial \Omega}{\partial \underset{\sim}{\boldsymbol{\sigma}}}, \quad \dot{p} = \frac{\partial \Omega}{\partial a - R} \tag{176}$$

In order to evidence the kind of gradient elastoviscoplastic models we aim at, we illustrate the case of a quadratic free energy potential:

$$\begin{aligned} \rho\psi &= \frac{1}{2} \underset{\sim}{\boldsymbol{\varepsilon}}^e : \underset{\approx}{\boldsymbol{C}} : \underset{\sim}{\boldsymbol{\varepsilon}}^e + R_0 p + \frac{1}{2} H p^2 + \frac{1}{2} H_\phi e^2 + \frac{1}{2} A \underline{\boldsymbol{K}} \cdot \underline{\boldsymbol{K}} \\ \underset{\sim}{\boldsymbol{\sigma}} &= \underset{\approx}{\boldsymbol{C}} : \underset{\sim}{\boldsymbol{\varepsilon}}^e, \quad R = R_0 + Hp, \quad a = H_\phi e + \beta \dot{e}, \quad \underline{\boldsymbol{b}} = A \underline{\boldsymbol{K}} + \kappa \dot{\underline{\boldsymbol{K}}} \end{aligned}$$

The viscoplastic potential is based on the yield function that introduces the equivalent stress measure σ_{eq} and a threshold

$$\Omega(\underset{\sim}{\boldsymbol{\sigma}}, a - R) = \frac{K}{n+1} \left\langle \frac{\sigma_{eq} + a - R}{K} \right\rangle^{n+1}$$

$$\dot{\underset{\sim}{\boldsymbol{\varepsilon}}}^p = \dot{p} \frac{\partial \sigma_{eq}}{\partial \underset{\sim}{\boldsymbol{\sigma}}}, \quad \dot{p} = \left\langle \frac{\sigma_{eq} + a - R}{K} \right\rangle^n$$

where $\langle \cdot \rangle$ denotes the positive part of the quantity in brackets, and K and n are usual viscosity parameters. The decomposition (175) and the generalized balance (159) become

$$a = H_\phi(\phi - p) + \beta(\dot{\phi} - \dot{p}) = \operatorname{div}(A \underline{\boldsymbol{K}} + \kappa \dot{\underline{\boldsymbol{K}}}) \tag{177}$$

We finally obtain the following linear partial differential equation, under the condition of plastic loading, in the absence of volume and inertial forces:

$$H_\phi \phi - A \Delta \phi + \beta \dot{\phi} - \kappa \Delta \dot{\phi} = H_\phi p + \kappa \dot{p} \tag{178}$$

where Δ is the Laplace operator. When the viscous parts are dropped in (175), the Helmholtz type equation used in strain gradient plasticity and damage (Peerlings et al., 2001; Engelen et al., 2003; Forest, 2009) is retrieved. It is classically used for the regularization of strain localization phenomena. The rate dependent part in the previous equation is expected to be useful in the simulation of strain rate localization phenomena which occur for instance in strain ageing materials (Mazière et al., 2010).

Under plastic loading, the equivalent stress can then be decomposed into the following contributions:

$$\sigma_{eq} = R - a + K\dot{p}^{1/n} = R_0 + Hp - A\Delta\phi - \kappa\Delta\dot{\phi} + K\dot{p}^{1/n} \tag{179}$$

If $\kappa = 0$, the micromorphic model is retrieved. If, furthermore, the constraint $\phi \equiv p$ is enforced, Aifantis well–known strain gradient plasticity model is recovered.

Decomposition of the generalized strain measures. It is proposed now to consider the decomposition of the additional dof and its gradient into elastic and plastic parts:

$$\phi = \phi^e + \phi^p, \quad \underline{\boldsymbol{K}} = \underline{\boldsymbol{K}}^{\,e} + \underline{\boldsymbol{K}}^{\,p} \tag{180}$$

The decomposition of ϕ itself is allowed only if it is an objective quantity. This would not apply for instance for $\phi \equiv \underset{\sim}{\boldsymbol{R}}$, the Cosserat microrotation. But it is allowed for a strain variable (Forest and Sievert, 2006). Such generalized kinematic decompositions were proposed in (Forest and Sievert, 2006) for strain gradient, Cosserat and micromorphic media, also at finite deformation. It is generalized here for more general dofs, possibly related to physically coupled phenomena.

The selected state variables then are

$$STATE = \{\underset{\sim}{\boldsymbol{\varepsilon}}^e, \quad \phi^e, \quad \underline{\boldsymbol{K}}^{\,e}, \quad p\} \tag{181}$$

which leads to the following Clausius–Duhem inequality

$$(\underset{\sim}{\boldsymbol{\sigma}} - \rho\frac{\partial\psi}{\partial\underset{\sim}{\boldsymbol{\varepsilon}}^e}) : \dot{\underset{\sim}{\boldsymbol{\varepsilon}}}^e + (a - \rho\frac{\partial\psi}{\partial\phi^e})\dot{\phi}^e + (\underline{\boldsymbol{b}} - \rho\frac{\partial\psi}{\partial\underline{\boldsymbol{K}}^{\,e}})\cdot\dot{\underline{\boldsymbol{K}}}^{\,e} + \underset{\sim}{\boldsymbol{\sigma}} : \dot{\underset{\sim}{\boldsymbol{\varepsilon}}}^p + a\dot{\phi}^p + \underline{\boldsymbol{b}}\cdot\dot{\underline{\boldsymbol{K}}}^{\,p} - R\dot{p} \geq 0 \tag{182}$$

The retained state laws are

$$\underset{\sim}{\boldsymbol{\sigma}} = \rho\frac{\partial\psi}{\partial\underset{\sim}{\boldsymbol{\varepsilon}}^e}, \quad a = \rho\frac{\partial\psi}{\partial\phi^e}, \quad \underline{\boldsymbol{b}} = \rho\frac{\partial\psi}{\partial\underline{\boldsymbol{K}}^{\,e}} \tag{183}$$

The residual dissipation then is

$$\underset{\sim}{\boldsymbol{\sigma}} : \dot{\underset{\sim}{\boldsymbol{\varepsilon}}}^p + a\dot{\phi}^p + \underline{\boldsymbol{b}} \cdot \dot{\underline{\boldsymbol{K}}}^{\,p} - R\dot{p} \geq 0 \tag{184}$$

A simple choice of dissipation potential is

$$\Omega(\underset{\sim}{\boldsymbol{\sigma}}, R, a) = \frac{K}{n+1}\left\langle \frac{\sigma_{eq}+a-R}{K}\right\rangle^{n+1} + \frac{K_a}{m_a+1}\left(\frac{|a|}{K_a}\right)^{m_a+1} + \frac{K_b}{m_b+1}\left(\frac{b_{eq}}{K_b}\right)^{m_b+1}$$

where b_{eq} is a norm of $\underline{\boldsymbol{b}}$ and from which the evolution rules are derived

$$\underset{\sim}{\dot{\boldsymbol{\varepsilon}}}^p = \dot{p}\frac{\partial \sigma_{eq}}{\partial \underset{\sim}{\boldsymbol{\sigma}}}, \quad \dot{p} = -\frac{\partial \Omega}{\partial R} = \left\langle \frac{\sigma_{eq}+a-R}{K}\right\rangle^{n}, \tag{185}$$

$$\dot{\phi}^p = \frac{\partial \Omega}{\partial a} = \dot{p} + \left(\frac{|a|}{K_a}\right)^{m_a} \operatorname{sign} a, \; \underline{\dot{\boldsymbol{K}}}^p = \frac{\partial \Omega}{\partial \underline{\boldsymbol{b}}} = \left(\frac{b_{eq}}{K_b}\right)^{m_b} \frac{\partial b_{eq}}{\partial \underline{\boldsymbol{b}}} \tag{186}$$

The time variation of the additional dof therefore deviates from the cumulated plastic strain rate by a viscous term characterized by the material parameters K_a and m_a. The residual dissipation rate becomes

$$(\sigma_{eq} - R + a)\dot{p} + \frac{|a|^{m_a+1}}{K_a^{m_a}} + \left(\frac{b_{eq}}{K_b}\right)^{m_b} \frac{\partial b_{eq}}{\partial \underline{\boldsymbol{b}}} \cdot \underline{\boldsymbol{b}} \geq 0 \tag{187}$$

which is indeed always positive.

Let us illustrate the type of partial differential equation provided by such a model. For that purpose, a simple quadratic free energy potential is chosen:

$$\rho\psi = \frac{1}{2}\underset{\sim}{\boldsymbol{\varepsilon}}^e : \underset{\approx}{\boldsymbol{C}} : \underset{\sim}{\boldsymbol{\varepsilon}}^e + R_0 p + \frac{1}{2}Hp^2 + \frac{1}{2}H_\phi \phi^{e2} + \frac{1}{2}A\underline{\boldsymbol{K}}^e \cdot \underline{\boldsymbol{K}}^e \tag{188}$$

As a result, the corresponding state laws can be combined with the extra–balance equation (159):

$$a = H_\phi \phi^e = \operatorname{div} \underline{\boldsymbol{b}} = \operatorname{div}(A\underline{\boldsymbol{K}}^e) \tag{189}$$

which leads to the following partial differential equation, under the condition of material homogeneity:

$$H_\phi(\phi - \phi^p) = A\Delta\phi - A \operatorname{div} \underline{\boldsymbol{K}}^p \tag{190}$$

If $K_a = \infty$ (infinite viscosity), equation (186) shows that ϕ^p coincides with p. If, furthermore, $K_b = \infty$, the plastic part of $\underline{\boldsymbol{K}}$ vanishes. The equation (189) then reduces to the Helmholtz–type equation (178) where β and κ are set to zero. An alternative expression of (189) can be worked out by taking the viscous laws into account

$$a = K_a(\dot{\phi}^p - \dot{p}) = \operatorname{div} \underline{\boldsymbol{b}} = \operatorname{div} K_b \underline{\dot{\boldsymbol{K}}}^p \tag{191}$$

which leads to the following partial differential equation

$$K_a(\dot{\phi}^p - \dot{p}) = K_b \,\mathrm{div}\, \dot{\underline{\boldsymbol{K}}}^p \tag{192}$$

When the elastic contributions ϕ^e and $\underline{\boldsymbol{K}}^e$ are neglected, the previous equation reduces to

$$K_a(\dot{\phi} - \dot{p}) = K_b \Delta \dot{\phi} \tag{193}$$

which is identical to (178) after taking $A = H_\phi = 0$.

5.3 Phase field models for elastoviscoplastic materials

In this section, the additional degree of freedom is a phase field variable. We show how the constitutive framework for elastoviscoplastic materials can be embedded in the existing phase field approach which combines diffusion and phase field equations to model the motion of boundaries between phases. The migration of interfaces and growth of precipitates are strongly influenced by the mechanical behaviour of the phases.

One observes in current literature a strong endeavour to develop microstructure evolution simulation schemes coupled with complex mechanical material behaviour ranging from heterogeneous elasticity to general elastoviscoplasticity. The main difficulty of such a task lies in the tight coupling between the complex interface evolutions and the fields, common to many moving boundary problems. The phase field approach has emerged as a powerful method for easily tackling the morphological evolutions involved in phase transformations. Phase field models have incorporated elasticity quite early (Wang et al., 1993) and have succeeded in predicting some complex microstructure evolutions driven by the interplay of diffusion and elasticity. It is only very recently that some phase field models have been enriched with nonlinear mechanical behaviour, extending the range of applications and materials which can be handled by the phase field approach (Ubachs et al., 2004; Gaubert et al., 2008; Ammar et al., 2009b; Gaubert et al., 2010).

There are essentially two ways of introducing linear and nonlinear mechanical constitutive equations into the standard phase field approach:

1. The material behaviour is described by a unified set of constitutive equations including material parameters that explicitly depend on the concentration or the phase variable. Each parameter is usually interpolated between the limit values known for each phase. This is the formulation adopted in the finite element simulations of Cahn–Hilliard like equations coupled with viscoplasticity in (Ubachs et al., 2004, 2007) for tin–lead solders. The same methodology is used in (Gaubert et al., 2008, 2010) to simulate the role of viscoplasticity on

rafting of γ' precipitates in single crystal nickel base superalloys under load.

2. One distinct set of constitutive equations is attributed to each individual phase k at any material point. Each phase at a material point then possesses its own stress/strain tensor $\underset{\sim}{\boldsymbol{\sigma}}_k, \underset{\sim}{\boldsymbol{\varepsilon}}_k$. The overall strain and stress quantities $\underset{\sim}{\boldsymbol{\sigma}}, \underset{\sim}{\boldsymbol{\varepsilon}}$ at this material point must then be averaged or interpolated from the values attributed to each phase. This is particularly important for points inside the smooth interface zone. At this stage, several mixture rules are available to perform this averaging or interpolation. This approach makes possible to mix different types of constitutive equations for each phase, like hyperelastic nonlinear behaviour for one phase and conventional elastic–plastic model with internal variables for the other one. No correspondence of material parameters is needed between the phase behaviour laws. This is the approach proposed in (Steinbach and Apel, 2006) for incorporating elasticity in a multi–phase field model. For that purpose, the authors resort to a well–known homogeneous stress hypothesis taken from homogenization theory in the mechanics of heterogeneous materials (Besson et al., 2009). In the present work, we propose to generalize this procedure to nonlinear material behaviour and to other mixture rules also taken from homogenization theory.

It must be emphasized that the latter procedure is very similar to what has already been proposed for handling diffusion in phase field models by (Kim et al., 1999). Two concentration fields c_α and c_β are indeed introduced, and the real concentration field is obtained by a mixture rule together with an internal constraint on the diffusion potentials. Introducing two concentration fields gives an additional degree of freedom for controlling the energy of the interface with respect to its thickness. If this possibility is not obvious when mechanics is introduced, adding a degree of freedom for describing the stresses/strains within a diffuse interface could be valuable to get rid of some spurious effects due to unrealistic interface thickness.

Coupling with diffusion. In the context of mass diffusion and phase field evolution, the local form of the energy principle is

$$\dot{e} = \underset{\sim}{\boldsymbol{\sigma}} : \dot{\underset{\sim}{\boldsymbol{\varepsilon}}} + a\dot{\phi} + \underline{\boldsymbol{b}} \cdot \boldsymbol{\nabla}\dot{\phi} \tag{194}$$

The total strain is partitioned into the elastic strain $\underset{\sim}{\boldsymbol{\varepsilon}}^e$, the eigenstrain $\underset{\sim}{\boldsymbol{\varepsilon}}^\star$ due to phase transformation and the plastic strain $\underset{\sim}{\boldsymbol{\varepsilon}}^p$:

$$\underset{\sim}{\boldsymbol{\varepsilon}} = \underset{\sim}{\boldsymbol{\varepsilon}}^e + \underset{\sim}{\boldsymbol{\varepsilon}}^\star + \underset{\sim}{\boldsymbol{\varepsilon}}^p \tag{195}$$

According to the thermodynamics of irreversible processes, the second law states that the variation of entropy is always larger than or equal to the rate of entropy flux induced by diffusion:

$$T\dot{\eta} - \boldsymbol{\nabla}.(\mu \underline{\boldsymbol{J}}) \geqslant 0 \tag{196}$$

where $\underline{\boldsymbol{J}}$ is the diffusion flux and μ is the chemical potential. The conservation law for mass diffusion is then

$$\dot{c} = -\boldsymbol{\nabla}.\underline{\boldsymbol{J}} \tag{197}$$

Accordingly, the fundamental inequality containing first and second principles in the isothermal case is written as

$$-\rho\dot{\psi} + \underset{\sim}{\boldsymbol{\sigma}} : \underset{\approx}{\dot{\boldsymbol{\varepsilon}}} + a\dot{\phi} + \underline{\boldsymbol{b}} \cdot \boldsymbol{\nabla}\dot{\phi} + \mu\dot{c} - \underline{\boldsymbol{J}}.\boldsymbol{\nabla}\mu \geqslant 0 \tag{198}$$

Assuming that the free energy density depends on the order parameter ϕ and its gradient, the concentration c, the elastic strain $\underset{\approx}{\boldsymbol{\varepsilon}}^e$ and the set of internal variables V_k associated to material hardening[5]:

$$STATE = \{\phi, \quad \boldsymbol{\nabla}\phi, \quad c, \quad \underset{\approx}{\boldsymbol{\varepsilon}}^e, \quad V_k\}$$

The Clausius-Duhem inequality now becomes:

$$\left(a - \rho\frac{\partial\psi}{\partial\phi}\right)\dot{\phi} + \left(\underline{\boldsymbol{b}} - \rho\frac{\partial\psi}{\partial\boldsymbol{\nabla}\phi}\right)\cdot\boldsymbol{\nabla}\dot{\phi} + \left(\mu - \rho\frac{\partial\psi}{\partial c}\right)\dot{c} + \left(\underset{\sim}{\boldsymbol{\sigma}} - \frac{\partial\psi}{\partial\underset{\approx}{\boldsymbol{\varepsilon}}^e}\right) : \underset{\approx}{\dot{\boldsymbol{\varepsilon}}}^e - \underline{\boldsymbol{J}}.\boldsymbol{\nabla}\mu + \underset{\sim}{\boldsymbol{\sigma}} : \underset{\approx}{\dot{\boldsymbol{\varepsilon}}}^p - \rho\frac{\partial\psi}{\partial V_k}\dot{V}_k \geqslant 0 \tag{199}$$

The following reversible mechanisms and corresponding state laws are chosen:

$$\underline{\boldsymbol{b}} = \rho\frac{\partial\psi}{\partial\boldsymbol{\nabla}\phi}, \quad \mu = \rho\frac{\partial\psi}{\partial c}, \quad \underset{\sim}{\boldsymbol{\sigma}} = \rho\frac{\partial\psi}{\partial\underset{\approx}{\boldsymbol{\varepsilon}}^e}, \quad A_k := \rho\frac{\partial\psi}{\partial V_k} \tag{200}$$

The residual dissipation then is

$$\left(a - \rho\frac{\partial\psi}{\partial\phi}\right)\dot{\phi} - \underline{\boldsymbol{J}}.\boldsymbol{\nabla}\mu + \underset{\sim}{\boldsymbol{\sigma}} : \underset{\approx}{\dot{\boldsymbol{\varepsilon}}}^p - A_k\dot{V}_k \geqslant 0 \tag{201}$$

Three contributions appear in the above residual dissipation rate. The first is the phase field dissipation, associated with configuration changes of atoms and related to the evolution of the order parameter:

$$D_\phi = a^v\dot{\phi} \quad \text{with} \quad a^v = a - \rho\frac{\partial\psi}{\partial\phi} \tag{202}$$

[5]In this section, the notation for internal variables is changed to $(V_k)_{k\in\{\alpha,\beta\}}$ since α is now an index denoting one phase.

where a^v is the chemical force associated with the dissipative processes (Gurtin, 1996). The second contribution is the chemical dissipation due to diffusion, associated with mass transport. The last contribution is the mechanical dissipation, as discussed earlier.

An efficient way of defining the complementary laws related to the dissipative processes and ensuring the positivity of the dissipation for any thermodynamic process is to assume the existence of a dissipation potential $\Omega(a^v, \boldsymbol{\nabla}\mu, \underset{\sim}{\boldsymbol{\sigma}}, A_k)$, which is a convex function of its arguments:

$$\dot{\phi} = \frac{\partial \Omega}{\partial a^v}, \quad \underline{\boldsymbol{J}} = -\frac{\partial \Omega}{\partial \boldsymbol{\nabla}\mu}, \quad \dot{V}_k = -\frac{\partial \Omega}{\partial A_k} \quad , \quad \dot{\underset{\sim}{\boldsymbol{\varepsilon}}}^p = \frac{\partial \Omega}{\partial \underset{\sim}{\boldsymbol{\sigma}}} \tag{203}$$

These equations represent the evolution law for the order parameter, the diffusion flux as well as the evolution laws for the internal variables.

Partition of free energy and dissipation potential. The total free energy is postulated to have the form of a Ginzburg-Landau free energy functional accounting for interfaces through the square of the order parameter gradient. The free energy density ψ is then split into a chemical free energy density ψ_{ch}, a coherent mechanical energy density ψ_{mech}, and the square of the order parameter gradient:

$$\rho\psi(\phi, \boldsymbol{\nabla}\phi, c, \underset{\sim}{\boldsymbol{\varepsilon}}^e, V_k) = \rho\psi_{\text{ch}}(\phi, c) + \rho\psi_{\text{mech}}(\phi, c, \underset{\sim}{\boldsymbol{\varepsilon}}, V_k) + \frac{A}{2}\boldsymbol{\nabla}\phi \cdot \boldsymbol{\nabla}\phi \tag{204}$$

The irreversible part of the behaviour is described by the dissipation potential, which can be split into three parts related to the three contributions in the residual dissipation in Eq.(201): the phase field part $\Omega_\phi(\phi, c, a^v)$, the chemical part $\Omega_c(\phi, c, \boldsymbol{\nabla}\mu)$ and the mechanical dissipation potential $\Omega_{\text{mech}}(\phi, c, \underset{\sim}{\boldsymbol{\sigma}}, A_k)$:

$$\Omega(a^v, \boldsymbol{\nabla}\mu, \phi, c, \underset{\sim}{\boldsymbol{\sigma}}, A_k) = \Omega_\phi(c, \phi, a^v) + \Omega_c(c, \phi, \boldsymbol{\nabla}\mu) + \Omega_{\text{mech}}(\phi, c, \underset{\sim}{\boldsymbol{\sigma}}, A_k) \tag{205}$$

The chemical free energy density ψ_{ch} of a binary alloy is a function of the order parameter ϕ and of the concentration field c. The coexistence of both phases α and β discriminated by ϕ is possible if ψ_{ch} is non–convex with respect to ϕ. Following (Kim et al., 1998), ψ_{ch} is built with the free energy densities of the two phases ψ_α and ψ_β as follows:

$$\psi_{\text{ch}}(\phi, c) = h(\phi)\psi_\alpha(c) + (1 - h(\phi))\psi_\beta(c) + W g(\phi) \tag{206}$$

Here, the interpolating function $h(\phi)$ is chosen as $h(\phi) = \phi^2(3 - 2\phi)$, and $g(\phi) = \phi^2(1-\phi)^2$ is the double well potential accounting for the free energy

penalty of the interface. The height W of the potential barrier is related to the interfacial energy σ and the interfacial thickness δ as $W = 6\Lambda\sigma/\delta$. Assuming that the interface region ranges from θ to $1-\theta$, then $\Lambda = \log((1-\theta)/\theta)$. In the present work $\theta = 0.05$ (Kim et al., 1998; Ammar et al., 2009a).

The densities ψ_α and ψ_β are chosen to be quadratic functions of the concentration only:

$$\rho\psi_\alpha(c) = \frac{k_\alpha}{2}(c-a_\alpha)^2 \quad \text{and} \quad \rho\psi_\beta(c) = \frac{k_\beta}{2}(c-a_\beta)^2 \tag{207}$$

where a_α and a_β are the unstressed equilibrium concentrations of both phases which correspond respectively to the minima of ψ_α and ψ_β in the present model. k_α and k_β are the curvatures of the free energies.

Quadratic expressions are chosen for the chemical dissipation, which ensures the positivity of the dissipation rate:

$$\Omega_\phi(a^v) = \frac{1}{2}(1/\beta)a^{v2} \quad \text{and} \quad \Omega_c(\boldsymbol{\nabla}\mu) = \frac{1}{2}L(\phi)\boldsymbol{\nabla}\mu.\boldsymbol{\nabla}\mu \tag{208}$$

where a^v is given by Eq. (202), β is inversely proportional to the interface mobility and $L(\phi)$ is the Onsager coefficient, related to the chemical diffusivities D_α and D_β in both phases by means of the interpolation function $h(\phi)$ as:

$$L(\phi) = h(\phi)D_\alpha/k_\alpha + (1-h(\phi))D_\beta/k_\beta \tag{209}$$

The state laws and evolution equations for the phase field and chemical contributions can be derived as:

$$\underline{\boldsymbol{b}} = A\boldsymbol{\nabla}\phi, \quad \mu = \rho\frac{\partial\psi_{\text{ch}}}{\partial c} + \rho\frac{\partial\psi_{\text{mech}}}{\partial c} \tag{210}$$

$$\dot{\phi} = \frac{1}{\beta}a^v = \frac{1}{\beta}\left(a - \rho\frac{\partial\psi_{\text{ch}}}{\partial\phi} - \rho\frac{\partial\psi_{\text{mech}}}{\partial\phi}\right), \quad \underline{\boldsymbol{J}} = -L(\phi)\boldsymbol{\nabla}\mu \tag{211}$$

Substituting the previous equations into the balance equations for generalized stresses and mass concentration, the Ginzburg-Landau and usual diffusion equations are retrieved, which represent respectively the evolution equations for order parameter and concentration:

$$\operatorname{div}\underline{\boldsymbol{b}} - a = -\beta\dot{\phi} + \operatorname{div}(A\boldsymbol{\nabla}\phi) - \rho\frac{\partial\psi_{\text{ch}}}{\partial\phi} - \rho\frac{\partial\psi_{\text{mech}}}{\partial\phi} = 0 \tag{212}$$

$$\dot{c} = -\boldsymbol{\nabla}.(-L(\phi)\boldsymbol{\nabla}\mu) = -\boldsymbol{\nabla}.\left(-L(\phi)\left(\boldsymbol{\nabla}\frac{\partial\rho\psi_{\text{ch}}}{\partial c} + \boldsymbol{\nabla}\frac{\partial\rho\psi_{\text{mech}}}{\partial c}\right)\right) \tag{213}$$

Note the coupling of mechanics and diffusion and phase field evolution through the partial derivatives of the mechanical free energy with respect to concentration and order parameter.

Multiphase approach for the mechanical contribution. The second contribution to the free energy density is due to mechanical effects. Assuming that elastic behaviour and hardening are uncoupled, the mechanical part of the free energy density $\rho\psi_{\text{mech}}$ is decomposed into a coherent elastic energy density $\rho\psi_e$ and a plastic part $\rho\psi_p$ as:

$$\rho\psi_{\text{mech}}(\phi, c, \underset{\sim}{\boldsymbol{\varepsilon}}, V_k) = \rho\psi_e(\phi, c, \underset{\sim}{\boldsymbol{\varepsilon}}) + \rho\psi_p(\phi, c, V_k) \tag{214}$$

Moreover, the irreversible mechanical behaviour, related to the dissipative processes, is obtained by a plastic dissipation potential $\Omega_{\text{mech}}(\phi, c, \underset{\sim}{\boldsymbol{\sigma}}, A_k)$. It is assumed to be a function of order parameter, concentration, Cauchy stress tensor as well as the set of thermodynamic force associated variables A_k in order to describe the hardening state in each phase.

In the diffuse interface region where both phases coexist, we propose to use well-known results of homogenization theory to interpolate the local behaviour. The homogenization procedure in the mechanics of heterogeneous materials consists in replacing an heterogeneous medium by an equivalent homogeneous one, which is defined by an effective constitutive law relating the macroscopic variables, namely macroscopic stress $\underset{\sim}{\boldsymbol{\sigma}}$ and strain $\underset{\sim}{\boldsymbol{\varepsilon}}$ tensors, which are obtained by averaging the corresponding non-uniform local stress and strain in each phase. Each material point within a diffuse interface can be seen as a local mixture of the two abutting phases α and β with proportions given by complementary functions of ϕ. The strain and stress at each material point are then defined by the following mixture laws which would proceed from space averaging in a conventional homogenization problem, but which must be seen as arbitrary interpolations in the present case:

$$\underset{\sim}{\boldsymbol{\varepsilon}} = \chi\, \underset{\sim}{\boldsymbol{\varepsilon}}_\alpha + (1-\chi)\, \underset{\sim}{\boldsymbol{\varepsilon}}_\beta \quad \text{and} \quad \underset{\sim}{\boldsymbol{\sigma}} = \chi\, \underset{\sim}{\boldsymbol{\sigma}}_\alpha + (1-\chi)\, \underset{\sim}{\boldsymbol{\sigma}}_\beta \tag{215}$$

where $\underset{\sim}{\boldsymbol{\varepsilon}}_\alpha$, $\underset{\sim}{\boldsymbol{\varepsilon}}_\beta$ are local fictitious strains and $\underset{\sim}{\boldsymbol{\sigma}}_\alpha$, $\underset{\sim}{\boldsymbol{\sigma}}_\beta$ are local fictitious stresses in α and β phases respectively and $\chi(\underline{\boldsymbol{x}}, t)$ is a shape function which must take the value 0 in the β–phase and 1 in the α–phase. The following choice is made in the phase field context:

$$\chi(\underline{\boldsymbol{x}}, t) \equiv \phi(\underline{\boldsymbol{x}}, t) \tag{216}$$

The partition hypothesis, already used for the effective total strain tensor in Eq. (195), requires, in a similar way, a decomposition of the total strain in each phase into elastic, transformation and plastic parts:

$$\underset{\sim}{\boldsymbol{\varepsilon}}_\alpha = \underset{\sim}{\boldsymbol{\varepsilon}}^e_\alpha + \underset{\sim}{\boldsymbol{\varepsilon}}^\star_\alpha + \underset{\sim}{\boldsymbol{\varepsilon}}^p_\alpha \quad \text{and} \quad \underset{\sim}{\boldsymbol{\varepsilon}}_\beta = \underset{\sim}{\boldsymbol{\varepsilon}}^e_\beta + \underset{\sim}{\boldsymbol{\varepsilon}}^\star_\beta + \underset{\sim}{\boldsymbol{\varepsilon}}^p_\beta \tag{217}$$

where each point may depend on the local concentration c, but not on order parameter ϕ. In the proposed model, the elastoplastic and phase

field behaviours of each phase are treated independently and the effective behaviour is obtained using homogenization relation (215). It is assumed that the mechanical state of α and β phases at a given time are completely described by a finite number of local state variables $(\underset{\sim}{\varepsilon}^e_k, V_k)$ defined at each material point. The set of internal variables V_k, of scalar or tensorial nature, represents the state of hardening of phase k: for instance, a scalar isotropic hardening variable, and a tensorial kinematic hardening variable. According to the homogenization theory, the effective elastic and plastic free energy densities are given by the rule of mixtures as follows:

$$\rho\psi_e(\phi, c, \underset{\sim}{\varepsilon}) = \phi\,\rho\psi_{e\alpha}(c, \underset{\sim}{\varepsilon}^e_\alpha) + (1-\phi)\rho\psi_{e\beta}(c, \underset{\sim}{\varepsilon}^e_\beta) \tag{218}$$

$$\rho\psi_p(\phi, c, V_k) = \phi\,\rho\psi_{p\alpha}(c, V_\alpha) + (1-\phi)\rho\psi_{p\beta}(c, V_\beta) \tag{219}$$

Similarly, a mixture rule is used to mix the dissipation potentials of the individual phases:

$$\Omega_{\text{mech}}(\phi, c, \underset{\sim}{\sigma}, A_k) = \phi\,\Omega_{\text{mech}_\alpha}(c, \underset{\sim}{\sigma}_\alpha, A_\alpha) + (1-\phi)\,\Omega_{\text{mech}_\beta}(c, \underset{\sim}{\sigma}_\beta, A_\beta) \tag{220}$$

where the $A_{\alpha,\beta}$ are the thermodynamic forces associated with the internal variables attributed to each phase.

Knowing the free energy and dissipation potentials, the evolution of all variables can be computed. The remaining questions is the way of estimating the previously defined fictitious stress and strain tensors $\underset{\sim}{\varepsilon}_{\alpha,\beta}, \underset{\sim}{\sigma}_{\alpha,\beta}$ from the knowledge of the stress and strain tensors $\underset{\sim}{\varepsilon}$ and $\underset{\sim}{\sigma}$. Several homogenization schemes exist in the literature that can be used to define these new fictitious variables. The most simple schemes are the Voigt/Taylor and Reuss/Static models. We develop the Voigt/Taylor scenario in the sequel.

Voigt/Taylor model coupled phase field mechanical theory. According to Voigt's scheme, the fictitious strains are not distinguished from the local strain. The local stress is then computed in terms of the fictitious stress tensors by averaging with respect to both phases weighted by the volume fractions:

$$\underset{\sim}{\sigma} = \phi\,\underset{\sim}{\sigma}_\alpha + (1-\phi)\,\underset{\sim}{\sigma}_\beta, \quad \underset{\sim}{\varepsilon} = \underset{\sim}{\varepsilon}_\alpha = \underset{\sim}{\varepsilon}_\beta \tag{221}$$

The stresses of both phases $\underset{\sim}{\sigma}_\alpha$ and $\underset{\sim}{\sigma}_\beta$ are given by Hooke's law for each phase:

$$\underset{\sim}{\sigma}_\alpha = \underset{\approx}{C}_\alpha : (\underset{\sim}{\varepsilon}_\alpha - \underset{\sim}{\varepsilon}^\star_\alpha - \underset{\sim}{\varepsilon}^p_\alpha), \quad \underset{\sim}{\sigma}_\beta = \underset{\approx}{C}_\beta : (\underset{\sim}{\varepsilon}_\beta - \underset{\sim}{\varepsilon}^\star_\beta - \underset{\sim}{\varepsilon}^p_\beta) \tag{222}$$

where $\underset{\approx}{C}_\alpha$ and $\underset{\approx}{C}_\beta$ are respectively the tensor of elasticity moduli in α and β phases. As a result,

$$\underset{\sim}{\sigma} = \phi\,\underset{\approx}{C}_\alpha : (\underset{\sim}{\varepsilon}_\alpha - \underset{\sim}{\varepsilon}^\star_\alpha - \underset{\sim}{\varepsilon}^p_\alpha) + (1-\phi)\underset{\approx}{C}_\beta : (\underset{\sim}{\varepsilon}_\beta - \underset{\sim}{\varepsilon}^\star_\beta - \underset{\sim}{\varepsilon}^p_\beta) \tag{223}$$

From the above relation, it follows that the strain-stress relationship in the homogeneous effective medium obeys Hooke's law with the following equation:

$$\underset{\sim}{\boldsymbol{\sigma}} = \underset{\approx}{\boldsymbol{C}}_{\text{eff}} : (\underset{\sim}{\boldsymbol{\varepsilon}} - \underset{\sim}{\boldsymbol{\varepsilon}}^{p} - \underset{\sim}{\boldsymbol{\varepsilon}}^{\star})$$

where the effective elasticity tensor $\underset{\approx}{\boldsymbol{C}}_{\text{eff}}$ is obtained from the mixture rule of the elasticity matrix for both phases:

$$\underset{\approx}{\boldsymbol{C}}_{\text{eff}} = \phi\, \underset{\approx}{\boldsymbol{C}}_{\alpha} + (1-\phi)\underset{\approx}{\boldsymbol{C}}_{\beta} \tag{224}$$

and the effective eigenstrain $\underset{\sim}{\boldsymbol{\varepsilon}}^{\star}$ and plastic strain $\underset{\sim}{\boldsymbol{\varepsilon}}^{p}$ vary continuously between their respective values in the bulk phases as follows:

$$\begin{aligned} \underset{\sim}{\boldsymbol{\varepsilon}}^{\star} &= \underset{\approx}{\boldsymbol{C}}_{\text{eff}}^{-1} : (\phi\, \underset{\approx}{\boldsymbol{C}}_{\alpha} : \underset{\sim}{\boldsymbol{\varepsilon}}_{\alpha}^{\star} + (1-\phi)\underset{\approx}{\boldsymbol{C}}_{\beta} : \underset{\sim}{\boldsymbol{\varepsilon}}_{\beta}^{\star}) \\ \underset{\sim}{\boldsymbol{\varepsilon}}^{p} &= \underset{\approx}{\boldsymbol{C}}_{\text{eff}}^{-1} : (\phi\, \underset{\approx}{\boldsymbol{C}}_{\alpha} : \underset{\sim}{\boldsymbol{\varepsilon}}_{\alpha}^{p} + (1-\phi)\underset{\approx}{\boldsymbol{C}}_{\beta} : \underset{\sim}{\boldsymbol{\varepsilon}}_{\beta}^{p}) \end{aligned} \tag{225}$$

In the case of nonhomogeneous elasticity, it must be noted that $\underset{\sim}{\boldsymbol{\varepsilon}}^{\star}$ and $\underset{\sim}{\boldsymbol{\varepsilon}}^{p}$ are not the average of their respective values for each phase.

The proposed approach differs from the one most commonly used in phase field models, as popularized by Khachaturyan and co-workers, e.g. (Khachaturyan, 1983). The latter rely on mixture laws for all quantities within the interface, including the elastic moduli, the transformation and plastic strain. The effect of these different choices on the simulation of moving phase boundaries has been tested in (Ammar et al., 2009b) and (Ammar et al., 2011). In particular, the impact of plasticity on the kinetics of precipitate growth has been evidenced.

6 Summary and Outlook

The general thermomechanical setting for modeling size effects in the mechanics and thermodynamics of materials is based on the main assumption that microstructure effects can be accounted for by the introduction of additional degrees of freedom in addition to displacement, temperature and concentration. The additional dof and its gradient are expected to contribute to the power of internal forces of the medium and to arise in the energy local balance equations and/or entropy inequality. They induce generalized stresses that fulfill an additional balance equation with associated extra boundary conditions. A clear separation between balance equations and constitutive functionals is adopted in the formulation. Constitutive equations derive from the definition of a specific free energy density and dissipation potential.

The crossing of mechanical and physical approaches turns out to be fertile in providing motivated coupling between both kinds of phenomena. As an example, we have shown that the mechanics of heterogeneous materials can be useful to develop a sophisticated and flexible constitutive framework of coupled viscoplasticity and diffusion.

It was not possible to address applications that already exist in this context. In particular, the presented models predict that viscoplasticity affects the morphology and kinetics of precipitate growth in metals or during oxidation (Ammar et al., 2009a; Gaubert et al., 2010; Ammar et al., 2011).

Special attention must now be dedicated to more precise description of coherent vs. incoherent interfaces (Murdoch, 1978; Johnson and Alexander, 1986; Appolaire et al., 2010), and the associated specific interface conditions that can be deduced from asymptotic analysis of phase field models. On the other hand, the targeted applications of strain gradient plasticity are crystal plasticity and grain boundary migration (Cordero et al., 2010; Mayeur et al., 2011; Abrivard, 2009), whereas strain rate gradients are thought to be relevant for ageing materials (Mazière et al., 2010).

Bibliography

Guillaume Abrivard. *A coupled crystal plasticity–phase field formulation to describe microstructural evolution in polycrystalline aggregates*. PhD, Mines ParisTech, 2009.

E.C. Aifantis. On the microstructural origin of certain inelastic models. *Journal of Engineering Materials and Technology*, 106:326–330, 1984.

K. Ammar, B. Appolaire, G. Cailletaud, F. Feyel, and F. Forest. Finite element formulation of a phase field model based on the concept of generalized stresses. *Computational Materials Science*, 45:800–805, 2009a.

K. Ammar, B. Appolaire, G. Cailletaud, and S. Forest. Combining phase field approach and homogenization methods for modelling phase transformation in elastoplastic media. *European Journal of Computational Mechanics*, 18:485–523, 2009b.

K. Ammar, B. Appolaire, G. Cailletaud, and S. Forest. Phase field modeling of elasto-plastic deformation induced by diffusion controlled growth of a misfitting spherical precipitate. *Philosophical Magazine Letters*, 91:164–172, 2011.

B. Appolaire, E. Aeby-Gautier, J. D. Teixeira, M. Dehmas, and S. Denis. Non-coherent interfaces in diffuse interface models. *Philosophical Magazine*, 90:461–483, 2010.

R.J. Asaro. Crystal plasticity. *J. Appl. Mech.*, 50:921–934, 1983.

O. Aslan and S. Forest. Crack growth modelling in single crystals based on higher order continua. *Computational Materials Science*, 45:756–761, 2009.

O. Aslan and S. Forest. The micromorphic versus phase field approach to gradient plasticity and damage with application to cracking in metal single crystals. In R. de Borst and E. Ramm, editors, *Multiscale Methods in Computational Mechanics*, pages 135–154. Lecture Notes in Applied and Computational Mechanics 55, Springer, 2011.

O. Aslan, N. M. Cordero, A. Gaubert, and S. Forest. Micromorphic approach to single crystal plasticity and damage. *International Journal of Engineering Science*, 49:1311–1325, 2011.

V.P. Bennett and D.L. McDowell. Crack tip displacements of microstructurally small surface cracks in single phase ductile polycrystals. *Engineering Fracture Mechanics*, 70(2):185–207, 2003.

J. Besson, G. Cailletaud, J.-L. Chaboche, S. Forest, and M. Blétry. *Non–Linear Mechanics of Materials*. Series: Solid Mechanics and Its Applications, Vol. 167, Springer, ISBN: 978-90-481-3355-0, 433 p., 2009.

B.A. Bilby, R. Bullough, L.R.T. Gardner, and E. Smith. Continuous distributions of dislocations iv: Single glide and plane strain. *Proc. Roy. Soc. London*, A236:538–557, 1957.

P. Cermelli and M.E. Gurtin. On the characterization of geometrically necessary dislocations in finite plasticity. *Journal of the Mechanics and Physics of Solids*, 49:1539–1568, 2001.

Y. Chen and J.D. Lee. Connecting molecular dynamics to micromorphic theory. (I) instantaneous and averaged mechanical variables. *Physica A*, 322:359–376, 2003a.

Y. Chen and J.D. Lee. Connecting molecular dynamics to micromorphic theory. (II) balance laws. *Physica A*, 322:377–392, 2003b.

Y. Chen and J.D. Lee. Determining material constants in micromorphic theory through phonon dispersion relations. *International Journal of Engineering Science*, 41:871–886, 2003c.

W.D. Claus and A.C. Eringen. Three dislocation concepts and micromorphic mechanics. In *Developments in Mechanics, Vol. 6. Proceedings of the 12th Midwestern Mechanics Conference*, pages 349–358, 1969.

W.D. Claus and A.C. Eringen. Dislocation dispersion of elastic waves. *International Journal of Engineering Science*, 9:605–610, 1971.

J.D. Clayton, D.J. Bamman, and D.L. McDowell. A geometric framework for the kinematics of crystals with defects. *Philosophical Magazine*, 85: 3983–4010, 2005.

N.M. Cordero, A. Gaubert, S. Forest, E. Busso, F. Gallerneau, and S. Kruch. Size effects in generalised continuum crystal plasticity for two–phase laminates. *Journal of the Mechanics and Physics of Solids*, 58:1963–1994, 2010.

W. Ehlers and W. Volk. On theoretical and numerical methods in the theory of porous media based on polar and non–polar elasto–plastic solid materials. *Int. J. Solids Structures*, 35:4597–4617, 1998.

R.A.B. Engelen, M.G.D. Geers, and F.P.T. Baaijens. Nonlocal implicit gradient-enhanced elasto-plasticity for the modelling of softening behaviour. *International Journal of Plasticity*, 19:403–433, 2003.

A.C. Eringen and W.D. Claus. A micromorphic approach to dislocation theory and its relation to several existing theories. In J.A. Simmons, R. de Wit, and R. Bullough, editors, *Fundamental Aspects of Dislocation Theory*, pages 1023–1062. Nat. Bur. Stand. (US) Spec. Publ. 317, II, 1970.

A.C. Eringen and E.S. Suhubi. Nonlinear theory of simple microelastic solids. *Int. J. Engng Sci.*, 2:189–203, 389–404, 1964.

Y. Estrin. Dislocation density related constitutive modelling. In *Unified Constitutive Laws of Plastic Deformation*, pages 69–106. Academic Press, 1996.

A. Finel, Y. Le Bouar, A. Gaubert, and U. Salman. Phase field methods: Microstructures, mechanical properties and complexity. *Comptes Rendus Physique*, 11:245–256, 2010.

M. Fivel and S. Forest. *Plasticité cristalline et transition d'échelle : cas du monocristal*. Techniques de l'Ingénieur, M4016, 23 pages, 2004a.

M. Fivel and S. Forest. *Plasticité cristalline et transition d'échelle : cas du polycristal*. Techniques de l'Ingénieur, M4017, 11 pages, 2004b.

S. Forest. The micromorphic approach for gradient elasticity, viscoplasticity and damage. *ASCE Journal of Engineering Mechanics*, 135:117–131, 2009.

S. Forest. Some links between cosserat, strain gradient crystal plasticity and the statistical theory of dislocations. *Philosophical Magazine*, 88: 3549–3563, 2008.

S. Forest and E. C. Aifantis. Some links between recent gradient thermo-elasto-plasticity theories and the thermomechanics of generalized continua. *International Journal of Solids and Structures*, 47:3367–3376, 2010.

S. Forest and R. Sedláček. Plastic slip distribution in two–phase laminate microstructures: Dislocation–based vs. generalized–continuum approaches. *Philosophical Magazine A*, 83:245–276, 2003.

S. Forest and R. Sievert. Elastoviscoplastic constitutive frameworks for generalized continua. *Acta Mechanica*, 160:71–111, 2003.

S. Forest and R. Sievert. Nonlinear microstrain theories. *International Journal of Solids and Structures*, 43:7224–7245, 2006.

S. Forest, F. Barbe, and G. Cailletaud. Cosserat modelling of size effects in the mechanical behaviour of polycrystals and multiphase materials. *International Journal of Solids and Structures*, 37:7105–7126, 2000.

S. Forest, F. Pradel, and K. Sab. Asymptotic analysis of heterogeneous Cosserat media. *International Journal of Solids and Structures*, 38:4585–4608, 2001.

M. Frémond and B. Nedjar. Damage, gradient of damage and principle of virtual power. *Int. J. Solids Structures*, 33:1083–1103, 1996.

E. Fried and M.E. Gurtin. Continuum theory of thermally induced phase transitions based on an order parameter. *Physica D*, 68:326–343, 1993.

A. Gaubert, A. Finel, Y. Le Bouar, and G. Boussinot. Viscoplastic phase field modellling of rafting in ni base superalloys. In *Continuum Models and Discrete Systems CMDS11*, pages 161–166. Mines Paris Les Presses, 2008.

A. Gaubert, Y. Le Bouar, and A. Finel. Coupling phase field and viscoplasticity to study rafting in ni-based superalloys. *Philosophical Magazine*, 90:375–404, 2010.

P. Germain. La méthode des puissances virtuelles en mécanique des milieux continus, première partie : théorie du second gradient. *J. de Mécanique*, 12:235–274, 1973a.

P. Germain. The method of virtual power in continuum mechanics. part 2 : Microstructure. *SIAM J. Appl. Math.*, 25:556–575, 1973b.

P. Grammenoudis and Ch. Tsakmakis. Micromorphic continuum Part I: Strain and stress tensors and their associated rates. *International Journal of Non–Linear Mechanics*, 44:943–956, 2009.

P. Grammenoudis, Ch. Tsakmakis, and D. Hofer. Micromorphic continuum Part II: Finite deformation plasticity coupled with damage. *International Journal of Non–Linear Mechanics*, 44:957–974, 2009.

W. Günther. Zur Statik und Kinematik des Cosseratschen Kontinuums. *Abhandlungen der Braunschweig. Wiss. Ges.*, 10:195–213, 1958.

M.E. Gurtin. A gradient theory of single–crystal viscoplasticity that accounts for geometrically necessary dislocations. *Journal of the Mechanics and Physics of Solids*, 50:5–32, 2002.

M.E. Gurtin. Generalized Ginzburg–Landau and Cahn–Hilliard equations based on a microforce balance. *Physica D*, 92:178–192, 1996.

M.E. Gurtin and L. Anand. Nanocrystalline grain boundaries that slip and separate: A gradient theory that accounts for grain-boundary stress and conditions at a triple-junction. *Journal of the Mechanics and Physics of Solids*, 56:184–199, 2008.

M.E. Gurtin and L. Anand. Thermodynamics applied to gradient theories involving the accumulated plastic strain: The theories of Aifantis and Fleck & Hutchinson and their generalization. *Journal of the Mechanics and Physics of Solids*, 57:405–421, 2009.

C.B. Hirschberger and P. Steinmann. Classification of concepts in thermodynamically consistent generalized plasticity. *ASCE Journal of Engineering Mechanics*, 135:156–170, 2009.

William C. Johnson and J. Iwan D. Alexander. Interfacial conditions for thermomechanical equilibrium in two-phase crystals. *Journal of Applied Physics*, 9:2735–2746, 1986.

A.G. Khachaturyan. *Theory of structural transformations in solids.* John Wiley & Sons, 1983.

S.G. Kim, W.T. Kim, and T Suzuki. Interfacial compositions of solid and liquid in a phase–field model with finite interface thickness for isothermal solidification in binary alloys. *Physical Review E*, 58(3):3316–3323, 1998.

S.G. Kim, W.T. Kim, and T Suzuki. Phase–field model for binary alloys. *Physical Review E*, 60(6):7186–7197, 1999.

E. Kröner. On the physical reality of torque stresses in continuum mechanics. *Int. J. Engng. Sci.*, 1:261–278, 1963.

E. Kröner. Initial studies of a plasticity theory based upon statistical mechanics. In M.F. Kanninen, W.F. Adler, A.R. Rosenfield, and R.I. Jaffee, editors, *Inelastic Behaviour of Solids*, pages 137–147. McGraw-Hill, 1969.

E. Kröner and C. Teodosiu. Lattice defect approach to plasticity and viscoplasticity. In A. Sawczuk, editor, *Problems of Plasticity, International Symposium on Foundations of Plasticity, Warsaw.* Noordhoff International Publishing Leyden, 1972.

M. Lazar and G.A. Maugin. Dislocations in gradient micropolar–I: screw dislocation. *Journal of the Mechanics and Physics of Solids*, 52:2263–2284, 2004.

M. Lazar and G.A. Maugin. On microcontinuum field theories: the eshelby stress tensor and incompatibility conditions. *Philosophical Magazine*, 87: 3853–3870, 2007.

M. Lazar, G.A. Maugin, and E.C. Aifantis. Dislocations in second strain gradient elasticity. *International Journal of Solids and Structures*, 43: 1787–1817, 2006.

J.D. Lee and Y. Chen. Constitutive relations of micromorphic thermoplasticity. *International Journal of Engineering Science*, 41:387–399, 2003.

J. Mandel. Une généralisation de la théorie de la plasticité de W.T. Koiter. *International Journal of Solids and Structures*, 1:273–295, 1965.

J. Mandel. *Plasticité classique et viscoplasticité.* CISM Courses and Lectures No. 97, Udine, Springer Verlag, Berlin, 1971.

J. Mandel. Equations constitutives et directeurs dans les milieux plastiques et viscoplastiques. *Int. J. Solids Structures*, 9:725–740, 1973.

G.A. Maugin. The method of virtual power in continuum mechanics: Application to coupled fields. *Acta Mechanica*, 35:1–70, 1980.

J.R. Mayeur, D.L. McDowell, and D.J. Bammann. Dislocation–based micropolar single crystal plasticity: Comparison if multi– and single cristerion theories. *Journal of the Mechanics and Physics of Solids*, 59:398–422, 2011.

M. Mazière, J. Besson, S. Forest, B. Tanguy, H. Chalons, and F. Vogel. Numerical aspects in the finite element simulation of the portevin-le chatelier effect. *Computer Methods in Applied Mechanics and Engineering*, 199:734–754, 2010.

L. Méric, P. Poubanne, and G. Cailletaud. Single crystal modeling for structural calculations. Part 1: Model presentation. *J. Engng. Mat. Technol.*, 113:162–170, 1991.

C. Miehe. A multifield incremental variational framework for gradient-type standard dissipative solids, in press. *Journal of the Mechanics and Physics of Solids*, 2011.

C. Miehe, F. Welchinger, and M. Hofacker. Thermodynamically–consistent phase field models of fracture: Variational principles and multifield FE implementations. *International Journal for Numerical Methods in Engineering*, 83:1273–1311, 2010a.

C. Miehe, F. Welchinger, and M. Hofacker. A phase field model of electromechanical fracture. *Journal of the Mechanics and Physics of Solids*, 58:1716–1740, 2010b.

R.D. Mindlin. Micro–structure in linear elasticity. *Arch. Rat. Mech. Anal.*, 16:51–78, 1964.

A. I. Murdoch. A thermodynamical theory of elastic material interfaces. *Q. J. Mech. appl. Math.*, 29:245–275, 1978.

J.F. Nye. Some geometrical relations in dislocated crystals. *Acta Metall.*, 1:153–162, 1953.

R.H.J. Peerlings, M.G.D. Geers, R. de Borst, and W.A.M. Brekelmans. A critical comparison of nonlocal and gradient–enhanced softening continua. *Int. J. Solids Structures*, 38:7723–7746, 2001.

A. Rajagopal, P. Fischer, E. Kuhl, and P. Steinmann. Natural element analysis of the cahn-hilliard phase-field model. *Computational Mechanics*, 46: 471–493, 2010.

R.A. Regueiro. On finite strain micromorphic elastoplasticity. *International Journal of Solids and Structures*, 47:786–800, 2010.

C. Sansour, S. Skatulla, and H. Zbib. A formulation for the micromorphic continuum at finite inelastic strains. *Int. J. Solids Structures*, 47:1546–1554, 2010.

Schäfer,H. Eine Feldtheorie der Versetzungen im Cosserat-Kontinuum. *ZAMP*, 20:891–899, 1969.

I. Steinbach and M. Apel. Multi phase field model for solid state transformation with elastic strain. *Physica D*, 217:153–160, 2006.

P. Steinmann. Views on multiplicative elastoplasticity and the continuum theory of dislocations. *International Journal of Engineering Science*, 34: 1717–1735, 1996.

B. Svendsen. Continuum thermodynamic models for crystal plasticity including the effects of geometrically-necessary dislocations. *J. Mech. Phys. Solids*, 50:1297–1329, 2002.

C. Teodosiu. A dynamic theory of dislocations and its applications to the theory of the elastic-plastic continuum. In J.A. Simmons, R. de Wit, and R. Bullough, editors, *Fundamental Aspects of Dislocation Theory*, pages 837–876. Nat. Bur. Stand. (US) Spec. Publ. 317, II, 1970.

C. Teodosiu and F. Sidoroff. A theory of finite elastoviscoplasticity of single crystals. *Int. J. of Engng Science*, 14:165–176, 1976.

R.L.J.M. Ubachs, P.J.G. Schreurs, and M.G.D. Geers. A nonlocal diffuse interface model for microstructure evolution of tin–lead solder. *Journal of the Mechanics and Physics of Solids*, 52:1763–1792, 2004.

R.L.J.M. Ubachs, P.J.G. Schreurs, and M.G.D. Geers. Elasto-viscoplastic nonlocal damage modelling of thermal fatigue in anisotropic lead-free solder. *Mechanics of Materials*, 39:685–701, 2007.

Y. Wang, L.-Q. Chen, and A.G. Khachaturyan. Kinetics of strain-induced morphological transformation in cubic alloys with a miscibility gap. *Acta Metallurgica et Materialia*, 41:279–296, 1993.

A. Zeghadi, S. Forest, A.-F. Gourgues, and O. Bouaziz. Ensemble averaging stress–strain fields in polycrystalline aggregates with a constrained surface microstructure–Part 2: Crystal plasticity. *Philosophical Magazine*, 87:1425–1446, 2007.